

# ORIGIN AND DYNAMICAL EVOLUTION OF COMETS AND THEIR RESERVOIRS

Alessandro Morbidelli

CNRS, Observatoire de la Côte d'Azur, Nice, France

February 3, 2008

## Abstract

This text was originally written to accompany a series of lectures that I gave at the '35th Saas-Fee advanced course' in Switzerland and at the Institute for Astronomy of the University of Hawaii. It reviews my current understanding of the dynamics of comets and of the origin and primordial sculpting of their reservoirs. It starts discussing the structure of the Kuiper belt and the current dynamics of Kuiper belt objects, including scattered disk objects. Then it discusses the dynamical evolution of Jupiter family comets from the trans-Neptunian region, and of long period comets from the Oort cloud. The formation of the Oort cloud is then reviewed, as well as the primordial sculpting of the Kuiper belt. Finally, these issues are revisited in the light of a new model of giant planets evolution that has been developed to explain the origin of the late heavy bombardment of the terrestrial planets.

## 1 Introduction

Comets are often considered to be the gateway for understanding Solar System formation. In fact, they are probably the most primitive objects of the Solar System because they formed in distant regions where the relatively cold temperature preserved the pristine chemical conditions. For this reason they have been the target of very sophisticated and expensive space missions like *Giotto*, *Stardust* and *Rosetta* for in-situ analysis or sample return. To best exploit the information collected by ground based and space based observations, however, it is necessary to know where comets come from, where they formed, and how they evolved in the distant past. For instance, did they form at 5, 30 or at 100 AU? Are they chunks of larger objects that presumably underwent significant thermal and collisional alteration or are they pristine planetesimals that could never grow larger?

In addition, the orbital structure of the comet reservoirs records information of the dynamical processes that occurred when the Solar System was taking

shape. For example, it carries evidence of the migration of the giant planets, and/or of close encounters of our Sun with other stars. Modeling these dynamical processes and comparing their outcomes with the observed structures, gives us a unique opportunity to reconstruct the history of the formation of the planets and of their primordial evolution.

The purpose of this chapter is to review our current understanding of comets from the dynamical point of view and underline the open issues which still need more investigation. The first part is devoted to the current Solar System. In Section 2 I describe the orbital and dynamical properties of the trans-Neptunian population: the Kuiper belt and the scattered disk. Section 3 is devoted to the evolution of comets from their parent reservoirs –the trans-Neptunian population or the Oort cloud– to the inner Solar System. As we know the current Solar System quite well –the orbits of the planets, its galactic environment– the results discussed in this part are quite secure. In contrast, the second part of the chapter focusses on more controversial topics, as it is devoted to the origin of the Solar System, namely how the comet reservoirs formed and acquired their current shapes. More precisely, section 4 is devoted to the formation of the Oort cloud, section 5 to the primordial sculpting of the trans-Neptunian population and section 6 discusses a recently proposed connection between these events and the Late Heavy Bombardment of the terrestrial planets. In the final section I will speculate on a scenario of solar system primordial evolution that would put all these aspects together in a coherent scheme.

## 2 The trans-Neptunian population

Our observational knowledge of the trans-Neptunian population<sup>1</sup> is very recent. The first object, Pluto, was discovered in 1930, but unfortunately this discovery was not quickly followed by the detection of other trans-Neptunian objects. Thus, Pluto was thought to be an exceptional body –a planet– rather than a member of a numerous small body population, of which it is not even the largest in size. It was only in 1992, with the advent of CCD cameras and a lot of perseverance, that another trans-Neptunian object –1992 QB<sub>1</sub>– was found [82]. Now, 13 years later, we know more than 1,000 trans-Neptunian objects. Of them, about 500 have been observed for at least three years. A time-span of 3 years is required in order to compute their orbital elements with some confidence. In fact, the trans-Neptunian objects move very slowly, and most of their apparent motion is simply a parallax effect. Our knowledge of the orbital structure of the trans-Neptunian population is therefore built on these  $\sim 500$  objects.

Before moving to discuss the orbital structure of the trans-Neptunian population, in the next subsection I briefly overview the basic facts of orbital dynamics.

---

<sup>1</sup>There is no general consensus on nomenclature, yet. In this work I call ‘trans-Neptunian population’ the collection of small bodies with semi-major axis (or equivalently orbital period) larger than that of Neptune, with the exception of the Oort cloud (semi-major axis larger than 10,000 AU).

The expert reader can move directly to section 2.2.

## 2.1 Brief tutorial of orbital dynamics

Neglecting mutual perturbations, all bodies in the Solar System move relative to the Sun in an elliptical orbit, the Sun being at one of the two foci of the ellipse. Therefore, it is convenient for astronomers to characterize the relative motion of a body by quantities that describe the geometrical properties of its orbital ellipse and its instantaneous position on the ellipse. These quantities are usually called *orbital elements*.

The shape of the ellipse can be completely determined by two orbital elements: the semi-major axis  $a$  and the eccentricity  $e$  (Fig. 1). The name *eccentricity* comes from  $e$  being the ratio between the distance of the focus from the center of the ellipse and the semi-major axis of the ellipse. The eccentricity is therefore an indicator of how much the orbit differs from a circular one:  $e = 0$  means that the orbit is circular, while  $e = 1$  means that the orbit is a segment of length  $2a$ , the Sun being at one of the extremes. Among all “elliptical” trajectories, the latter is the only collisional one, if the physical radii of the bodies are neglected. A semi-major axis of  $a = \infty$  and  $e = 1$  denote parabolic motion, while the convention  $a < 0$  and  $e > 1$  is adopted for hyperbolic motion. I will not deal with these kinds of unbounded motion in this chapter, hence I will concentrate, hereafter, on the elliptic case. On an elliptic orbit, the closest point to the Sun is called the *perihelion*, and its heliocentric distance  $q$  is equal to  $a(1 - e)$ ; the farthest point is called the *aphelion* and its distance  $Q$  is equal to  $a(1 + e)$ .

To denote the position of a body on its orbit, it is convenient to use an orthogonal reference frame  $q_1, q_2$  with origin at the focus of the ellipse occupied by the Sun and  $q_1$  axis oriented towards the perihelion of the orbit. Alternatively, polar coordinates  $r, f$  can be used. The angle  $f$  is usually called the *true anomaly* of the body. From Fig. 1, with elementary geometrical relationships one has

$$q_1 = a(\cos E - e) , \quad q_2 = a\sqrt{1 - e^2} \sin E \quad (1)$$

and

$$r = a(1 - e \cos E) , \quad \cos f = \frac{\cos E - e}{1 - e \cos E} \quad (2)$$

where  $E$ , as Fig. 1 shows, is the angle subtended at the center of the ellipse by the projection –parallel to the  $q_2$  axis– of the position of the body on the circle which is tangent to the ellipse at perihelion and aphelion. This angle is called the *eccentric anomaly*. The quantities  $a$ ,  $e$  and  $E$  are enough to characterize the position of a body in its orbit.

From Newton equations, it is possible to derive [25] the evolution law of  $E$  with respect to time, usually called the *Kepler equation*:

$$E - e \sin E = n(t - t_0) \quad (3)$$

where

$$n = \sqrt{\mathcal{G}(m_0 + m_1)} a^{-3/2} \quad (4)$$

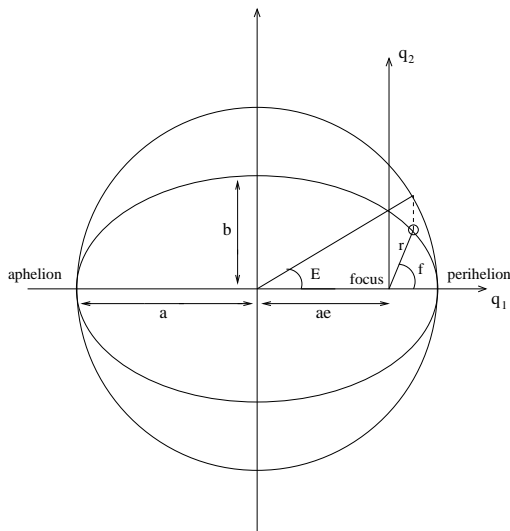


Figure 1: Keplerian motion: definition of  $a$ ,  $e$  and  $E$ .

is the orbital frequency, or *mean motion*, of the body,  $m_0$  and  $m_1$  are the masses of the Sun and of the body respectively and  $\mathcal{G}$  is the gravitational constant;  $t$  is the time and  $t_0$  is the time of passage at perihelion.

Astronomers like to introduce a new angle

$$M = n(t - t_0) \quad (5)$$

called the *mean anomaly*, as an orbital element that changes linearly with time.  $M$  also denotes the position of the body in its orbit, through equations (3) and (2).

To characterize the orientation of the ellipse in space, with respect to an arbitrary orthogonal reference frame  $(x, y, z)$  centered on the Sun, one has to introduce three additional angles (see Fig. 2). The first one is the inclination  $i$  of the orbital plane (the plane which contains the ellipse) with respect to the  $(x, y)$  reference plane. If the orbit has a nonzero inclination, it intersects the  $(x, y)$  plane in two points, called the *nodes* of the orbit. Astronomers distinguish between an *ascending* node, where the body passes from negative to positive  $z$ , and a *descending* node, where the body plunges towards negative  $z$ . The orientation of the orbital plane in space is then completely determined when one gives the angular position of the ascending node from the  $x$  axis. This angle is traditionally called the *longitude of ascending node*, and is usually denoted by  $\Omega$ . The last angle that needs to be introduced is the one characterizing the orientation of the ellipse in its plane. The *argument of perihelion*  $\omega$  is defined as the angular position of the perihelion, measured in the orbital plane relative to the line connecting the central body to the ascending node.

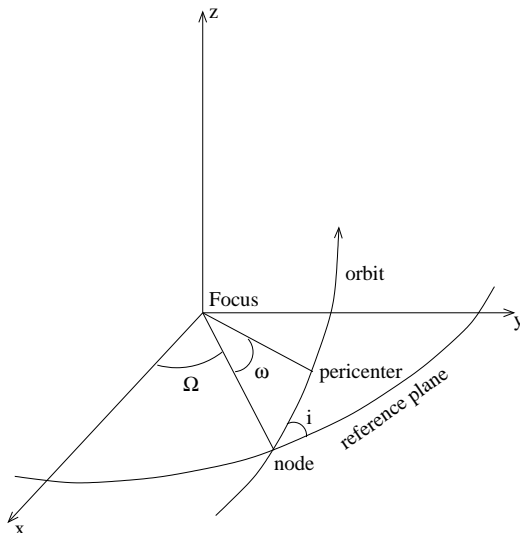


Figure 2: Keplerian motion: definition of  $i$ ,  $\Omega$  and  $\omega$ .

In the definition of the orbital elements above, note that when the inclination is zero,  $\omega$  and  $M$  are not defined, because the position of the ascending node is not determined. Moreover,  $M$  is not defined also when the eccentricity is zero, because the position of the perihelion is not determined. Therefore, it is convenient to introduce the *longitude of perihelion*  $\varpi = \omega + \Omega$  and the *mean longitude*  $\lambda = M + \omega + \Omega$ . The first angle is well defined when  $i = 0$ , while the second one is well defined when  $i = 0$  and/or  $e = 0$ .

In absence of external perturbations, the orbital motion is perfectly elliptic. Thus, the orbital elements  $a, e, i, \varpi, \Omega$  are fixed, and  $\lambda$  moves linearly with time, with frequency (4). When a small perturbation is introduced (for instance the presence of an additional planet), two effects are produced. First, the motion of  $\lambda$  is no longer perfectly linear. Correspondingly, the other orbital elements have short periodic oscillations with frequencies of order of the orbital frequencies. Second, the angles  $\varpi$  and  $\Omega$  start to rotate slowly. This motion is called *precession*. Typical precession periods in the Solar System are of order of 10,000–100,000 years. Correspondingly,  $e$  and  $i$  have long periodic oscillations, with periods of order of the precession periods.

The regularity of these short periodic and long periodic oscillations is broken when one of the following two situations occur: (i) the perturbation becomes large, for instance when there are close approaches between the body and the perturbing planet, or when the mass of the perturber is comparable to that of the Sun (as in the case of encounters of the Solar System with other stars) or (ii) the perturbation becomes resonant. In either of these cases the orbital elements  $a, e, i$  can have large non-periodic, irregular variations.

A resonance occurs when the frequencies of  $\lambda, \varpi$  or  $\Omega$  of the body, or an inte-

ger combination of them, are in an integer ratio with one of the time frequencies of the perturbation. If the perturber is a planet, the perturbation is modulated by the planet orbital frequency and precession frequencies. We speak of *mean-motion resonance* when  $k d\lambda/dt = k' d\lambda'/dt$ , with  $k$  and  $k'$  integer numbers and  $\lambda'$  denoting the mean longitude with the planet. We speak of *linear secular resonance* when  $d\varpi/dt = d\varpi'/dt$  or  $d\Omega/dt = d\Omega'/dt$ , prime variables referring again to the planet. Other types of resonances exist in more complicated systems (non-linear secular resonances, three-body resonances, Kozai resonance etc.). I will return to discuss resonant motion more specifically in subsection 2.3, when reviewing the dynamical properties of some trans-Neptunian sub-populations.

## 2.2 The structure of the trans-Neptunian population

The trans-Neptunian population is “traditionally” subdivided in two sub-populations: the *scattered disk* and the *Kuiper belt*. The definition of these sub-populations is not unique, with the Minor Planet center and various authors often using slightly different criteria. Here I propose a partition based on the dynamics of the objects and their relevance for the reconstruction of the primordial evolution of the outer Solar System, keeping in mind that all bodies in the Solar System must have been formed on orbits typical of an accretion disk (e.g. with very small eccentricities and inclinations).

I call *scattered disk* the region of the orbital space that can be visited by bodies that have encountered Neptune within a Hill’s radius<sup>2</sup>, at least once during the age of the Solar System, assuming no substantial modification of the planetary orbits. The bodies that belong to the scattered disk in this classification do not provide us any relevant clue to uncover the primordial architecture of the Solar System. In fact their current eccentric orbits might have been achieved starting from quasi-circular ones in Neptune’s zone by pure dynamical evolution, in the framework of the current architecture of the planetary system.

I call *Kuiper belt* the trans-Neptunian region that cannot be visited by bodies encountering Neptune. Therefore, the non-negligible eccentricities and/or inclinations of the Kuiper belt bodies cannot be explained by the scattering action of the planet on its current orbit, but they reveal that some excitation mechanism, which is no longer at work, occurred in the past (see section 5).

To categorize the observed trans-Neptunian bodies into scattered disk and Kuiper belt, one can refer to previous works on the dynamics of trans-Neptunian bodies in the framework of the current architecture of the planetary system. For the  $a < 50$  AU region, one can use the results by [35] and [99], who numerically mapped the regions of the  $(a, e, i)$  space with  $32 < a < 50$  AU that can lead to a Neptune encountering orbit within 4 Gy. Because dynamics are reversible, these are also the regions that can be visited by a body after having encountered the planet. Therefore, according to the definition above, they constitute the scattered disk. For the  $a > 50$  AU region, one can use the results in [103]

<sup>2</sup>The Hill’s radius is given by the formula  $R_H = a_p(m_p/3)^{1/3}$ , where  $m_p$  is the mass of the planet relative to the mass of the Sun and  $a_p$  is the planet’s semi-major axis. It corresponds approximately to the distance from the planet of the Lagrange equilibrium points  $L_1$  and  $L_2$ .

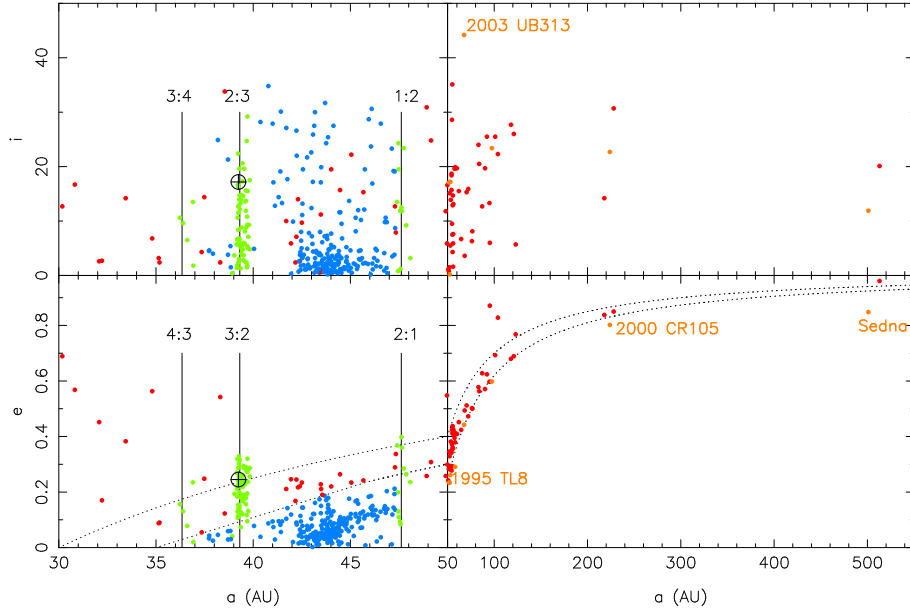


Figure 3: The orbital distribution of multi-opposition trans-Neptunian bodies, as of Aug. 26, 2005. Scattered-disk bodies are represented in red, extended scattered-disk bodies in orange, classical Kuiper belt bodies in blue and resonant bodies in green. We qualify that, in absence of long term numerical integrations of the evolution of all the objects and because of the uncertainties in the orbital elements, some bodies could have been mis-classified. Thus, the figure should be considered as an indicative representation of the various subgroups that compose the trans-Neptunian population. The dotted curves in the bottom left panel denote  $q = 30$  AU and  $q = 35$  AU; those in the bottom right panel  $q = 30$  AU and  $q = 38$  AU (right panel). The vertical solid lines mark the locations of the 3:4, 2:3 and 1:2 mean-motion resonances with Neptune. The orbit of Pluto is represented by a crossed circle.

and [36], where the the evolutions of the particles that encountered Neptune in [35] have been followed for another 4 Gy time-span. Despite the fact that the initial conditions did not cover all possible configurations, one can reasonably assume that these integrations cumulatively show the regions of the orbital space that can be possibly visited by bodies transported to  $a > 50$  AU by Neptune encounters. Again, according to my definition, these regions constitute the scattered disk.

Fig. 3 shows the  $(a, e, i)$  distribution of the trans-Neptunian bodies which have been observed during at least three oppositions. The bodies that belong to the scattered disk according to my criterion are represented as red dots. The Kuiper belt population is in turn subdivided in two sub-populations: the *resonant population* (green dots) and the *classical belt* (blue dots). The former is

made of objects located the major mean-motion resonances with Neptune (essentially the 3:4, 2:3 and 1:2 resonances, but also the 2:5 –see [20], while the classical belt objects are not in any noticeable resonant configuration. Mean-motion resonances offer a protection mechanism against close encounters with the resonant planet (see section 2.3). For this reason, the resonant population can have perihelion distances much smaller than those of the classical belt objects. Stable resonant objects can have even Neptune-crossing orbits ( $q < 30$  AU) as in the case of Pluto (see sect. 2.3). The bodies in the 2:3 resonance are often called *Plutinos*, for the similarity of their orbit with that of Pluto. According to [160], the scattered disk and the Kuiper belt constitute roughly equal populations, while the resonant objects, altogether, make about 10% of the classical objects.

Notice in Fig. 3 also the existence of bodies with  $a > 50$  AU, on highly eccentric orbits, which do not belong to the scattered disk according to my definition (magenta dots). Among them are 2000CR<sub>105</sub> ( $a = 230$  AU, perihelion distance  $q = 44.17$  AU and inclination  $i = 22.7^\circ$ ), Sedna ( $a = 495$  AU,  $q = 76$  AU) and the currently size-record holder 2003 UB<sub>313</sub> ( $a = 67.7$  AU,  $q = 37.7$  AU but  $i = 44.2^\circ$ ), although for some objects the classification is uncertain for the reasons explained in the figure caption. Following [53], I call these objects *extended scattered-disk* objects for three reasons. (i) They are very close to the scattered-disk boundary. (ii) Bodies of the sizes of the three objects quoted above (300–2000 km) presumably formed much closer to the Sun, where the accretion timescale was sufficiently short [146]. This implies that they have been transported in semi-major axis space (e.g. scattered), to reach their current locations. (iii) the lack of objects with  $q > 41$  AU and  $50 < a < 200$  AU should not be due to observational biases, given that many classical belt objects with  $q > 41$  AU and  $a < 50$  AU have been discovered (see Fig. 6). This suggests that the extended scattered-disk objects are *not* the highest eccentricity members of an excited belt beyond 50 AU. These three considerations indicate that in the past the true scattered disk extended well beyond its present boundary in perihelion distance. Why this was so, is particularly puzzling. Some ideas will be presented in sect. 5.

Given that the observational biases become more severe with increasing perihelion distance and semi-major axis, the currently known extended scattered-disk objects may be like the tip of an iceberg, e.g. the emerging representatives of a conspicuous population, possibly outnumbering the scattered-disk population [53].

**The excitation of the Kuiper belt.** An important clue to the history of the early outer Solar System is the dynamical excitation of the Kuiper belt. While eccentricities and inclinations of resonant and scattered objects are expected to have been affected by interactions with Neptune, those of the classical objects should have suffered no such excitation. Nonetheless, the confirmed classical belt objects have an inclination range up to at least 32 degrees and an eccentricity range up to 0.2, significantly higher than expected from a primordial disk, even accounting for mutual gravitational stirring.



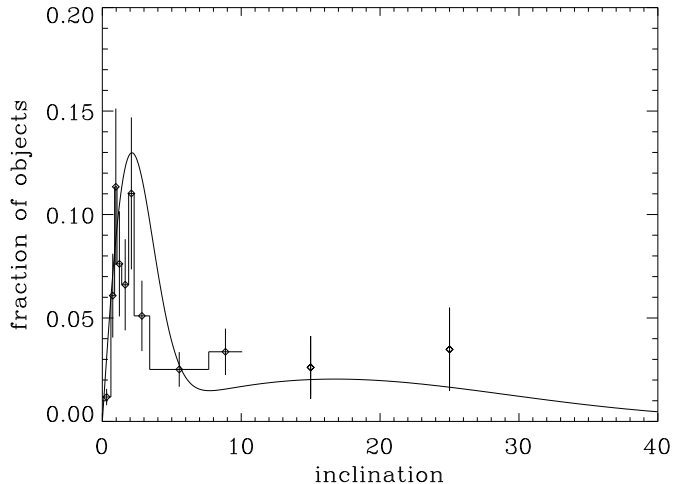


Figure 4: The inclination distribution (in deg.) of the classical Kuiper belt, from [125]. The points with error bars show the model-independent estimate constructed from a limited subset of confirmed classical belt bodies, while the smooth line shows the best fit two-population model  $f(i)di = \sin(i)[96.4 \exp(-i^2/6.48) + 3.6 \exp(-i^2/288)]di$  [14]. In this model  $\sim 60\%$  of the objects have  $i > 4^\circ$ .

The observed distributions of eccentricities and inclinations in the Kuiper belt are highly biased. High eccentricity objects have closer approaches to the Sun and thus they become brighter and are more easily detected. Consequently, the detection bias roughly follows curves of constant  $q$ . At first sight, this bias might explain why, in the classical belt beyond  $a = 44$  AU, the eccentricity tends to increase with semi-major axis. However, the resulting  $(a, e)$  distribution is significantly steeper than a curve  $q = \text{constant}$ . Thus, the apparent relative under-density of objects at low eccentricity in the region  $44 < a < 48$  AU is likely a real feature of the Kuiper belt distribution.

High inclination objects spend little time at low latitudes<sup>3</sup> at which most surveys take place, while low inclination objects spend zero time at the high latitudes where some searches have occurred. Using this fact, [14] computed a de-biased inclination distribution for classical belt objects (Figure 4).

A clear feature of this de-biased distribution is its bi-modality, with a sharp drop around 4 degrees and an extended, almost flat distribution in the 4–30 degrees range, demanded by the presence of objects with large inclinations.

<sup>3</sup>Latitude (angular height over a reference curve in the sky) and inclination should be defined with respect to the local Laplace plane (the plane normal to the orbital precession pole), which is a better representation for the plane of the Kuiper belt than is the ecliptic [38].

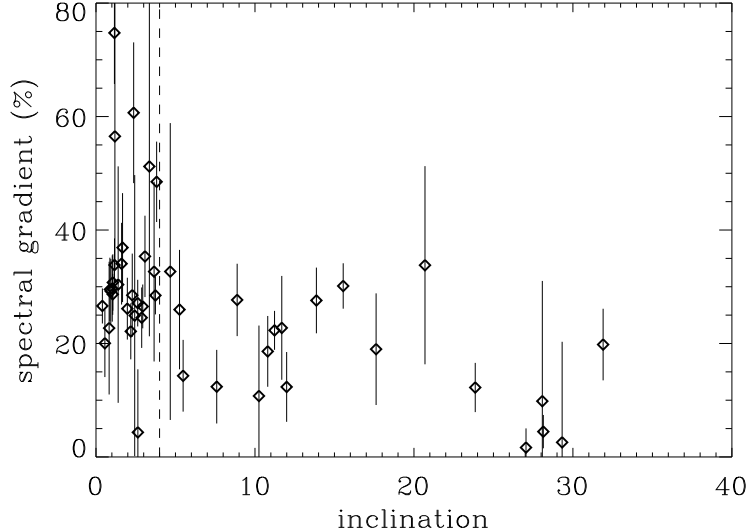


Figure 5: Color gradient versus inclination in the classical Kuiper belt (from [125], using the database in [65]). Color gradient is the slope of the spectrum, in % per 100nm, with 0% being neutral and large numbers being red. The hot and cold classical objects have significantly different distributions of color.

This bi-modality can be modeled with two Gaussian functions and suggests the presence of two distinct classical Kuiper belt populations, called hot ( $i > 4$ ) and cold ( $i < 4$ ) after [14].

**Physical evidence for two populations in the classical belt.** The co-existence of a hot and a cold population in the classical belt could be caused in one of two general manners. Either a subset of an initially dynamically cold population was excited, leading to the creation of the hot classical population, or the populations are truly distinct and formed separately. One manner in which one can attempt to determine which of these scenarios is more likely is to examine the physical properties of the two classical populations. If the objects in the hot and cold populations are physically different it is less likely that they were initially part of the same population.

The first suggestion of a physical difference between the hot and the cold classical objects came from [104] who noted that the intrinsically brightest classical belt objects (those with lowest absolute magnitudes) are preferentially found on high inclination orbits. This conclusion has been recently verified in a bias-independent manner in [163], with a survey for bright objects which covered  $\sim 70\%$  of the ecliptic and found many hot classical objects but few cold classical objects.

The second possible physical difference between hot and cold classical Kuiper belt objects is their colors, which relates in an unknown manner to surface composition and physical properties. Several possible correlations between orbital parameters and color were suggested by [156] and further investigated by [31]. The issue was clarified by [162] who quantitatively showed that for the classical belt, the inclination is correlated with color. In essence, the low inclination classical objects tend to be redder than higher inclination objects (see Fig. 5). This correlation has then been confirmed by several other authors [32] [38]. Whether or not there is also a correlation between colors and perihelion distances is still a matter of debate [32].

More interestingly, we see that the colors naturally divide into distinct low inclination and high inclination populations at precisely the location of the divide between the hot and cold classical objects. These populations differ at a 99.9% confidence level. Interestingly, the cold classical population also differs in color from the Plutinos and the scattered objects at the 99.8% and 99.9% confidence level, respectively, while the hot classical population appears identical in color to these other populations [162]. The possibility remains, however, that the colors of the objects, rather than being markers of different populations, are actually *caused* by the different inclinations. For example [150] has suggested that the higher average impact velocities of the high inclination objects will cause large scale resurfacing by fresh water ice which could be blue to neutral in color. However, a careful analysis shows that there is clearly no correlation between average impact velocity and color ([158]).

In summary, the significant color and size differences between the hot and cold classical objects imply that these two populations are physically different, in addition to being dynamically distinct.

**The radial extent of the Kuiper belt.** Another important property of interest for understanding the primordial evolution of the Kuiper belt is its radial extent. While initial expectations were that the mass of the Kuiper belt should smoothly decrease with heliocentric distance –or perhaps even increase in number density by a factor of  $\sim 100$  [146], back to the level given by the extrapolation of the minimum mass solar nebula [66] beyond the region of Neptune’s influence– the lack of detection of objects beyond about 50 AU soon began to suggest a drop off in number density ([83], [19], [160]). It was often argued that this lack of detections was the consequence of a simple observational bias caused by the extreme faintness of objects at greater distances from the sun, but [3], [4] showed convincingly that for a fixed absolute magnitude distribution, the number of objects with semi-major axis less than 50 AU was larger than the number greater than 50 AU, and thus some density decrease is present.

The characterization of the density drop beyond 50 AU was hampered by the small numbers of objects and thus weak statistics in individual surveys. A method to use all detected objects to estimate a radial distribution of the Kuiper belt and to test hypothetical radial distributions against the known observations was developed in [161]. The analysis reported in that work is reproduced in

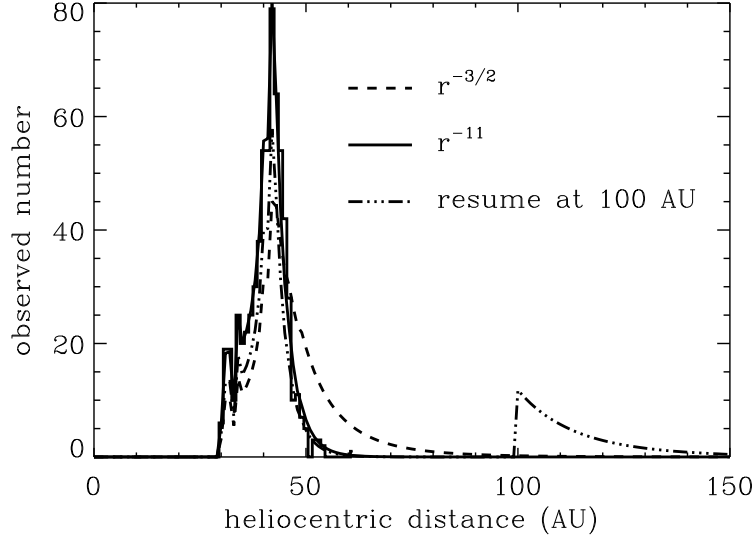


Figure 6: The observed radial distribution of Kuiper belt objects (solid histogram) compared to observed radial distributions expected for models where the surface density of Kuiper belt objects decreases by  $r^{-3/2}$  beyond 42 AU (dashed curve), where the surface density decreases by  $r^{-11}$  beyond 42 AU (solid curve), and where the surface density at 100 AU increases by a factor of 100 to the value expected from an extrapolation of the minimum mass solar nebula (dashed-dotted curve). From [125].

Fig. 6. The drop off beyond 42 AU of the heliocentric distance distribution of Kuiper belt objects at discovery is clearly inconsistent with a smooth decline of the surface density distribution proportional to  $r^{-3/2}$ . Instead, it can be fitted with a surface density distribution with a much sharper decay, as  $r^{-11 \pm 4}$  (error bars are  $3\sigma$ ), i.e. assuming the existence of an effective edge in the radial Kuiper belt distribution. This steep radial decay should presumably hold up to  $\sim 60$  AU, beyond which a much flatter distribution due to the scattered-disk objects should be found.

It has been conjectured [146] that, beyond some range of Neptune’s influence, the number density of Kuiper belt objects could increase back up to the level expected for the minimum mass solar nebula [66]. Such an increase can be ruled out at the  $3\sigma$  level within 115 AU from the Sun. Beyond this distance the biases due to the slow motions of the objects also become important, so few conclusion can be drawn from the current data about objects beyond this threshold. If the model is slightly modified to make the maximum object mass proportional to the surface density at a particular distance, a 100 times resumption of the Kuiper belt can still be ruled out inside 94 AU.

Although the drop off in the heliocentric distance distribution starts at 42 AU, a visual inspection of Fig. 3 shows that the edge of the Kuiper belt in semi-major axis space is precisely at the location of the 1:2 mean-motion resonance with Neptune. This is a very important feature, which points to a role of Neptune in the final positioning of the edge. I will come back to this in sect. 5.

**The missing mass of the Kuiper belt.** The absolute magnitude<sup>4</sup> distribution of the Kuiper belt objects can be determined from the so-called *cumulative luminosity function*, which is given by the number of detections that surveys reported as a function of their limiting magnitude, weighted by the inverse area of sky that the surveys covered. If one assumes that the albedo distribution of Kuiper belt objects is size independent, the slope of the absolute magnitude distribution can be readily converted into the slope of the cumulative size distribution.

The size distribution turns out to be very steep, with exponent of the cumulative power law exponent between  $-3.5$  and  $-3$  for bodies larger in diameter than  $\sim 200$  km [52]. Actually, the size distribution is slightly shallower for the hot population than for the cold population, as shown in a recent analysis [9] (see Fig. 7). This is not surprising, given that –as we have seen above– the hot and the cold populations contain roughly the same total number of objects, but the former hosts the largest members of the Kuiper belt.

The HST survey in [9] also reported the detection of a change in the size distribution for objects fainter than about 100 km in diameter. The slopes of the size distribution below this limit, however, remain very uncertain because of small number statistics. Some researchers still dispute the validity of the detection of any turnover of the size distribution (Kaavelars, private communication). Given these uncertainties, as well as uncertainties on the mean albedo of the Kuiper belt objects (required to convert a given absolute magnitude into a size) and their bulk density, the total mass of the Kuiper belt is uncertain up to an order of magnitude at least, its estimates ranging from  $0.01 M_{\oplus}$  ([9]) to  $0.1 M_{\oplus}$  ([52]).

Whatever the real value in this range (or slightly beyond), it appears nevertheless secure that the total mass of the Kuiper belt is now very small, in particular compared to the mass of the disk of solids from which the Kuiper belt objects had to form. There are two lines of argument to estimate the primordial mass.

A first argument follows the reasoning which led Kuiper to conjecture the existence of a band of small planetesimals beyond Neptune ([100]). The minimum mass solar nebula inferred from the total planetary mass (plus lost volatiles; [66]) smoothly declines from the orbit of Jupiter until the orbit of Neptune; why should it abruptly drop beyond the last planet? The extrapolation and the integration of this surface density distribution predicts that the original total

---

<sup>4</sup>The absolute magnitude  $H$  is a measure of the intrinsic brightness of an object. It corresponds to the visual magnitude that an object would have in the paradoxical situation of being simultaneously at 1 AU from the Sun and the Earth, at opposition!

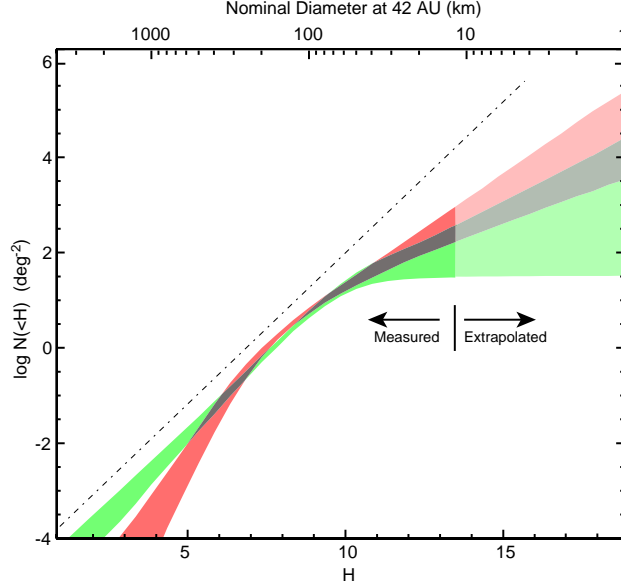


Figure 7: The  $H$ - or size-distribution in the Kuiper belt (adapted from [9] with the courtesy of Bernstein. The red and green bands show the uncertainties for the cold and the hot population, respectively (although the definition for hot and cold used in that work do not exactly match those adopted in this paper). Absolute magnitudes have been computed assuming that all detections occurred at 42 AU (the maximum of the radial surface density distribution of the Kuiper belt), and the conversion to diameters uses the assumption that the mean albedo is 4%.

mass of solids in the 30–50 AU range should have been  $\sim 30M_{\oplus}$ .

The second argument for a massive primordial Kuiper belt was brought to attention by Stern ([145]) who found that the objects currently in the Kuiper belt could not have formed in the present environment: collisions are sufficiently infrequent that 100 km objects cannot be built by pairwise accretion of the current population over the age of the solar system. Moreover, owing to the large eccentricities and inclinations of Kuiper belt objects –and consequently to their high encounter velocities– collisions that do occur tend to be erosive rather than accretional, making bodies smaller rather than larger. Stern suggested that the resolution of this dilemma is that the primordial Kuiper belt was both more massive and dynamically colder, so that more collisions occurred, and they were gentler and therefore generally accretional.

Following this idea, detailed modeling of accretion in a massive primordial Kuiper belt was performed [146], [147], [148] [88], [89], [90]. While each model includes different aspects of the relevant physics of accretion, fragmentation, and velocity evolution, the basic results are in approximate agreement. First,

with  $\sim 10 M_{\oplus}$  or more of solid material in an annulus from about 35 to 50 AU on very low eccentricity orbits ( $e \leq 0.001$ ), all models naturally produce of order a few objects the size of Pluto and approximately the right number of  $\sim 100$  km objects, on a timescale ranging from several  $10^7$  to several  $10^8$  y. The models suggest that the majority of mass in the disk was in bodies approximately 10 km and smaller. The accretion stopped when the formation of Neptune or other dynamical phenomena (see section 5) began to induce eccentricities and inclinations in the population high enough to move the collisional evolution from the accretional to the erosive regime.

A massive and dynamically cold primordial Kuiper belt is also required by the models that attempt to explain the formation of the observed numerous binary Kuiper belt objects ([54], [167], [51], [5]).

Therefore, the general formation picture of an initial massive Kuiper belt appears secure, and understanding the ultimate fate of the 99% of the initial Kuiper belt mass that appears to be no longer in the Kuiper belt is a crucial step in reconstructing the history of the outer Solar System.

### 2.3 Dynamics in the Kuiper belt

I now come to overview the dynamical properties in the Kuiper belt. Without pretension of being exhaustive, the goal is to understand which properties of the Kuiper belt orbital structure can be explained from the evolution of the objects in the framework of the current architecture of the Solar System and which, conversely, require an explanation built on a scenario of primordial sculpting (as in section 5).

Figure 8 shows a map of the dynamical lifetime of trans-Neptunian bodies as a function of their initial semi-major axis and eccentricity, for an inclination of  $1^\circ$  and a random choice of the orbital angles  $\lambda$ ,  $\varpi$  and  $\Omega$  ([35]). Similar maps, referring to different choices of the initial inclination or different projections on the orbital element space can be found in [99] and [35]. These maps have been computed numerically, by simulating the evolution of massless particles from their initial conditions, under the gravitational perturbations of the giants planets. The latter have been assumed to be initially on their current orbits. Each particle was followed until it suffered a close encounter with Neptune. Objects encountering Neptune, would then evolve in the scattered disk for a typical time of order  $\sim 10^8$  years (but much longer residence times in the scattered disk occur for a minority of objects), until they are transported by planetary encounters into the inner planets region or to the Oort cloud, or are ejected to the interstellar space. This issue is described in more detail in section 3.

In Figure 8 the colored strips indicate the timespan required for a particle to encounter Neptune, as a function of its initial semi-major axis and eccentricity. Strips that are colored yellow represent objects that survive for the length of the simulation,  $4 \times 10^9$  years (the approximate age of the Solar System) without encountering the planet. The figure also reports the orbital elements of the known Kuiper belt objects. Big dots refer to bodies with  $i < 4^\circ$ , consistent with the low inclination at which the stability map has been computed. Small dots

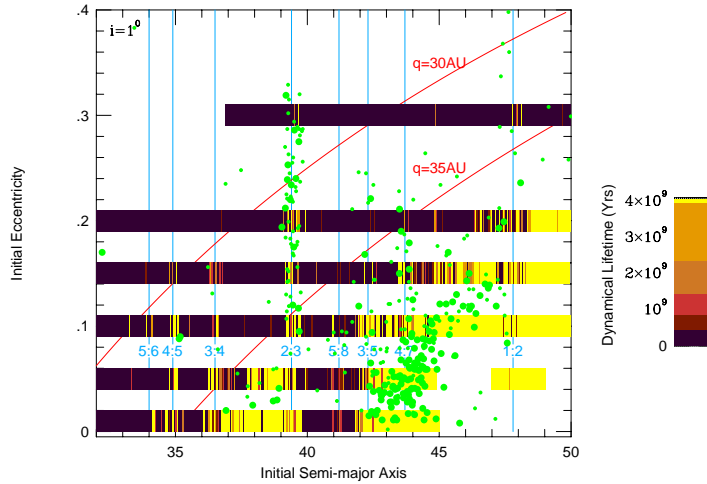


Figure 8: The dynamical lifetime for small particles in the Kuiper belt derived from 4 billion year integrations [35]. Each particle is represented by a narrow vertical strip of color, the center of which is located at the particle’s initial eccentricity and semi-major axis (initial orbital inclination for all objects was 1 degree). The color of each strip represents the dynamical lifetime of the particle. Strips colored yellow represent objects that survive for the length of the integration,  $4 \times 10^9$  years. Dark regions are particularly unstable on short timescales. For reference, the locations of the important Neptune mean-motion resonances are shown in blue and two curves of constant perihelion distance,  $q$ , are shown in red. The  $(a, e)$  elements of the Kuiper belt objects with well determined orbits are also shown as green dots. Large dots are for  $i < 4^\circ$ , small dots otherwise.

refer to objects with larger inclination and are plotted only for completeness.

As can be seen in the figure, the Kuiper belt has a complex dynamical structure, although some general trends can be easily explained.

**Stability limits imposed by close encounters with Neptune.** Most objects with perihelion distances less than  $\sim 35$  AU are unstable. This is due to the fact that they pass sufficiently close to Neptune so that they are destabilized during the encounters. In fact, in these cases Neptune’s gravity is no longer a ‘small perturbation’ relative to that of the Sun. The regularity of the oscillation of the orbital elements is broken. The semi-major axis suffers jumps at each encounter with the planet, and the eccentricity has correlated jumps in order to keep the perihelion distance roughly constant (more precisely, to conserve the



*Tisserand parameter*, see sect. 3). One encounter with Neptune after another, the object wanders over the  $(a, e)$  plane: the object is effectively a member of the scattered disk. Consequently, the  $q = 35$  AU curve can be considered as the approximate border between the Kuiper belt and the scattered disk, in the 30–50 AU semi-major axis range. The real border, however, has a more complicated, fractal structure, illustrated by the boundary between the black and the yellow regions in Fig. 8.

Not all bodies with  $q < 35$  AU are unstable. The exception is represented by objects in mean-motion resonances with Neptune. These objects, despite approaching (or even intersecting) the orbit of Neptune at perihelion, never approach the planet at short distance. This happens because the resonance plays a protection role against close encounters.

The stabilizing role of a mean-motion resonance can be understood in simple, qualitative terms. For instance, Figure 9 illustrates the mechanism for the case of Pluto (2:3 mean-motion resonance). The trajectory of Pluto is shown in the figure in a frame that rotates with Neptune. Pluto moves in a clockwise direction when further from the Sun than Neptune and moves in a counter-clockwise direction when closer to the Sun. In the figure, an object with Pluto’s eccentricity and exactly at Neptune 2:3 mean-motion resonance would have a trajectory that is a double-lobed structure oriented as in Fig. 9a. The configuration shown in the figure will remain fixed only if the object’s semi-major axis is *exactly* equal to that characterizing the location of the resonance. For an object with semi-major axis slightly displaced, the double-lobed structure will slowly precess in the rotating frame.

If the semi-major axis of the object is slightly larger than that corresponding to the exact location of the resonance the double-lobed trajectory will slowly precess towards that shown in Fig. 9b. If the precession continued indefinitely, eventually the trajectory would pass over the location of Neptune and a close encounter or a physical collision would occur. However, because the new trajectory is no longer symmetric with respect to Neptune, the object receives its largest acceleration ( $a_m$ ) from Neptune when in or near the upper lobe. At this point, the object is leading Neptune in its orbit and thus it is slowed down in its heliocentric motion. Consequently its semi-major axis decreases.

When the semi-major axis of the object becomes smaller than that corresponding to the exact location of the resonance the situation reverses. Now the double-lobed trajectory slowly precesses in the opposite direction. The configuration of Fig. 9a is restored, and then the trajectory continues to precess towards the configuration of Fig. 9c. In this case, the object gets its largest acceleration when it is near perihelion and is trailing Neptune in their orbits (near the lower lobe of the trajectory). Thus, the object’s orbital velocity is increased, increasing its semi-major axis.

When the semi-major axis of the object becomes again larger than the exact resonant value, the precession of the double-lobed trajectory reverses again. The trajectory goes back to the configuration of Fig. 9a and then to that of Fig. 9b, and the cycle repeats indefinitely. Each cycle is called a *libration*. Over a full libration cycle the pattern drawn by the object’s dynamics in the frame

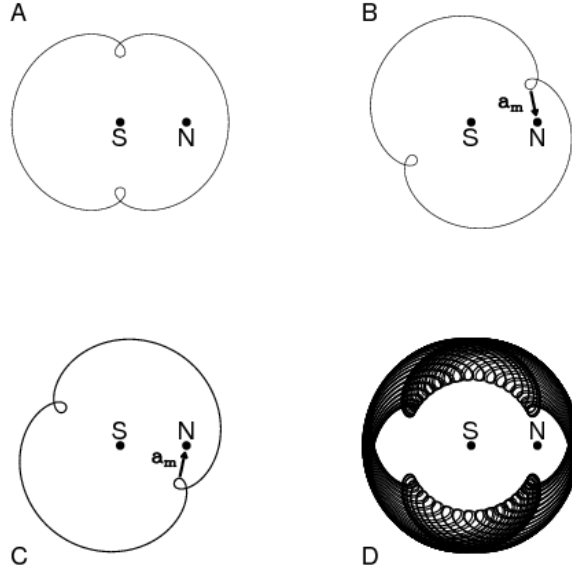


Figure 9: The dynamics of an object in the 2:3 mean-motion resonance with Neptune. The double-lobed curve represents the orbit of an object with the eccentricity of Pluto. The coordinate frame rotates counterclockwise at the average speed of Neptune. Thus, Neptune (dot labeled ‘N’) is stationary in this figure. The location of the Sun is labeled ‘S’. A) The orbit of an object whose semi-major axis is equal to that characterizing the exact location of the resonance. The gravitational perturbations of Neptune cancel out due to the symmetry in the geometry. Thus, this orbit does not precess in the rotating frame. B) If the symmetry is broken, there is a net acceleration due to Neptune. Here, the strongest perturbation ( $a_m$ ) is at the upper lobe. The object is leading Neptune at this lobe, so the net acceleration will decrease its semi-major axis. C) The strongest perturbation is in the lower lobe. Consequently, the object’s semi-major axis has to increase. D) The orbit of an object that *librates* in the resonance. Courtesy of H. Levison.

co-rotating with Neptune is that illustrated in Fig. 9d.

Therefore, the mean-motion resonance exerts on the object a *restoring torque* which reverses the precession of its double-lobed trajectory before a close encounter can occur. This of course happens only if the object is not too far from the exact resonance location, otherwise the precession is too fast and the mag-

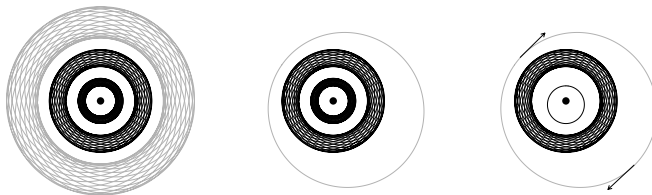


Figure 10: The dynamics of a secular resonance. Three orbits are shown in each panel. The inner two are planets, which are shown as black lines. The outer orbit (gray line) is for a small object. The orbits of each object are ellipses, and the ellipses are precessing due to the mutual gravitational effects of the planets. Left: The orbits of the objects over a period of time that is long compared to the precession time of the orbits. Here, we are looking in a fixed, non-rotating reference frame. Each orbit sweeps out a torus of possible positions. Center: The same as in the left plot, except that we are looking in a frame that rotates at the precession rate of the small outer body. Thus, its orbit is again an ellipse. This panel shows the geometry if no secular resonance exists. Note that the trajectories of the planets look axisymmetric. Therefore, there is no net torque on the outer small object. Right: Same as the middle plot, except that the outer object is in a secular resonance with the inner planet, i.e. both orbits precess at the same rate. As a result, the outer object no longer sees an axisymmetric gravitational perturbation from the inner planet. Indeed, it feels a significant torque. Courtesy of H. Levison.

nitude of the restoring torque is not sufficient. The limiting distance from the exact resonance location within which the restoring torque is effective defines the *resonance width*.

The analytic computation of resonance widths is detailed in [122]. This calculation, however, overestimates the width of the region where resonant objects are stable over the Solar System’s age. In fact, the situation is complicated by the interaction between the libration motion inside the resonance and the precession motion of the orbits of the object and of the perturbing planet. A detailed exploration of the stability region inside the two main mean-motion resonances of the Kuiper belt, the 2:3 and 1:2 resonances with Neptune, has been done in [130] [131]. Its description goes beyond the purposes of this chapter.

**Secular resonance instabilities.** In Fig. 8 one can see that the dark region extends significantly below the  $q = 35$  AU line for  $40 < a < 42$  AU (and also for  $35 < a < 36$  AU). The instability in these regions is due to the presence of a secular resonance, due to the fact that  $d\varpi/dt \sim d\varpi_N/dt$ , where  $\varpi$  is the perihelion longitude the object and  $\varpi_N$  that of Neptune.

This resonance forces large variation of the eccentricity of the trans-Neptunian object, so that –even if the initial eccentricity is null– the perihelion distance eventually decreases below 35 AU, and the object enters the scattered disk [79]

[120].

The destabilizing effect of a secular resonance between the longitude of perihelia can be understood in simple qualitative terms. Consider a simple case where the orbits of the object and of *two* planets are in the same plane. The presence of two planets is necessary, otherwise the planetary orbit would be a fixed, non-precessing ellipse. The orbit of the small body also precesses under the planets' perturbations. The left plot in Figure 10 shows the long-term trajectories of these objects in a fixed frame. The middle plot shows the same system in a frame that rotates with the precession rate of the small body. Note that the orbit of the small body (the outermost orbit) is, in this frame, a fixed ellipse. If the precession rates of the planetary orbits are different from that of the small body, the trajectories of the two planets in the rotating frame are still, on average, axisymmetric and thus the small body experiences no long-term torques. However, if one of the planets precesses at the same rate as the small body, as in the right plot in Figure 10, its long-term trajectory is also a fixed ellipse in the rotating frame, and it is no longer axisymmetric. Thus the small body feels a significant long-term torque, which can lead to a significant change in its eccentricity (which is related to the angular momentum).

The location of secular resonances in the Kuiper belt has been computed in [94]. This work showed that the secular resonance is present only at small inclination. Large inclination orbits with  $q > 35$  AU and  $40 < a < 42$  AU are therefore stable. Indeed, Figure 8 shows that many objects with  $i > 4^\circ$  (small dots) are present in this region. Only large dots, representing low-inclination objects, are absent.

**Chaotic diffusion in the Kuiper belt.** Fig. 8 also shows the presence of narrow bands with brown colors, crossing the yellow stability domain. These bands correspond to orbits which become Neptune-crossing only after billions of years of evolution. What is the nature of these weakly unstable orbits?

It has been found [131] that these orbits are in general associated either with high order mean-motion resonances with Neptune (i.e. resonances for which the equivalence  $k d\lambda/dt = k_N d\lambda_N/dt$  holds only for large values of the integer coefficients  $k, k_N$ ) or three-body resonances with Uranus and Neptune (which occur when  $k d\lambda/dt + k_N d\lambda_N/dt + k_U d\lambda_U/dt = 0$  occurs for some integers  $k, k_N$  and  $k_U$ ).

The dynamics of objects in these resonances is chaotic. The semi-major axis of the objects remain locked at the corresponding resonant value, while the eccentricity of objects is slowly modified. In an  $(a, e)$ -diagram like Fig. 11, each object's evolution leaves a vertical trace. This phenomenon is called *chaotic diffusion*. Eventually the growth of the eccentricity can bring the diffusing object above the  $q = 35$  AU curve. These resonances are too weak to offer an effective protection against close encounters with Neptune, unlike the low order resonances considered above. Thus, once above this critical curve, the encounters with Neptune start to change the semi-major axis of the objects, which leave their original resonance and evolve –from that moment on– in the

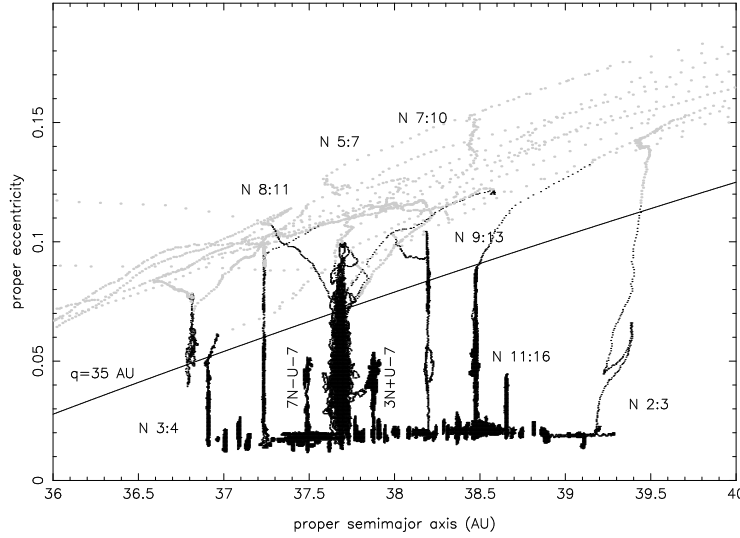


Figure 11: The evolution of objects initially at  $e = 0.015$  and semi-major axis distributed in the 36.5–39.5 AU range. The dots represent the proper semi-major axis and the eccentricity of the objects –computed by averaging their  $a$  and  $e$  over 10 My time intervals– over the age of the Solar System. They are plotted in grey after that the perihelion has decreased below 32 AU for the first time. Labels  $Nk : k_N$  denote the  $k : k_N$  two-body resonances with Neptune. Labels  $k_N N + k_U U + k$  denote the three-body resonances with Uranus and Neptune, that correspond to the equality  $k_N \dot{\lambda}_N + k_U \dot{\lambda}_U + k \dot{\lambda} = 0$ . Reprinted from [131].

scattered disk.

Notice from Fig. 11 that some resonances are so weak that, despite the resonant objects diffuse chaotically, they cannot reach the  $q = 35$  AU curve within the age of the Solar System. Therefore, these objects are ‘stable’ from the astronomical point of view.

Notice also that chaotic diffusion is effective only for selected resonances. The vast majority of the simulated objects are not affected by any macroscopic diffusion. They preserve their initial small eccentricity for the entire age of the Solar System. Thus, the current moderate/large eccentricities and inclinations of most of the Kuiper belt objects cannot be obtained from primordial circular and coplanar orbits by dynamical evolution in the framework of the current orbital configuration of the planetary system. Likewise, the region beyond the 1:2 mean-motion resonance with Neptune is totally stable. Thus, the absence of bodies beyond 48 AU cannot be explained by current dynamical instabilities. Also, the overall mass deficit of the Kuiper belt cannot be due objects escaping through resonances, because most of the inhabited Kuiper belt is stable for the current planetary architecture. Therefore, all these intriguing properties of

the Kuiper belt's structure must find an explanation in the framework of the formation and primordial evolution of the Solar System. This will be the topic of sect. 5.

## 2.4 Note on the scattered disk

We have seen above that the bodies that escape from the Kuiper belt and decrease their perihelion distance below 35 AU, without being protected by a low-order mean-motion resonance, enter the scattered disk.

Their subsequent evolution has been studied in detail in [103]. It was found that the median dynamical lifetime is  $\sim 50$  My, the typical end-states being the transport towards the inner Solar System (and the eventual ejection from the Solar System due to an encounter with Jupiter or Saturn; see sect. 3), a collision with a planet or the outward transport towards the Oort cloud (see sect. 4). This result suggests that the scattered disk could be a population of transient objects, which is sustained in steady state by a continuous flux of objects escaping from the Kuiper belt. In this case, the scattered disk would be, relative to the Kuiper belt, what the population of Near Earth Asteroids is, relative to the main asteroid belt.

However, [36] showed that about 1% of the scattered-disk objects can survive on trans-Neptunian orbits for the age of the Solar System. This opens the possibility that the current scattered disk is the remnant of a  $\sim 100\times$  more massive primordial structure, which presumably formed when the planets chased the left-over planetesimals from their neighborhoods. In this case, the scattered disk would not be in steady state, and it would have no direct relationship with the Kuiper belt.

How can we discriminate between these two hypotheses on the origin of the scattered disk? In the first case, if the scattered disk is sustained in steady state by the objects leaking out of the Kuiper belt, the number ratio between the Kuiper belt and scattered-disk populations must be large. Indeed:

$$N_{SD} = N_{KB} \times f_{esc} \times L_{SD}$$

where  $N_{SD}$  is the number of scattered-disk objects (larger than a given size),  $N_{KB}$  is the number of Kuiper belt objects (down to the same size),  $f_{esc}$  is the fraction of the Kuiper belt population that escapes into the scattered disk in the unit time (due to chaotic diffusion or collisional ejection) and  $L_{SD}$  is the mean lifetime in the scattered disk. Both  $L_{SD}$  and  $f_{esc}$  are small, so that  $N_{KB} \gg N_{SD}$ . In fact, in the case of the main asteroid belt and the NEA population, the number ratio is about 1,000.

In the second case, if the current scattered disk is the remnant of a much more massive primordial scattered population, there is no casual relationship between  $N_{KB}$  and  $N_{SD}$ . The current population of the scattered disk depends only on its primordial population, and not on the current Kuiper belt population.

Discovery statistics [160] suggest that the scattered disk and the Kuiper belt now contain roughly equal populations. This rules out (by orders of magnitude)

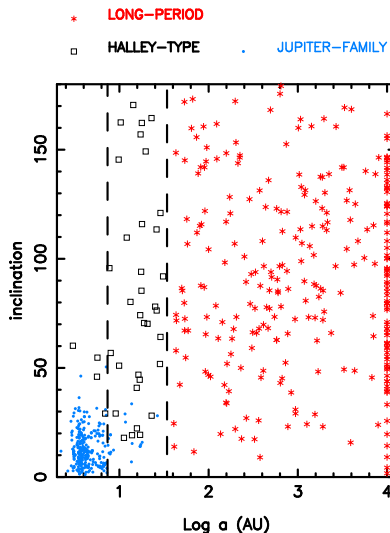


Figure 12: The distribution of comets according to their orbital semi-major axis and inclination. Here the orbital elements are defined at the moment of the comet’s last aphelion passage. Long period, Halley-type and Jupiter family comets are plotted as red stars, black squares and blue dots, respectively. The separation between Halley-types and Jupiter family comets has been made according to the value of their Tisserand parameter, following [101]. The vertical dashed lines correspond to orbital periods  $P = 20$  y and  $P = 200$  y, respectively. All long period comets with  $a > 10,000$  AU have been represented on the  $\log a = 4$  line.

the possibility that the scattered disk is sustained in steady state by the Kuiper belt. Only the scenario of [36] remains valid for the origin of the scattered disk.

### 3 The dynamics of comets

Comets are usually classified in categories according to their orbital period (Figure 12). Comets with orbital period  $P > 200$  y are called *long period comets* (LPCs); those with shorter period are called *short period comets* (SPCs). The threshold of 200 y is arbitrary, and has been chosen mostly for historical reasons: modern instrumental astronomy is about two centuries old, so that the long period comets that we see now are unlikely to have been observed in the past.

If the orbital distribution of the comets is plotted, like in Fig. 12, using the orbital elements that the comets had when they last passed at *aphelion* – which can be computed through a backward numerical integration – one sees a clustering of long period comets with  $a \sim 10^4$  AU. These comets are called *new comets* because they must pass through the giant planets system for the first

time. In fact, after a passage through the inner Solar System, it is unlikely that the semi-major axis remains of order  $10^4$  AU. It either decreases to  $\sim 10^3$  AU or the orbit becomes hyperbolic. The reason is that the binding energy of a new comet is  $E = -\mathcal{G}M_{\odot}/2a \sim 10^{-4}$ , but typically, during a close perihelion passage, the energy suffers a change of order of the mass of Jupiter relative to the Sun:  $10^{-3}$ . This change is not due to close encounters with the planet (which might not occur). It is due to the fact that the comet has a barycentric motion when it is far away, an heliocentric motion when it is close, and the distance of the barycentre from the Sun is of the order of the relative mass of Jupiter.

The short period comets are in turn subdivided in *Halley-type* (HTCs) and *Jupiter family* (JFCs). Historically, the partition between the two classes is done according to the orbital period being respectively longer or shorter than 20 y. This threshold has been chosen because there is an evident change in the inclination distribution at the corresponding value of semi-major axis (see Fig. 12). However, comets continuously change semi-major axis as a consequence of their encounters with the planets. In particular, all short period comets had to have a larger semi-major axis in the past, given that they come from the trans-planetary region. Thus, by adopting a partition between Halley-type and Jupiter family comets based on orbital period, one is confronted with the unpleasant situation of objects changing their classification during their lifetime.

This has motivated Levison [101] to classify short period comets according to their *Tisserand parameter* relative to Jupiter

$$T_J = \frac{a_J}{a} + 2\sqrt{\frac{a}{a_J}(1 - e^2)} \cos i . \quad (6)$$

This new classification makes sense, because the Tisserand parameter is quite well preserved during the comet's evolution. In Levison's classification, Halley-type and Jupiter family comets have  $T_J$  respectively smaller and larger than 2. Fig. 12 adopts this classification and shows that for most of the objects the classifications based on orbital period and on Tisserand parameter are in agreement, but a few objects (those with  $P < 20$  y and large inclination or those with  $P > 20$  y and low inclination) do change their classification depending on the adopted criterion.

**Tisserand parameter.** Given the importance of the Tisserand parameter in comet dynamics, it is useful to derive its expression (which outlines the limitations of its use) and discuss its properties.

The Tisserand parameter is an approximation of the Jacobi constant, which is an invariant of the dynamics of a small body in the framework of the restricted, circular, three-body problem.

The expression of the Jacobi constant is:

$$C_J = -(\dot{x}^2 + \dot{y}^2 + \dot{z}^2) + 2\left(\frac{1}{r} + \frac{m_p}{\Delta}\right) + 2H_z , \quad (7)$$



where  $\mathcal{G}M_{\oplus} = a_p = 1$  are assumed, and  $a_p, m_p$  are the semi-major axis and mass of the perturbing planet and  $H_z$  is the  $z$ -component of the small body's angular momentum. The quantity  $\Delta$  is the distance between the small body and the planet.

We write the kinetic energy of the small body as a function of its semi-major axis and heliocentric distance:

$$\frac{1}{2}(\dot{x}^2 + \dot{y}^2 + \dot{z}^2) = -\frac{1}{2a} + \frac{1}{r}, \quad (8)$$

while the  $z$ -component of the angular momentum can be written:

$$H_z = \sqrt{a(1-e^2)} \cos i. \quad (9)$$

Substituting (8) and (9) into (7) and neglecting the term  $m_p/\Delta$  one gets

$$C_J \sim T \equiv \frac{1}{a} + 2\sqrt{a(1-e^2)} \cos i, \quad (10)$$

where the right hand side coincides with (6), given that  $a$  is expressed in units of the planet's semi-major axis.

This derivation of the Tisserand formula shows that the Tisserand parameter is constant as long as the Jacobi constant is preserved, and  $m_p/\Delta$  is small. This last condition requires that the comet is not in a close encounter with the planet. During a close encounter, the Tisserand parameter has large and abrupt changes, but it returns to the value that it had before the encounter, once the distance to the planet increases back to large values. The conservation of the Jacobi constant, conversely, requires that the conditions of the restricted three-body problem are fulfilled, namely one planet must dominate the comet's evolution, and the effects of the planet's eccentricity must be negligible. This requires that the comet is not in a region where it can have encounters with *two* planets, otherwise the one-planet approximation does not hold. Also, it requires that the comet is not in a secular resonance with the planet, otherwise the effects of the planet's small eccentricity are enhanced.

One can demonstrate that, if a comet intersects the orbit of a planet, the Tisserand parameter  $T$  is related to the unperturbed relative velocity  $U$  at which it encounters the planet:

$$U = \sqrt{3-T},$$

where  $U$  is expressed in units of the planet's orbital velocity. The formula is not defined for  $T > 3$ , which implies that comets with such values of Tisserand parameter cannot intersect the orbit of the planet. Note however that comets non-intersecting the orbit of the planet can have  $T < 3$ . Only objects with  $T < 2\sqrt{2} \sim 2.83$  (the value for a parabolic trajectory with  $i = 0$  and  $q = a_p$ ) can be ejected on hyperbolic orbit in a single encounter with a planet.

### 3.1 Origin and evolution of Jupiter family comets

The fact that the JFCs have (by definition) a Tisserand parameter with respect to Jupiter that is distinct from that of HTC and LPCs suggests that the former

are not the small semi-major axis end of the distribution of the latter. The average low inclination of the JFCs, and the absence of retrograde comets in the JFC population (whichever of the two definitions for JFCs is adopted, see Fig. 12) argues that the source of JFCs must be a disk-like structure. In 1980 [41] proposed that the source of JFCs was the –at the time still putative– Kuiper belt, an hypothesis supported later in [34].

However, today we know that there are two distinct disk-like structures in the trans-Neptunian region: the Kuiper belt and the scattered disk. Which of the two is the source of JFCs? We have seen in sect. 2.4 that the scattered disk is too populated to be sustained in steady state by the objects leaking out of the Kuiper belt. If the scattered disk is not sustained in steady state, it means that the number of objects that leave the scattered disk –mostly evolving towards the inner solar system– is larger than the number of objects entering the scattered disk from the Kuiper belt. Thus, the scattered disk must dominate the JFC production, over the Kuiper belt.

The dynamical evolution of objects from the scattered disk to the JFC region has been studied in detail in [103], with statistics made on a large number of numerical simulations. The results illustrated in that paper essentially supersede all the results from the previous literature. Thus, most of what I report below is taken from that source. The origin and dynamics of JFCs has also been exhaustively reviewed in [37].

To evolve from the scattered disk to the JFC region, a comet has to pass from a Neptune-dominated dynamics to a Jupiter-dominated dynamics (see Fig. 13). The transfer process involving multiple planets, in principle the Tisserand parameter is not preserved. However, the planetary system is structured in such a way that the transfer chain from Neptune to Jupiter is piece-wise dominated by one single planet (see Fig. 13), and the values of the Tisserand parameters relative to the dominating planets are almost the same. For instance, consider a scattered-disk body with Tisserand parameter relative to Neptune  $T_N = 2.98$ . The conservation of the Tisserand parameter implies that the smallest perihelion distance to which Neptune can scatter this object is  $q = 17.7$  AU, just enough to become Uranus-crosser. In this orbit, the body has  $T_U = 2.96$ . If Uranus takes the control of this body, it can scatter it inwards down to  $q = 9.0$  AU, barely a Saturn crosser. The body has now  $T_S = 2.94$  and thus Saturn can lower its  $q$  to only 3.8 AU. With such a perihelion, the comet has a Tisserand parameter  $T_J = 2.82$ . Thus, the body never spends much time in a region where it can encounter two planets. The Tisserand parameter is therefore piece-wise conserved, and the final Tisserand parameter (with respect to Jupiter) is very close to the initial one (with respect to Neptune). Now, the bulk of the observed population in the scattered disk has  $2 < T_N < 3$ . Thus, at the end of the transfer chain, the bodies coming from the scattered disk will have  $2 < T_J < 3$ , namely they will be JFCs.

Because the Tisserand parameter remains close to 3, the inclination cannot grow to large values (the growth of  $i$  would decrease  $T$ , see (6)). So, the final inclination distribution is comparable to the inclination distribution in the scattered disk, i.e. mostly confined within 30 degrees. Figure 14 compares

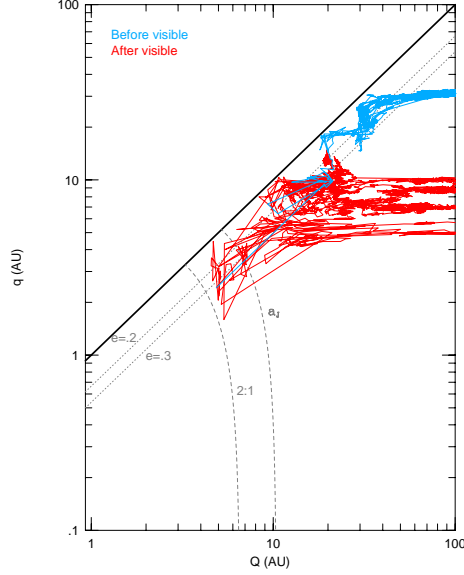


Figure 13: The evolution of an object from the scattered disk up to its ultimate ejection, projected over the plane representing perihelion vs. aphelion distance. The horizontal structure at  $q \sim 30$  AU represents the scattered disk. When the object evolves along a line  $q = \text{constant}$  or  $Q = \text{constant}$  its dynamics are essentially dominated by one single planet. This happens at least down to 10 AU, and during the final ejection phase. Blue lines denote the evolution before that the object becomes a visible JFC, red lines after. The criterion for first visibility is that  $q$  has decreased below 2.5 AU for the first time. From [103]

the  $(a, i, T_J)$  distribution of the observed short period comets (top panels) with the one obtained in the numerical simulation for the objects coming from the scattered disk, when their perihelion distance first decreases below 2.5 AU (a criterion for visibility as an active comet). As one sees, the objects with  $T_J < 2$  (HTCs) are not reproduced, while the observed and simulated distributions of the JFCs agree with each other in a remarkable way.

Nevertheless, a quantitative comparison would show that the inclination distribution of the simulated comets when they first become visible is slightly skewed towards low values relative to the observed distribution. Similarly, the distribution of the distances of the comets' nodes from Jupiter's orbit is also skewed towards small values. However, the dynamical lifetime of comets after they first become visible is of order  $10^5$  y. As time passes, the conservation of the Tisserand parameter degrades, as a result of the combined effects of Jupiter and

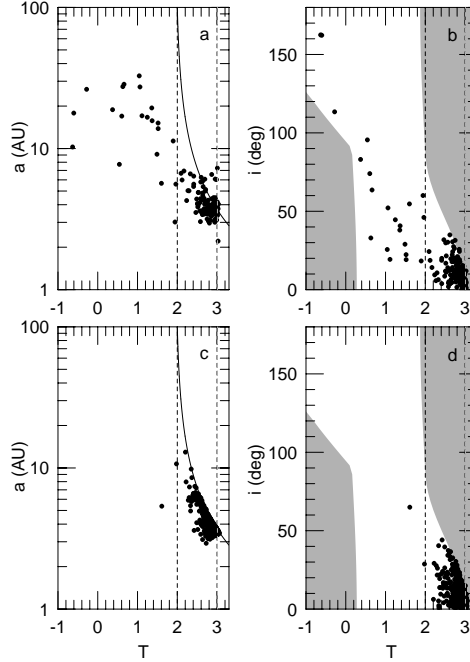


Figure 14: The distribution of short period comets projected over the  $(T_j, a)$  and  $(T_j, i)$  planes. Top panels: the observed distribution. Bottom panels: the distribution of the objects coming from the scattered disk, when they are visible ( $q < 2.5$  AU) for the first time. From [103].

Saturn and of secular resonances. Thus, the inclination is puffed up, and the distribution of  $\omega$  (initially strongly peaked around  $0^\circ$  and  $180^\circ$ ) is randomized. As a consequence, the nodal distance distribution is also puffed up<sup>5</sup>. Consequently, the agreement between the observed and simulated distributions first improves with the age of the comets, and then eventually degrades. Thus, [36] considered the distribution of all simulated objects, from the time they first become visible up to time  $\tau$ . Using a Kolmogorov-Smirnov test to measure quantitatively the statistical agreement between simulated and observed distributions, [36] concluded that the best match is achieved –simultaneously for the inclination and the nodal distance distributions– for  $\tau \sim 12,000$  y. The interpretation of this result is that this value of  $\tau$  corresponds to the typical physical lifetime of JFCs, after which the comets lose their activity and are no longer observed. Comparing the physical lifetime with the dynamical lifetime, [36] concluded that, if all faded JFCs are dormant objects with asteroidal appearance, the ratio between the number of dormant vs. active JFCs should be  $\sim 4$ .

<sup>5</sup>Some comets eventually evolve towards the  $T_J < 2$  region, although they never manage to reproduce the  $(a, i, T_J)$  distribution illustrated in the top panels of Fig. 14

The comparison between the  $q$  distribution of the simulated and observed JFCs suggests that the population of comets is observationally complete up to  $q \sim 2$  AU. There are  $\sim 40$  known JFCs with total absolute magnitude  $H_{10} < 9$ <sup>6</sup> and  $q < 2$  AU. The simulated  $q$  distribution indicates that there should be about 100 comets with  $q < 2.5$  AU, with the same total magnitude. If all faded JFCs are dormant, then we should expect an additional 400 bodies of asteroidal appearance on similar orbits. About 100 of them should have  $q < 1.3$  AU and belong to the NEO population. The size of these putative bodies is badly constrained, because the conversion from total magnitude to nuclear magnitude (i.e. the absolute magnitude of the nucleus, in absence of cometary activity) is poorly known. Published estimates for the nucleus size for  $H_{10} = 9$  comets range from  $D = 0.8$  km [6] to  $D = 4.5$  km [45], with a mean of about 2 km [45]. I will return to the nature of faded comets in sect. 3.4.

With this estimate of the total number of JFCs, from the rate at which scattered-disk bodies become JFCs and the mean lifetime of JFCs measured in the simulations, [36] computed that there should be  $4 \times 10^8$  of such objects (i.e. big enough to have total magnitude  $H_{10} < 9$  when active) in the scattered disk. The extrapolation of the size distribution observed in the scattered disk [9] is roughly consistent with this estimate.

**The orbit of comet P/Encke.** Despite the overall good agreement between the observed and the simulated distribution of JFCs shown in Fig. 14 there is one important difference that should not be overlooked: the orbit of comet P/Encke is not re-produced in the simulation of [103]. P/Encke is particular. It is the only active comet with an orbit totally interior to the orbit of Jupiter and  $T_J > 3$ . The aphelion distance of P/Encke is currently 4.1 AU, so that it is not scattered by Jupiter’s encounters. This implies that encounters with Jupiter cannot have emplaced the comet onto its current orbit.

It has been proposed that P/Encke reached its orbit from the  $T_J < 3$  region due to close encounters with the terrestrial planets, to the effect of non-gravitational forces<sup>7</sup>, or both [166][70][47][138]. Neither of these aspects have been included in the simulations of [103].

A quantitative model of the orbital distribution of JFCs accounting for terrestrial planets encounters and/or non-gravitational forces has never been done, so that we do not know if either of these effects naturally explains the existence of *one* active comet on orbits decoupled from Jupiter like that of P/Encke (as opposed to several comets or none). From the observational point of view, it seems that only very few objects should have followed Encke’s dynamical path. In fact, a search for objects with albedo typical of dormant cometary nuclei among the NEOs with  $T_J > 3$  ([50]) has showed that these objects, if they

<sup>6</sup>The total absolute magnitude is computed from the apparent magnitude  $V$  (of nucleus plus coma), the heliocentric and geocentric distances  $r$  and  $\Delta$  by the formula  $H_{10} = V + 5 \log \Delta + 10 \log r$ , instead of the usual formula for dormant bodies  $H = V + 5 \log \Delta + 5 \log r$ . The coefficient 10, instead of 5, accounts for the fact that the intensity of the activity of the comet is proportional to  $r^{-2}$ .

<sup>7</sup>for a recent review on non-gravitational forces acting on comet dynamics see [178]

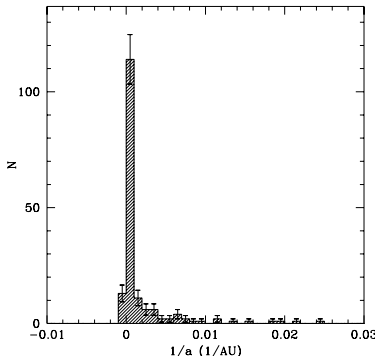


Figure 15: The differential distribution of LPCs as a function of the inverse semi-major axis. The big spike at  $1/a < 10^{-4}$  is due to the new comets, and is usually called the *Oort spike*. From [175].

exist, are rare.

### 3.2 Origin and evolution of Long period comets

In an historical paper, Oort ([134]) pointed out that the presence of numerous *new comets* with  $a > 10^4$  AU –which appears as a spike in the distribution of  $1/a$  of the LPCs (see Fig. 15)– argues for the existence of a reservoir of objects in that distant region. The fact that the inclination distribution of new comets is essentially isotropic, not only in  $\cos i$  (from -1 to 1, i.e. including also retrograde orbits), but also in  $\omega$  and  $\Omega$ , indicates that this reservoir must have a quasi-spherical symmetry, namely it has the shape of a cloud surrounding the Solar System. This cloud is now generally called the *Oort cloud*. In Oort’s view, *all* long period comets come from this cloud. The LPCs with  $a < 10^4$  AU are returning comets, which originally belonged to the new comet group when they first entered into the inner Solar System, but subsequently they had their orbit perturbed and acquired a more negative binding energy (smaller semi-major axis). This view remains essentially valid even today.

At such large distances from the Sun, the evolution of the comets in the Oort cloud is strongly affected by the overall gravitational field due to the mass distribution in the galaxy (the so-called *galactic tide*), and by sporadic passing stars and giant molecular clouds (GMCs).

Assuming that the galaxy has a disk-like structure and considering that the Sun is not at the center, the galactic tide has both “disk” and “radial” force components. In a coordinate system centered on the Sun, with  $x$ -axis pointing away from the galactic center,  $y$ -axis in the direction of the galactic rotation and  $z$ -axis towards the south galactic pole, the radial component of the tide can be expressed with forces along the  $x$  and  $y$  directions, respectively:

$$F_x = \Omega_0^2 x ; \quad F_y = -\Omega_0^2 y , \quad (11)$$

where  $\Omega_0$  is the frequency of revolution of the Sun around the galaxy. The disk component of the tide can be represented with a force along the  $z$  direction:

$$F_z = -4\pi\mathcal{G}\rho_0 z , \quad (12)$$

where  $\rho_0$  is the mass density in the solar neighborhood [73]. The disk component dominates over the radial component by a factor 8–10, so that typically only the disk component (12) is considered.

The effect of the disk tide is analogous to the Kozai effect for the dynamics of asteroids with high inclination relative to Jupiter’s orbit [97]. In the following, I denote the inclination of the comet relative to the galactic plane by  $\tilde{i}$  and the argument of perihelion by  $\tilde{\omega}$  (not to be confused with the inclination  $i$  and the argument of perihelion  $\omega$  relative to the Solar System plane; the two planes are inclined at 120 degrees relative to each other). The disk tide preserves  $a$  and the  $z$ -component of the angular momentum  $H_z = \sqrt{1 - e^2} \cos \tilde{i}$  of the comet, while its  $e$  and  $\tilde{i}$  change with the precession of  $\tilde{\omega}$ . The evolution is periodic;  $e$  has a maximum and  $\tilde{i}$  a minimum when  $\tilde{\omega} = 90^\circ, 270^\circ$ , while  $e$  has a minimum and  $\tilde{i}$  a maximum when  $\tilde{\omega} = 0^\circ, 180^\circ$ <sup>8</sup>. The difference between the maximum and minimum values of  $e$  and  $\tilde{i}$  increases when  $a$  increases or  $H_z$  decreases. There is no variation of  $e$  and  $\tilde{i}$  if  $\tilde{i} = 0$ .

Thus, Oort cloud comets with high inclination relative to the galactic plane, under the effect of the tide, increase their orbital eccentricity; their perihelion distance decreases and the object becomes planet-crosser. If this evolution is fast enough that  $q$  decreases from beyond 10 AU to less than  $\sim 3$  AU within half an orbital period the comet becomes active during its first dive into the inner solar system (i.e. without having interacted with Jupiter or Saturn during its previous orbits), namely it appears as a ‘new comet’. The perturbations from the planets remove the planet-crossing comets from the Oort cloud, by either decreasing their semi-major axis or ejecting them from the Solar System on hyperbolic orbits. Thus, the high inclination portion of the Oort cloud is progressively depleted. The role of passing stars and GMCs is to reshuffle the comet distribution in the Oort cloud, and to refill the high inclination region where comets are pushed into the planetary region by the disk’s tide. Of course, stars and GMCs can also directly deflect the cometary trajectories, injecting the comets into the inner solar system without the help of the galactic tide. This happens particularly during comet showers caused by close encounters between the Sun and these external perturbers [80][75]. These directly injected comets do not need to have a large inclination relative to the galactic plane.

The transfer of comets from the Oort cloud to the inner Solar System has been simulated by many authors, in particular by [75], [170] and, more recently [175]. In what follows I will mostly refer to this latter, most modern work.

In [175] the Oort cloud was modeled as a collection of objects with  $10,000 < a < 50,000$  AU, differential distribution  $N(a)da \propto a^{-1.5}$  and uniform distribution

---

<sup>8</sup>Here I assume that  $\tilde{i}$  is defined in the range between  $-90^\circ$  and  $90^\circ$  (negative  $\tilde{i}$  corresponding to retrograde orbits relative to the galactic plane), and by ‘maximum’ and ‘minimum’ I mean the maximum and minimum of  $|\tilde{i}|$

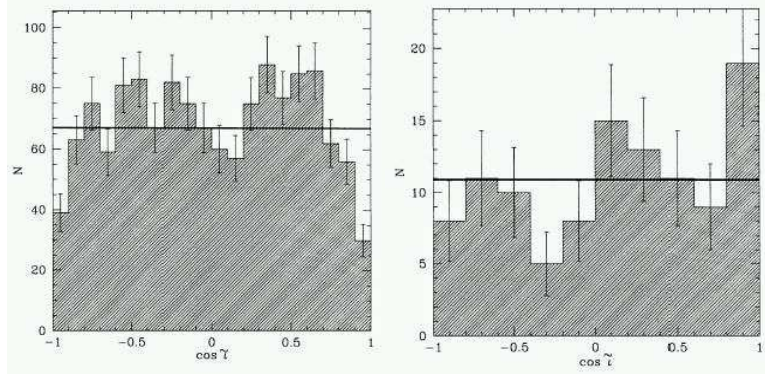


Figure 16: The inclination distribution relative to the galactic plane for new comets. (a) (left): result of a numerical simulation. (b) (right): the observed distribution. Here  $\tilde{i}$  is defined in the range between  $0^\circ$  and  $180^\circ$ ; values of  $\tilde{i}$  larger than  $90^\circ$  correspond to retrograde orbits relative to the galactic plane. From [175].

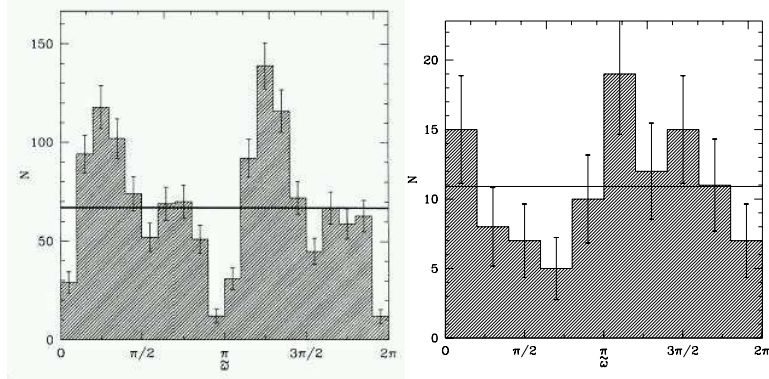


Figure 17: The same as Fig. 16, but for the distribution of the argument of perihelion relative to the galactic plane. From [175].

on each energy hyper-surface, consistent with an earlier model of Oort cloud formation[33]. The evolution of the comets was followed numerically, under the influence of the galactic disk's tide and of the 4 giant planets, the latter assumed to be on coplanar circular orbits. Stellar and GMCs passages, as well as the radial component of the galactic tide, were neglected. Figure 16a shows the  $\cos \tilde{i}$  distribution of the simulated comets at their first passage within 3 AU from the Sun (the limit assumed for comet physical activity and visibility). The distribution peaks at  $\cos \tilde{i} = \pm 0.5$  and is relatively depleted at  $\cos \tilde{i} = \pm 1$  and 0. This is the signature of the galactic tide. Comets with  $\tilde{i} \sim 0^\circ$  (or equivalently,  $\tilde{i} \sim 180^\circ$ ) have an oscillation of the perihelion distance which is too small to



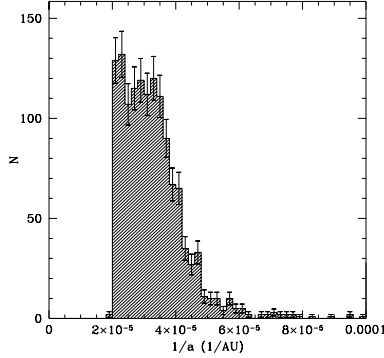


Figure 18: The distribution of  $1/a$  of the comets at their first appearance ( $q < 3$  AU) from the Oort cloud, according to [175]. The sharp fall-off at  $1/a = 2 \times 10^{-5} \text{ AU}^{-1}$  is due to the choice of the initial conditions ( $a < 50,000$  AU).

bring them from the trans-planet region into the visibility region. Comets with initial  $\tilde{t} \sim 90^\circ$  have their inclination decreased to lower values by the time that the perihelion distance is decreased below 3 AU. Similarly, Figure 17a shows the  $\tilde{\omega}$  distribution. The peaks at  $\tilde{\omega} \sim 1/4\pi$  and  $3/4\pi$  are, again, a signature of the galactic tide. In fact, the precession of  $\tilde{\omega}$  is counter-clockwise and the minimal  $q$  is achieved when  $\tilde{\omega} = \pi/2, 3/2\pi$ . Thus the perihelion distance decreases below the imposed threshold  $q = 3$  AU when  $\tilde{\omega}$  is *en route* from 0 to  $\pi/2$  or from  $\pi$  to  $3/2\pi$ . Figures 16b and 17b show the same distributions for the observed new comets. The observed and simulated distributions are quite similar, which confirms the dominant role of the galactic tide. However, the peak and valleys observed in the simulated distributions are not nearly as pronounced. This suggests that the direct injection of comets from the Oort cloud due to passing stars and/or GMCs (neglected in the simulation) has non-negligible importance.

Figure 18 shows the distribution of  $1/a$  for the comets at their first apparition, still according to the simulation in [175]. Notice the sharp fall off at  $a \lesssim 20,000$  AU ( $1/a \gtrsim 5 \times 10^{-5} \text{ AU}^{-1}$ ), that reproduces well the one observed in the  $1/a$  distribution of LPCs (see Fig. 15). Thus, essentially all comets at their first apparition have semi-major axis beyond 20,000 AU and therefore would be classified as ‘new comets’ by an observer. This sharp fall off is due to the so-called *Jupiter barrier*. It is due to the fact that new comets must have decreased their  $q$  from  $> 10$  AU to  $< 3$  AU in less than one orbital period, otherwise, they would have encountered Jupiter and Saturn during an earlier evolution, and most likely they would have been ejected from the Solar System. This condition is fulfilled only if the semi-major axis is larger than  $\sim 20,000$  AU. The implication of this result is that LPCs do not probe the Oort cloud inside this semi-major axis threshold, except during rare showers due to a very close encounter of a passing star with the Solar System (which allows a rapid decrease of  $q$  even for  $a < 20,000$  AU; see [74]). Therefore, our information on

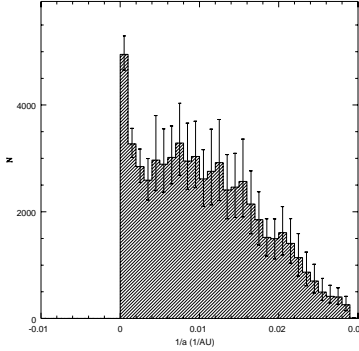


Figure 19: The distribution of the inverse semi-major axis of all LPCs, independent on the number of perihelion passages within 3 AU that they already suffered, according to the simulation in [175]. This distribution is very different from the observed distribution, illustrated on the same scale in Fig. 15

the inner Oort cloud does not come from the observations of comets, but solely from models of Oort cloud formation (see sect. 4).

From the fraction of the Oort cloud population that enters the visibility region per unit time, and the flux of new comets with  $H_{10} < 11$  and  $q < 3$  AU estimated from observations, [175] concluded that the Oort cloud population with  $a > 20,000$  AU and  $H_{10} < 11$  is  $10^{12}$ . This estimate agrees with [171], and is 2 times higher than that in [75], which gives a measure of its uncertainty. For the reason explained just above, the estimated population in the Oort cloud with smaller semi-major axis is totally dependent on its formation model.

The evolution of the comets, from their first apparition to their ultimate dynamical elimination, has also been followed in [175]. If the orbital elements of all comets at every passage at  $q < 3$  AU are added up (without limitation on the number of perihelion passages that they already suffered), the resulting distribution of  $1/a$  (Fig. 19) is very different from the observed distribution (Fig. 15). In particular, the ratio between the number of comets in the Oort spike and the number of returning comets is much smaller than observed. This problem was already pointed out in [134]. As suggested by Oort himself, this mismatch indicates that comets from the Oort cloud have a very limited physical lifetime: after a few perihelion passages they fade away from visibility, either by becoming inactive or by disrupting. In [175] it was shown that a very good match with the observed distribution of LPCs can be achieved if one assumes that the probability  $P_m$  that a comet is still active after  $m$  perihelion passages within 3 AU decays as  $m^{-0.6}$ . This fading law implies that only 10% of the comets survive more than 50 passages and only 1% of them survive more than 2,000 passages. Other equally drastic fading laws, such as  $P_m = 1$  for  $m \leq 6$  and  $p_m = 0.04$  for  $m > 6$  [169], can also reproduce the observed distribution of LPCs.

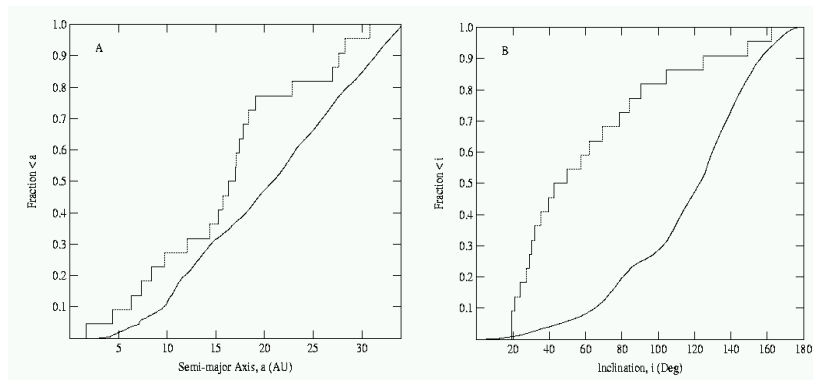


Figure 20: Comparison between the cumulative orbital element distributions of the observed HTCs (dotted line) and those produced in the integrations of [105] (solid line). (a) Semi-major axis distributions ; (b) inclination distributions. Note the significant disagreement in the inclination distributions. Only comets with  $q < 1.3$  AU are considered.

Therefore, the conclusion is that comets from the Oort cloud fade very quickly, in just a few revolutions. This is a very different behavior with respect to that of JFCs, which have a physical lifetime of  $\sim 10,000$  y, namely they remain active for about 1,000 revolutions. The fate of faded comets (disruption versus inactivity) for both LPCs and JFCs is discussed in sect. 3.4.

### 3.3 Note on Halley-type comets

The Halley-type comets have been traditionally considered as the low semi-major axis end of the returning LPC distribution. Indeed, at a first glance, the distribution of HTCs and of returning LPCs (apart from the semi-major axis range that they cover) appear fairly similar.

Under the effects of close encounters with Jupiter and Saturn, some returning comets can have their semi-major axis decreased to less than 34.2 AU. At that point, their orbital period becomes shorter than 200 y, so that, by convention, they are classified as short period comets. They are predominantly HTCs, and not JFCs, because their Tisserand parameter relative to Jupiter is typically smaller than 2. The reason for this is that new comets from the Oort cloud, having  $q < 3$ ,  $a \sim \infty$ ,  $e \sim 1$  must have  $T_J < 2.15$ , and the Tisserand parameter remains roughly conserved during the subsequent evolution down to the SPC region, due to the predominance of Jupiter's scattering action. The transfer of comets from the Oort spike to the HTC region typically requires a large number of revolutions. Thus, the HTCs should belong to the small fraction ( $\sim 4\%$ ) of Oort cloud comets that do not fade away rapidly.

This transfer process from the Oort cloud to the HTC region has been recently revisited in [105], using state of the art numerical simulations. It was

found that, if the semi-major axis distribution of the HTC obtained in the simulations matches fairly well the observed distribution, the inclination distributions are profoundly different (Fig. 20). In particular, the median inclination distribution of the observed HTCs is 45 degrees, and 80% of them have a prograde orbit, whereas the median inclination of the HTCs obtained in the simulation is 120 degrees and only 25% of them have prograde orbit. The reason for which the simulated distribution is skewed towards retrograde objects is that the latter have a longer dynamical lifetime (100,000 y, as opposed to 60,000 y for prograde HTCs).

In [105] the solution that the authors proposed to solve the mismatch between the inclination distributions was that part of the HTCs come from the inner Oort cloud ( $a < 20,000$  AU) and that the latter has a disk-like structure, with inclinations within 50 degrees from the ecliptic. However, modern formation models of the Oort Cloud (see sect. 4 and Fig. 23) show that retrograde orbits in the Oort cloud start to appear beyond 6,000–7,000 AU, and a flattened region can be found only inside this boundary in semi-major axis. However, this region is too tightly bound to the Sun to be an abundant source of comets.

In [109] it was proposed that part of the HTCs come from the distant end of the scattered disk. They would be objects that, pushed outwards by Neptune, eventually feel the galactic tide and have the perihelion decreased deeper into the planetary region ( $q < 25$  AU). However, all these objects would appear first as prograde long period comets, whereas there is no trace of an overabundance of prograde comets in the new LPC population (Rickman, private communication).

In conclusion, the problem of the inclination distribution of HTCs is currently unsolved. It is possible that part of the solution is that HTCs, even if more resistant than new LPCs, cannot be active for more than  $\sim 10,000$  y, as it is the case for JFCs. This would bring the median value of the inclination distribution of the simulated ‘active’ comets down to  $\sim 90^\circ$ , or even less ([43]). Moreover, the median inclination of the currently observed HTCs might be smaller than in reality, due to observational biases and/or small number statistics. In fact, an update of the HTC catalog with respect to that used in [105], shows an increase of the median inclination from 45 to 60 degrees. In addition, the HTCs catalog might be contaminated by a few prograde objects coming from the JFC population (see sect. 3.1). Finally, I notice that in the simulations of [175], 65% of the short period comets were on prograde orbits. Why this result is different from that in [105] (25%) is not clear. The efficiency of transfer of comets from the Oort cloud to the SPC region is very small, so that it is possible that the results of any model based on numerical simulations is dominated by small number statistics. Definitely, the issue of the origin of HTCs needs to be investigated further, and a quantitative model of their distribution remains to be done.

### 3.4 The fate of faded comets

We have seen in sections 3.1 and 3.2 that there is quite strong evidence that comets fade after a limited number of revolutions, and that the rate at which

they do so is different for JFCs and LPCs. What happens to the faded comets? Do they remain on orbit around the Sun as dormant asteroid-like objects, or do they disintegrate into smaller, undetectable pieces?

To answer this question it is necessary to look for asteroid-like objects on orbits typical of these comets, and compute if their number is consistent with the one expected assuming that all faded comets are dormant and accounting for the discovery biases.

Several Near Earth Asteroids (NEA) have been discovered on orbits typical of JFCs, with  $2 < T_J < 3$ . The NEA model developed in [12], calibrated on Spacewatch discoveries, argues that the asteroid belt is not a sufficient source of these objects. This model implies that, among the NEA population,  $60 \pm 40$  objects with  $H < 18$  are dormant JFCs. A similar model ([174]), developed using the more extended dataset provided by the LINEAR survey, estimates  $\sim 70$  dormant JFCs in the NEA population in the same magnitude range (for comparison, the total number of NEAs with  $H < 18$  is estimated to be  $\sim 1,200$  [154]). Assuming 4% albedo –typical of cometary nuclei without activity–,  $H = 18$  corresponds to  $D = 1.7$  km. As we have seen in sect. 3.1, [36] estimate the existence of  $\sim 100$  faded JFCs in the NEO region with diameter of about 2.0 km.

An independent confirmation that many/most NEAs with  $T_J < 3$  are dormant comets come from spectroscopic observations ([50], [11]), which show that the albedo distributions of the NEAs with, respectively,  $T_J > 3$  and  $T_J < 3$  are totally different. The latter have much darker albedos than the former. In conclusion, there is solid evidence that at least a significant fraction of JFCs –if not all– become dormant when they fade.

The situation is totally different for LPCs and HTC, as shown in [107]. The steep fading law required to explain the observed number ratio between new and returning comets (see sect. 3.2) implies that for every active returning comet there should be 20 faded comets. Thus, if all faded comets were dormant, the model in [175] would imply the existence of  $4 \times 10^6$  objects, with  $q < 3$  AU and semi-major axis distribution similar to that of Fig. 19. Again, the absolute magnitude  $H$  of these objects, corresponding to comets with  $H_{10} < 11$  when in activity, is very uncertain. Assuming that they have  $H < 18$  –with cumulative distribution  $N(< H) \propto 10^{0.28H}$  as in [172]– [107] estimated that 1 object out of 20,000 should have been discovered by asteroid surveys, namely  $\sim 200$  objects. However, only 2 ‘asteroidal’ objects have been discovered on LPC orbits. Similarly, if all faded comets were dormant, the model in [105] estimates that there should be 100,000 inactive HTCs with  $H < 18$  and  $q < 2.5$  AU. Of these, [107] estimated that 1,000 should have been discovered by asteroid surveys. This estimate is again 100 times larger than the number of actual discoveries of ‘asteroids’ on corresponding orbits. Thus, the conclusion seems to be that only  $\sim 1\%$  of the comets from the Oort cloud become dormant when they fade. The remaining 99% apparently split in smaller undetectable fragments (like in the case of comet LINEAR C/2001 A2), if not into dust trails.

In summary, JFCs and LPCs seem to fade away due to different physical processes. This may be surprising, given that both are thought to be similar

mixtures of ice and rock. However, evolutionary processes could affect comets' susceptibility to disruption. For example, over long timescales, JFCs could have lost more volatiles than LPCs because they have been stored in the scattered disk, at closer heliocentric distances and thus higher temperatures than in the Oort cloud. JFCs could be more porous, and thus less susceptible to disruption resulting from volatile pressure buildup, due to a relatively violent collisional environment. Finally, the dynamical pathways that LPCs and JFCs take on their way into the inner Solar System might lead to very different thermal histories for the two populations. To jump over the Jupiter barrier, in one orbital period LPCs have to evolve from very distant orbits (with perihelia outside the planetary region) to orbits that closely approach the Sun. On the other hand, objects from the scattered disk slowly move through the planetary region, taking  $\sim 10$  My to evolve onto orbits with  $q < 2.5 AU$  ([103]). Perhaps LPCs disrupt because of strong thermal gradients or volatile pressure buildup, while JFCs survive because they are warmed more slowly.

## 4 The formation of the Oort cloud

For the formation of the Oort cloud it is intuitive to invoke the mechanism described in the previous section for the origin of LPCs, but 'played' in 'reverse mode'. Imagine an early time when the Oort cloud was still empty and the giant planets' neighborhoods were full of icy planetesimals. The scattering action of the planets dispersed the planetesimals throughout the solar system. Some were moved onto eccentric orbits with large semi-major axis, but with perihelion distance still in the planetary region. Those of them which reached a semi-major axis of  $\sim 10,000$  AU started to feel a galactic tide strong enough to modify their orbit on a timescale of an orbital period. During the scattering process, these planetesimals remained relatively close to the ecliptic plane, so that their inclination relative to the galactic plane  $\tilde{i}$  was  $\sim 120^\circ$ . Due to their large  $e$  and  $\tilde{i}$  the effect of the tide on the evolution of  $e, \tilde{i}$  was prominent. The planetesimals with  $\tilde{\omega}$  between  $90^\circ$  and  $180^\circ$  (or, symmetrically, between  $270^\circ$  and  $360^\circ$ ) had their eccentricity decreased. This lifted their perihelion distances beyond the planets' reach, so that they could not be scattered any more: they became Oort cloud objects. The precession of  $\tilde{\Omega}$  and the random passage of rogue stars randomized the planetesimals' distribution, giving to the Oort cloud the structure that is inferred from LPCs observations.

This scenario, originally proposed in [100], was first simulated in [39], [40] using a Monte Carlo method to represent the effects of repeated, uncorrelated encounters of the planetesimals with the giant planets and passing stars (the role of the galactic tide was not yet taken into account). The first simulation of Oort cloud formation using direct numerical simulations and accounting for the galactic tide was done in [33]. To save computing time, however, the simulations were started with comets already on low inclination, high eccentricity orbits: initial  $a = 2,000$  AU and  $q$  uniformly distributed between 5 and 35 AU.

The Oort cloud formation has been recently revisited in [30] (see also [29]),

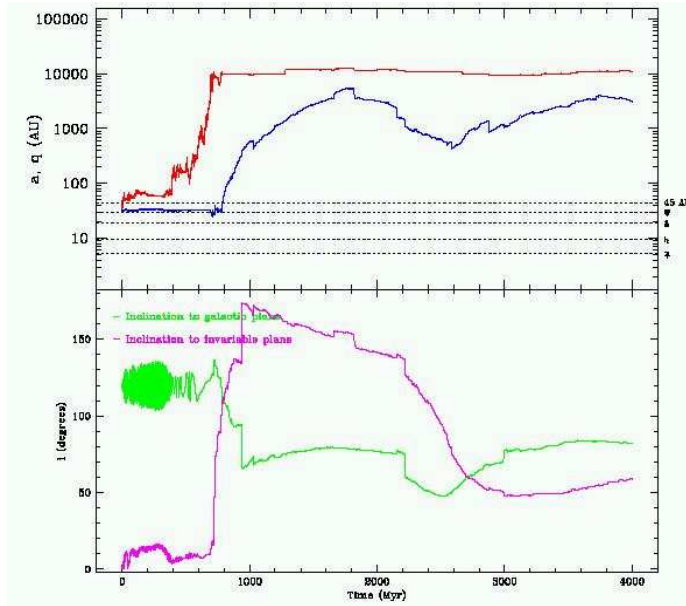


Figure 21: An example of evolution of a comet from the vicinity of Neptune into the Oort cloud, from [30]. The top panel shows the evolution of the object’s semi-major axis (red) and perihelion distance (blue). The bottom panel shows the inclinations relative to the galactic plane (green) and Solar System invariable plane (the plane orthogonal to the total angular momentum of the planetary system; in magenta).

using more modern numerical simulation techniques. They started with more realistic initial conditions, assuming planetesimals initially distributed in the 4–40 AU zone with small eccentricities and inclination. The giant planets were assumed to be on their current orbits, and the migration of planets in response to the dispersion of the planetesimals (see sect. 5), was neglected. The evolution of the planetesimals was followed for 4 Gy, under the gravitational influence of the 4 giant planets, the galactic tide (both radial and disk components - see (11), (12)-), and passing stars. Both the tide and the statistics of passing stars were calibrated using the current galactic environment of the Sun. A stellar density of  $0.041 M_{\odot}/\text{pc}^3$  was assumed, with stellar masses distributed in the range  $0.11\text{--}18.24 M_{\odot}$  and relative velocities between 1.7 and 158 km/s (with a median value of 46 km/s). In total the simulation in [30] recorded  $\sim 50,000$  stellar encounters within 1 pc from the Sun, in 4 Gy. In the following discussion of Oort cloud formation, I mostly refer to the results of this work.

Fig. 21 shows an example of the evolution of a comet from the neighborhood of Neptune to the Oort cloud. With a sequence of encounters, the object is first scattered by Neptune to larger semi-major axis, while keeping the perihelion distance slightly beyond 30 AU, as typical of scattered-disk bodies. After about

700 My, the random walk in semi-major axis brings the body's semi-major axis to  $\sim 10,000$  AU. At this time the galactic tide starts to be effective, and the perihelion distance is rapidly lifted above 45 AU. Neptune's scattering action ceases and the further changes in semi-major axis are due to the effects of distant stellar encounters. When the body starts to feel the galactic tide, its inclination relative to the galactic plane is 120 degrees. As the perihelion distance is lifted (namely the eccentricity decreases), the inclination decreases towards 90 degrees<sup>9</sup>. A stellar passage causes a sudden jump of  $\tilde{i}$  down to  $65^\circ$  just before  $t = 1$  Gy. This allows the tide to enhance its action, bringing the perihelion distance of the object beyond 1,000 AU and the inclination  $\tilde{i}$  up to  $80^\circ$ . This configuration is reached at  $t = 1.7$  Gy, when  $\tilde{\omega}$  is 0 or 180 degrees. From this time onwards the galactic tide reverses its action, decreasing  $q$  and  $\tilde{i}$ . In principle the action of the galactic tide is periodic, so that the object's perihelion should be decreased back to planetary distances. However, the jumps in  $a, q, \tilde{i}$  caused by the stellar encounters break this reversibility. The oscillation of  $q$  becomes more shallow and the object never comes back into the planetary region within the age of the Solar System. Notice finally that during this evolution, the inclination relative to the invariable plane is strongly changed. It is turned to retrograde, and then back to prograde values, as the longitude of galactic node  $\tilde{\Omega}$  precesses.

Not all particles follow this evolution, though. Those which come to interact closely with Jupiter and Saturn are mostly ejected from the Solar System. Those which have distant encounters with Saturn are transported more rapidly and further out in semi-major axis with respect to the evolution shown in Fig. 21. The strength of the galactic tide increases with  $a$ ; thus, for the comets that are scattered to  $a \sim 20,000$  y or beyond, the oscillation period of  $q$  and  $\tilde{i}$  is shorter than for the particle in Fig. 21.

Figures 22 and 23 give a global illustration of the Oort cloud formation process, showing snapshots of the  $(a, q)$  and  $(a, i)$  distributions of all planetesimals at 0 (initial conditions), 1, 10, 100 My and 1, 4 Gy. The planetesimals in these plots are color-coded according to their initial position: Jupiter region objects are magenta; Saturn region objects are blue; Uranus region objects are green; Neptune region objects are red and trans-Neptunian objects are black. Figure 22 shows that, after only 1 My, a scattered disk is formed by Jupiter and Saturn, out of particles initially in the Jupiter-Uranus region. This scattered disk differs from the current scattered disk because most of its objects have  $q < 10$  AU. Particles originally in Neptune's region or beyond have not been scattered out yet. At 10 My a signature of the galactic tide starts to be visible. The Oort cloud begins to form. Particles with  $a > 30,000$ , mostly from Jupiter-Saturn region, have their perihelia lifted beyond the orbits of the planets. Neptune's particles start to populate the scattered disk. From 100 My to 1 Gy, particles continue to enter the Oort cloud from the scattered disk. The population of

<sup>9</sup>Notice that, for the dynamical evolution forced by the galactic disk tide, the decrease of  $\tilde{i}$  from 120 to 90 degrees, is equivalent to an increase from 60 to 90 degrees, in agreement with what has been said in the previous section on the anti-correlation of the evolutions of eccentricity and inclination.



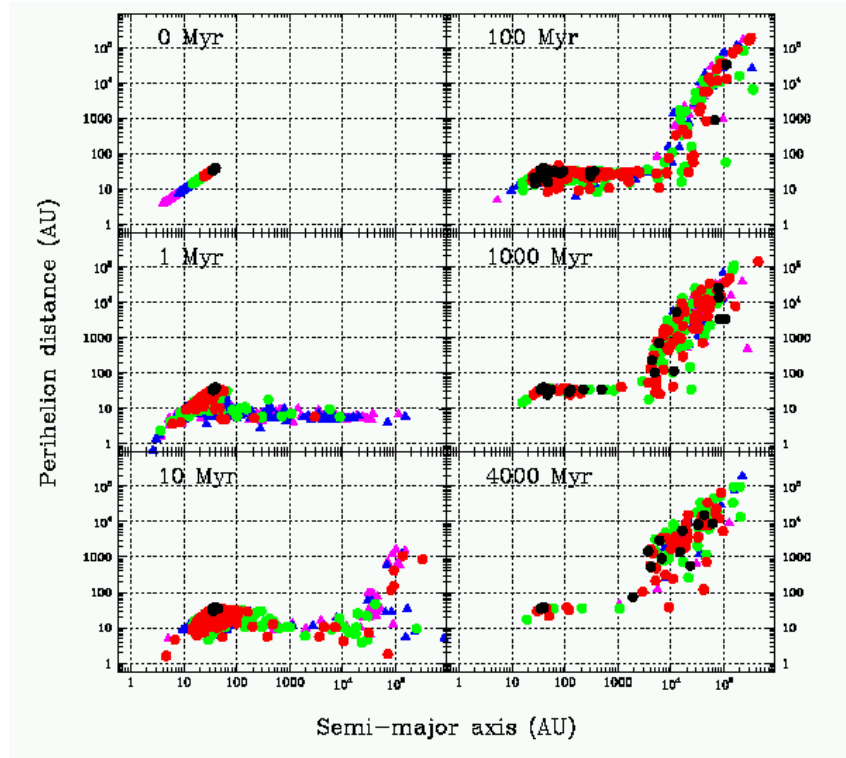


Figure 22: Scatter plot of osculating barycentric pericenter distance vs. osculating barycentric semi-major axis, at various times in the Oort cloud formation simulations of [30]. The points are color-coded to reflect the region in which the simulated comets formed. Each panel is labeled by the simulation time that it corresponds to.

the Oort cloud peaks at 840 My, at which time 7.55% of the initial particles occupy the cloud. Objects from the Uranus-Neptune region gradually replace those from Jupiter-Saturn zone. The latter have been lost during stellar encounters, as they predominantly occupied the very outer part of the Oort cloud ( $a > 30,000$  AU). Due to the longer time over which the galactic tide has acted and to stellar encounters, the population of bodies with perihelion distances above 100 AU can have semi-major axes as low as 3,000 AU. The Oort cloud with  $a < 20,000$  AU is usually called the inner Oort cloud, or Hills cloud from [77]. The last panel in Fig. 22, representing the distribution at 4Gy, should correspond to the current structure of the Oort cloud. The distribution remains nearly the same as that at 1 Gy, but the Oort cloud population has declined slightly in number.

Figure 23 shows the evolution of the particles inclinations. After 1 Myr the planets have scattered the comets into moderately inclined orbits. After 10

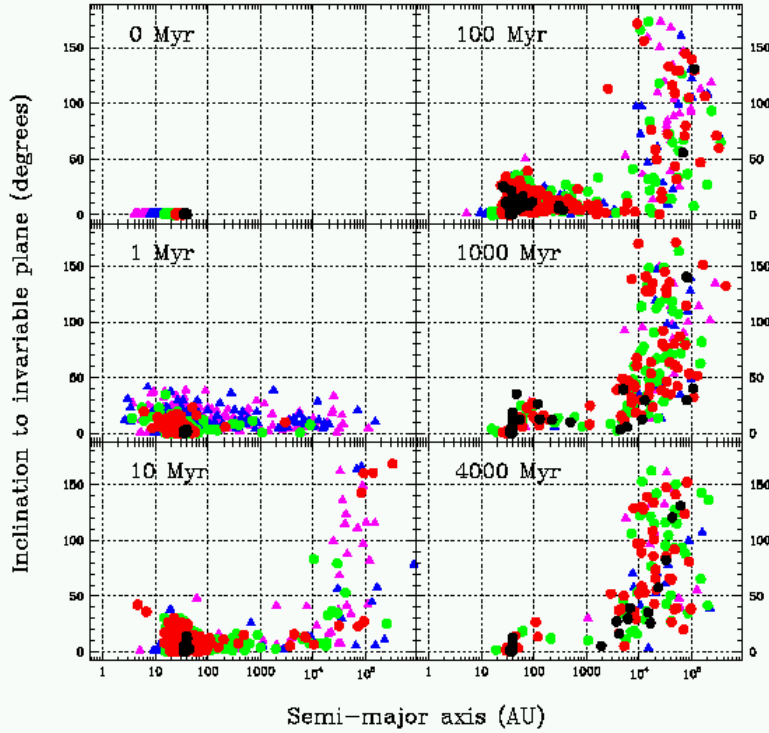


Figure 23: The same as Fig. 22 but for osculating barycentric inclination relative to the Solar System mid-plane vs. osculating barycentric semi-major axis. From [30].

My the particles with  $a > 30,000$  AU have been perturbed by the galactic tide and passing stars into a nearly isotropic distribution of inclinations. As time continues, tides affect the inclinations of particles closer to the Sun, so that at 4,000 My inclinations are clearly isotropic for  $a > 20,000$  AU.

The final Oort cloud contains roughly equal populations in the inner and outer parts, with radial distribution  $N(r)dr \propto 1/r^3$ . About 5% to 9% of the planetesimals initially in the Uranus-Neptune-transneptunian region remain in the Oort cloud at the end of the simulation. Conversely, only 2% of the planetesimals originally in the Jupiter-Saturn region do so. The scattering action of these planets is too strong to deposit a large fraction of planetesimals in the Oort cloud. The reason is the same as invoked to explain the Jupiter's barrier for the new-LPCs distribution (see sect. 3.2). In energy space, the Oort cloud is  $10^{-4}$  wide, whereas the random walk in energy of particles scattered by Jupiter and Saturn has steps of width  $\sim 10^{-3}$ , e.g. proportional to the masses of these planets relative to that of the Sun. Thus, most of the particles scattered by these planets go directly from a scattered-disk or-

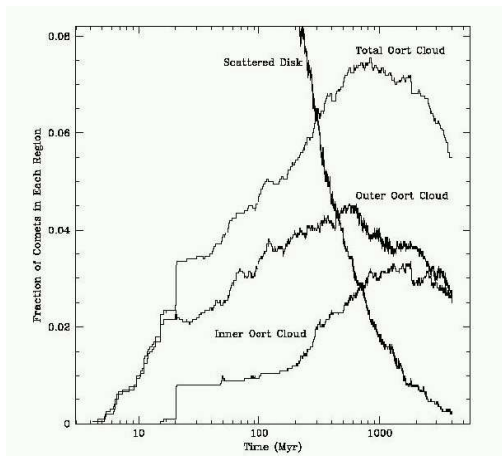


Figure 24: Fraction of the initial planetesimal population that is in the Oort cloud, in its inner and outer parts and in the scattered disk, as a function of time. From [30].

bit ( $\text{Energy} < -10^{-3}$ ) to unbound orbit ( $\text{Energy} > 0$ ), without passing through the Oort cloud ( $-10^{-4} < \text{Energy} < 10^{-3}$ ).

Figure 24 shows the evolution of the mass in the Oort cloud as a function of time. The formation and the erosion of the Oort cloud are not separate processes. Throughout the Solar System history, in parallel with new planetesimals entering the Oort cloud from the scattered disk, other comets left the cloud, because the galactic tide pushed their perihelion back into the planetary region or passing stars put them on hyperbolic orbits. Thus, on the one hand, the flux of LPCs started as soon as the first planetesimals reached  $\sim 10,000$  AU (10 My). On the other hand the supply of new objects to the Oort cloud is still ongoing today [48]. However, as mentioned above, the mass in the cloud peaks at about 800 My. Before this date the formation process dominated over the erosion process. Then –because the mass of the scattered disk dropped– the erosion process became predominant, and the total mass in the cloud decayed to  $\sim 5.5\%$  of the mass originally in the planetesimals’ disk. The outer Oort cloud formed faster than the inner cloud –because of the contribution of planetesimals from Jupiter-Saturn region– but then it eroded faster, because its objects are less gravitationally bound to the Sun.

#### 4.1 Problems with the classical scenario

The classical scenario of Oort cloud formation discussed above meets two problems, when confronted with the quantitative constraints provided by the current Solar System.

As we have seen in sect. 3.2, the outer Oort cloud should currently contain  $10^{12}$  comets with  $H_{10} < 11$ . The estimates of the nuclear size of a  $H_{10} = 11$

comet range from 1 km [7] to 2.3 km [171]. Assuming, as in [107] that a  $H_{10} = 11$  comet has  $D \sim 1.7$  km, and assuming also a cumulative size distribution proportional to  $D^{-2}$  and a density of  $0.6 \text{ g/cm}^3$  (as for P/Halley), one obtains a total mass of  $3 \times 10^{28} \text{ g}$ , namely  $3M_{\oplus}$ . Because the overall efficiency of formation of the outer Oort cloud is small (2.5%), this implies that the original planetesimal disk in the Jupiter-Neptune region was  $\sim 100M_{\oplus}$ . This seems rather high compared to the total mass of solids associated with the minimal mass solar nebula [66]. Also, numerical simulations show that a planetesimal disk more massive than  $30\text{--}50M_{\oplus}$  would have driven Neptune beyond 30 AU and Jupiter and Saturn would have passed across their mutual 2:5 mean-motion resonance (see sects. 5 and 6). The uncertainty in the conversion between  $H_{10}$  magnitude and size, however, allows enough wiggle room to make consistent estimates. For instance, it would be enough that the nuclear size of  $H_{10} = 11$  comets is 1.3 km (instead of the assumed 1.7) to bring the required mass of the planetesimal disk to a more reasonable value of  $50M_{\oplus}$ .

A second, more compelling problem concerns the number ratio between the comet populations in the Oort cloud and in the scattered disk. We have seen in sect. 3.1 that the scattered disk, to be a sufficient source of JFCs, has to contain  $4 \times 10^8$  comets with  $H_{10} < 9$ . The number of comets with  $H_{10} < 11$  depends on the exponent of the  $H_{10}$  distribution of comets, which is highly debated. Using the largest value available in the literature (0.7 [45]) the scattered disk should have  $10^{10}$   $H_{10} < 11$  comets. Using the exponent for the nuclear magnitude distribution in [172][107] (0.28) and assuming a linear scaling between nuclear magnitude and  $H_{10}$ , the number of  $H_{10} < 11$  comets in the scattered disk reduces to  $1.5 \times 10^9$ . Because the number of comets in the outer Oort cloud with  $H_{10} < 11$  is  $10^{12}$ , the comet number ratio *inferred from observations* between the outer Oort cloud and the scattered disk is in the range 100–1,000. However, in the simulations in [30], the final ratio is  $\sim 10$  (see Fig. 24).

The way out of this problem is much more difficult than for the total mass problem. The discrepancy does not depend on assumed relationships between total magnitude and size, nor on density. It cannot be alleviated with any reasonable assumption of the exponent of the  $H_{10}$  distribution. Also, different assumptions of the initial planetesimal distribution in the disk would not help. The point is that most of the Oort cloud is made of planetesimals from the Uranus–Neptune–trans-Neptunian zone, which have to pass through the scattered disk to reach the cloud. Thus, there is a causal relationship between the final numbers of comets in the scattered disk and Oort cloud. To change this relationship, it would be necessary that a much larger number of planetesimals could reach the Oort cloud without passing through the scattered disk. This requires that Jupiter and Saturn were more effective in the real Oort cloud building process than in the simulations of [30]. A possible scenario in which this can occur is discussed below.

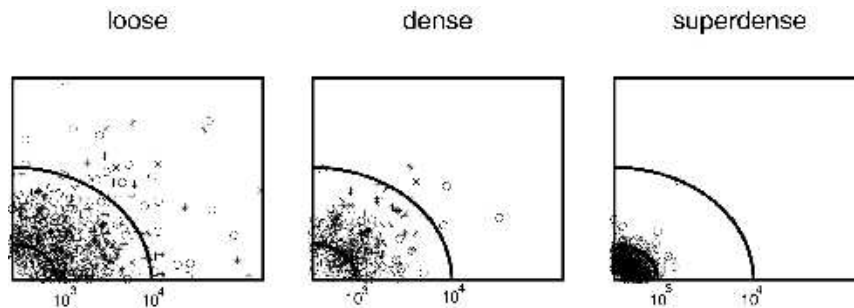


Figure 25: A sketch showing how comets trapped in the Oort cloud would appear distributed in the circumsolar space, for three kinds of star clusters surrounding the Sun. The radii of the circles are expressed in AU. Stars denote comets coming from Jupiter-Saturn zone, while open circles denote bodies from the Uranus-Neptune zone. From [46].

## 4.2 Oort cloud formation in a dense galactic environment

It is now known that most stars form in clusters. In [44] it was pointed out that a denser galactic environment would have exerted a stronger tide on the scattered planetesimals. In addition, stellar encounters would have been more effective, because of the slower relative velocities and smaller approach distances typical of a cluster environment. As a consequence, the threshold semi-major axis value beyond which planetesimals could be decoupled from the planets would have been  $\sim 1,000$  AU, instead of the current value of  $\sim 10,000$  AU. In other words, the Oort cloud would have extended closer to the Sun, covering the region with binding energy down to  $-10^{-3}$  in normalized units. Because this width is of the same order as the energy change suffered by planetesimals crossing the orbits of Jupiter and Saturn, the role of these gas giants in building the Oort cloud would be greatly enhanced.

Simulations of Oort cloud formation in a dense environment have been done in [46]. Three kinds of environments were considered: (i) a loose cluster with 10 stars/pc<sup>3</sup>; (ii) a dense cluster with 25 stars/pc<sup>3</sup> and (iii) a super-dense cluster with 100 stars/pc<sup>3</sup>. In all cases, all stars solar were assumed to have a solar mass (compare with the current stellar density of  $0.041M_{\odot}/\text{pc}^3$  [30]). The average relative velocity among the stars was assumed to be 1 km/s, typical of star clusters [10] (instead of the current  $\sim 40$  km/s). In addition, a placental molecular cloud containing  $10^5$  molecules of Hydrogen per cm<sup>3</sup> was assumed (the current molecular density is  $\sim 3$  g/cm<sup>3</sup>). The initial conditions of the planetesimals were similar to those in [33]. Comets were placed on initial orbits with  $100 < a < 250$  AU and  $q$  ranging from 4 to 30 AU.

Fig. 25 shows the result of these simulations. As expected, the denser the cluster, the more bound to the Sun becomes the resulting Oort cloud. Notice however that the outer part of the cloud (beyond  $10^4$  AU) becomes totally empty, because all comets beyond this limit are stripped off by the passing stars. Thus,

a mechanism would be required to transfer the comets from the massive inner Oort cloud to the outer cloud, in order to explain the current flux of LPCs (which come from the outer cloud only). Less effective stellar encounters, occurring during the dispersal of the cluster and in the current galactic environment, might be responsible for this process.

In terms of efficiency of Oort cloud formation, [46] found that about 30% of the initial planetesimals were trapped in the cloud, namely a factor of 6 higher than in [30]. However, this new efficiency is of the same order of that found in [33], which used initial conditions similar to those in [46], but no star cluster. Thus, it is unclear if the difference in efficiency between [46] and [30] is due to the different choice of initial conditions (in which case the efficiency in [30] is more accurate because the initial conditions are more realistic) or to the presence of the cluster. Moreover, conversely to what expected, the final contribution of Jupiter and Saturn to the formation of the Oort cloud (i.e. the fraction of the planetesimal population with initial  $q < 10$  AU that ended in the cloud) was minimal. This happened because the planetesimals scattered by Jupiter and Saturn typically ended in the outer part of the cloud, and were subsequently stripped away by the numerous stellar encounters.

Thus, at the current state of the art, the formation of the Oort cloud in a stellar cluster has not yet been proven to be the solution for the Oort cloud/scattered disk ratio problem. More precise simulations –starting from a disk of planetesimals on low eccentricity orbits as in [30]– are required. Moreover it would be more realistic to do these simulations accounting for gas-drag, given that the gas-disk was present for most of the time that the Sun spent in the cluster. Gas drag could protect comets from ejection (Levison, private communication), thus increasing the fraction of planetesimals from Jupiter–Saturn zone that are trapped in the cloud. Moreover, it would be necessary to quantify more precisely which mechanism could transfer the comets from the massive inner Oort cloud –produced in the dense environment– to the outer Oort cloud –where comets must reside at the current time to produce LPCs.

**Sedna: an inner Oort cloud object?** One piece of evidence for a moderate stellar cluster surrounding the early Sun is provided by Sedna. The distribution of the extended scattered-disk bodies shows a clear tendency: the perihelion distance is larger for bodies with larger semi-major axis. The bodies in the 50–100 AU range have  $q < 41.5$  AU; 2000 CR<sub>105</sub> ( $a = 222$  AU) has  $q = 44.3$  AU and Sedna ( $a = 495$  AU) has  $q = 76$  AU. Although only a few such bodies are known –and one should be careful about small number statistics– the lack of objects with perihelion distances comparable to those of 2000 CR<sub>105</sub> and Sedna but smaller semi-major axes seems significant. In fact, observational biases (given an object’s perihelion distance and absolute magnitude, and a survey’s limiting magnitude of detection) sharply favor the discovery of objects with smaller semi-major axes. So, it would be unlikely that the first two discovered bodies with  $q > 44$  AU have  $a > 200$  AU if the real semi-major axis distribution in the extended scattered disk were skewed toward smaller  $a$ .

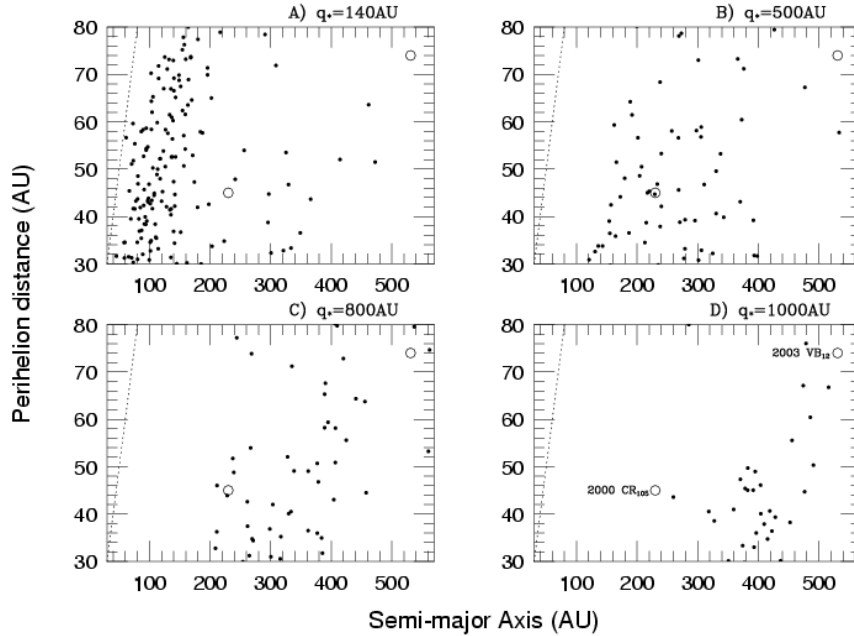


Figure 26: The extended scattered disk that results from passing stars. In all cases the passing star had  $1 M_{\odot}$  and was on a hyperbolic orbit with relative velocity of 1 km/s. Only the perihelion distance of the stellar orbit is varied from panel to panel. The particles were initially in the scattered disk created in the simulation of [30], at  $t = 10^5$  y. The two open circles show the orbits of Sedna and 2000 CR<sub>105</sub>. From [123].

Assuming that the extended scattered-disk bodies belonged to the scattered disk until a perturbation lifted their perihelion distance beyond Neptune’s reach, the fact that  $q$  increases with  $a$  is a clear signature that the perturbation had to grow in magnitude with increasing heliocentric distance. Passing stars produce this very signature [46][123][139]. In particular, it was shown in [123] that an encounter with a Solar mass star at 800 AU with an unperturbed relative velocity of 1 km/s (see Fig. 26) would have produced a distribution of extended scattered-disk objects that overlaps the orbits of Sedna and 2000 CR<sub>105</sub> and does not extend to smaller semi-major axes. Closer stellar encounters would still produce a distribution overlapping the orbits of Sedna and 2000 CR<sub>105</sub>, but such distribution would extend to smaller semi-major axes, inconsistent with the lack of detections of large- $q$  bodies at small  $a$ . More distant encounters would not reproduce the orbits of Sedna and/or 2000 CR<sub>105</sub> (see Fig. 26). The best

‘fit distance’ of the stellar encounter depends on the stellar mass. A star with  $M = 1/4M_{\odot}$  should have passed at  $\sim 400$  AU in order to produce a distribution similar to that in Fig. 26C.

Stellar encounters at such short distances from the Sun were statistically possible only if the Sun was embedded in a cluster, supporting the necessity of building models of Oort cloud formation in the framework of a dense galactic environment. If this view is correct, then the outer part of the extended scattered disk smoothly joins the inner Oort cloud. In particular, Sedna could be considered the first discovered object in the inner Oort cloud!

## 5 The primordial sculpting of the Kuiper belt

In section 2 I have shown that many properties of the Kuiper belt cannot be explained in the framework of the current Solar System:

- i) the existence of the resonant populations,
- ii) the excitation of the eccentricities in the classical belt,
- iii) the co-existence of a cold and a hot population with different physical properties,
- iv) the presence of an outer edge at the location of the 1:2 mean-motion resonance with Neptune,
- v) the mass deficit of the Kuiper belt,
- vi) the existence of the extended scattered-disk population (with the exception of 2000 CR<sub>105</sub> and Sedna, whose orbits can be explained in the framework of the Oort cloud formation in a dense galactic environment, as just discussed above).

These puzzling aspects of the trans-Neptunian population reveal that the latter has been sculpted when the Solar System was different, due to mechanisms that are no longer at work. Like detectives at the scene of a crime, trying to reconstruct what happened from the available clues, astronomers have tried to reconstruct how the Solar System formed and evolved from the traces left in the structure of the Kuiper belt. A large number of mechanisms have been proposed so far to explain some of the properties of the Kuiper belt listed above. For space limitation, here I debate only those which, in my opinion –in light of our current observational knowledge of the Kuiper belt– played a role in in the primordial sculpting of the trans-Neptunian population. I will try to put the various scenarios together, in order to build-up a consistent view of the primordial sculpting of the Kuiper belt. For a more exhaustive review see [125].



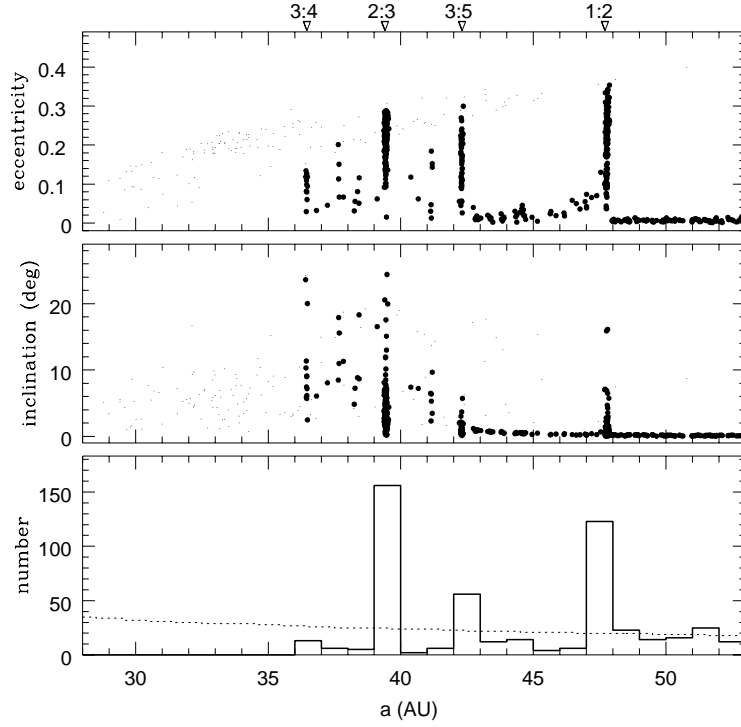


Figure 27: Final distribution of the Kuiper belt bodies according to the sweeping resonances scenario (courtesy of R. Malhotra). The simulation is done by numerically integrating, over a 200 My time-span, the evolution of 800 test particles on initial quasi-circular and coplanar orbits. The planets are forced to migrate (Jupiter: -0.2 AU; Saturn: 0.8 AU; Uranus: 3 AU; Neptune: 7 AU) and reach their current orbits on an exponential timescale of 4 My. Large solid dots represent ‘surviving’ particles (i.e., those that have not suffered any planetary close encounters during the integration time); small dots represent the ‘removed’ particles at the time of their close encounter with a planet (e.g. bodies that entered in the scattered disk and whose evolution was not followed further). In the lowest panel, the solid line is the histogram of semi-major axes of the ‘surviving’ particles; the dotted line is the initial distribution. The locations of the main mean-motion resonances are indicated above the top panel.

## 5.1 Origin of the resonant populations

It was shown in [42] that, while scattering away the primordial planetesimals from their neighboring regions, the giant planets had to migrate in semi-major axis as a consequence of angular momentum conservation. Given the giant planets' configuration in our Solar System, migration should have had a general trend. As discussed above concerning Oort cloud formation, the ice giants have difficulty in ejecting planetesimals on hyperbolic orbits. Apart from the few percent of planetesimals that they can permanently store in the Oort cloud or in the scattered disk, the remaining planetesimals (the large majority) are eventually scattered inwards, towards Saturn and Jupiter. Thus, the ice giants, by reaction, have to move outwards. Jupiter, on the other hand, eventually ejects from the Solar System almost all of the planetesimals that it encounters: thus it has to move inwards. The fate of Saturn is more difficult to predict, *a priori*. However, modern numerical simulations show that this planet also moves outwards, although only by a few tenths of AU for reasonable disk's masses [67][59].

In [112][113] it was realized that, following Neptune's migration, the mean-motion resonances with Neptune also migrated outwards, sweeping the primordial Kuiper belt until they reached their present positions. From adiabatic theory [76], some of the Kuiper belt objects swept by a mean-motion resonance were captured into resonance; they subsequently followed the resonance in its migration, while increasing their eccentricities. This model accounts for the existence of the large number of Kuiper belt objects in the 2:3 mean-motion resonance with Neptune (and also in other resonances) and explains their large eccentricities (see Fig. 27). Neptune had to migrate  $\sim 7$  AU in order to reproduce quantitatively the observed range of eccentricities of the resonant bodies. In [113], it was also showed that the bodies captured in the 2:3 resonance can acquire large inclinations, comparable to those of Pluto and other objects. The mechanisms that excite the inclination during the capture process have been investigated in detail in [56], who concluded that, although large inclinations can be achieved, the resulting proportion of high inclination vs. low inclination bodies, as well as their distribution in the eccentricity vs. inclination plane, do not reproduce well the observations. According to [57] (see sect. 5.2) most high inclination Plutinos were captured from the scattered-disk population during Neptune's migration, rather than from an originally cold Kuiper belt as in [113].

The mechanism of adiabatic capture into resonance requires that Neptune's migration happened very smoothly. If Neptune had encountered a significant number of large bodies (Lunar mass or more), its jerky migration would have jeopardized capture into resonances. For instance, direct simulations of Neptune's migration in [67] –which modeled the disk with Lunar to Martian-mass planetesimals– did not obtain any permanent capture. Adiabatic captures into resonance can be seen in numerical simulations only if the disk is modeled using many more, smaller mass planetesimals [57][59][68]. The constraint set by the capture process on the maximum size of the planetesimals comprising the bulk

of the mass in the disk has been recently estimated in [128].

## 5.2 Origin of the hot population

An appealing mechanism for the origin of the hot population, also in the framework of the planet migration scenario, has been proposed in [57]. Like in [67], [57] simulated Neptune’s migration by the interaction with a massive planetesimal disk, extending from beyond Neptune’s initial position. But, taking advantage of improved computer technology, 10,000 particles were used to simulate the disk population, with individual masses roughly equal to twice Pluto’s mass. For comparison, [67] used only 1,000 particles, with Lunar to Martian masses. Moreover, Neptune was started at  $\sim 15$  AU, instead of 23 AU as in [67].

In the simulations of [57], during its migration Neptune scattered the planetesimals and formed a massive scattered disk. Some of the scattered bodies decoupled from the planet, by decreasing their eccentricities through the interaction with some secular or mean-motion resonance. If Neptune had not been migrating, the decoupled phases would have been transient –as often observed in the integrations of [36]. In fact, the dynamics are reversible, so that the eccentricity would have eventually increased back to Neptune-crossing values. But Neptune’s migration broke the reversibility, and some of the decoupled bodies managed to escape from the resonances and remained permanently trapped in the Kuiper belt. As shown in Fig. 28, the current Kuiper belt would therefore be the result of the superposition in  $(a, e)$ -space of these bodies with the local population, originally formed beyond 30 AU, which stays dynamically cold because they were only moderately excited (by the resonance sweeping mechanism, as in Fig. 27).

The migration mechanism is sufficiently slow (several  $10^7$  y) that the scattered particles have the time to acquire very large inclinations, consistent with the observed hot population. The resulting inclination distribution of the bodies in the classical belt is bimodal, because it results from the superposition of two different populations, each having its own inclination distribution. If the number of objects in the cold population is properly scaled<sup>10</sup>, the resulting distribution can quantitatively reproduce the de-biased inclination distribution computed in [14] from the observations.

Assuming that the bodies’ color varied in the primordial disk with heliocentric distance, the scenario proposed in [57] qualitatively explains why the scattered objects and hot classical belt objects –which mostly come from regions inside  $\sim 30$  AU– appear to have similar color distributions, while the cold classical objects –the only ones that actually formed in the trans-Neptunian region– have a different distribution. Similarly, assuming that the maximum size of the objects was a decreasing function of the heliocentric distance at which they formed, the scenario also explains why the biggest Kuiper belt objects are all in the hot population.

---

<sup>10</sup>The cold population is not depleted in [57], while only a fraction of a percent of the scattered disk remains trapped in the hot population. So the former would outnumber the latter by orders of magnitudes unless some other mechanism trimmed it down; see sect. 5.4.

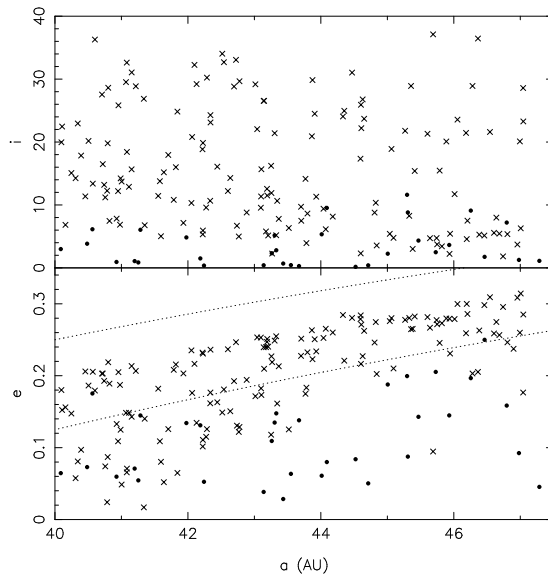


Figure 28: The orbital distribution in the classical belt according to the simulations in [57]. The dots denote the local population, which is only moderately dynamically excited. The crosses denote the bodies that were originally inside 30 AU. Therefore, the resulting Kuiper belt population is the superposition of a dynamically cold population and a dynamically hot population, which gives a bi-modal inclination distribution comparable to that observed. The dotted curves in the eccentricity vs. semi-major axis plot correspond to  $q = 30$  AU and  $q = 35$  AU. Courtesy of R. Gomes.

The mechanism uncovered in [57] would also have important implications for two other trans-Neptunian sub-populations: the Plutinos and the extended scattered disk. In the simulations, some scattered objects also reached stable Plutino orbits, with orbital properties remarkably similar to those of the observed objects. Because, on the contrary, the final  $(e, i)$  distribution of the Plutinos captured by resonance sweeping from the cold population is not consistent with observations [56], this suggests that the Plutinos have been predominantly captured from the scattered disk. The fact that the Plutinos have a color distribution similar to that of the hot population (see [163]), without a predominant red component typical of the cold population, also supports this scenario.

An extended scattered disk is also formed in [57] (see also [58][60]), beyond 50 AU. However, orbits similar to that of Sedna are not achieved in these simulations. Orbits like that of 2000 CR<sub>105</sub> are obtained in [58], but the resulting population with  $q \sim 45$  AU is skewed towards small semi-major axis, which—as discussed before—is probably inconsistent with observations. It is probable that this large perihelion distance population simulated in [58] really exists, but it

is very small in number so that none of these objects has yet been discovered. In this case, 2000 CR<sub>105</sub> (and Sedna of course) would be representative of a more conspicuous population with  $a > 200$  AU, decoupled from the planets by a stellar encounter during the Oort cloud formation time [123]. Conversely, the observed extended scattered-disk bodies with  $q \sim 39\text{--}40$  AU and  $a \sim 50\text{--}100$  AU most likely achieved their current orbits as shown in [57][58].

### 5.3 Origin of the outer edge of the Kuiper belt

The existence of an outer edge of the Kuiper belt is a very intriguing property. Several mechanisms for its origin have been proposed, none of which has raised the general consensus of the community of the experts. These mechanisms can be grouped in three classes.

**Destroying the distant planetesimal disk.** It has been shown with numerical simulations in [16] that a Martian mass body residing for 1 Gy on an orbit with  $a \sim 60$  AU and  $e \sim 0.15\text{--}0.2$  could have scattered into Neptune-crossing orbits most of the Kuiper belt bodies originally in the 50–70 AU range, leaving this region strongly depleted and dynamically excited. As shown in Fig. 6 the apparent edge at 50 AU might simply be the inner edge of a similar gap in the distribution of Kuiper belt bodies. A problem with this scenario is that there are no evident dynamical mechanisms that would ensure the later removal of the massive body from the system. In other words, the massive body should still be present, somewhere in the  $\sim 50 - 70$  AU region. A Mars-size body with 4% albedo at 70 AU would have apparent magnitude brighter than 20. In addition its inclination should be small, both in the scenario where the it was originally a scattered-disk object whose eccentricity (and inclination) were damped by dynamical friction ([16]) and in that where the body reached its required heliocentric distance by migrating through the primordially massive Kuiper belt ([59]). Thus, in view of its brightness and small inclination, it is unlikely that the putative Mars-size body could escape detection in the numerous wide field ecliptic surveys that have been performed up to now, and in particular in that led by Trujillo and Brown ([163]).

A second possibility is that the planetesimal disk was truncated by the passage of a star in the vicinity of the Sun. The eccentricities and inclinations of the planetesimals resulting from a stellar encounter depend critically on  $a/D$ , where  $a$  is their semi-major axis and  $D$  is the heliocentric distance of the stellar encounter [81][95]. A stellar encounter at  $\sim 200$  AU would make most of the bodies beyond 50 AU so eccentric that they intersect the orbit of Neptune, which eventually would produce the observed edge [117]. An interesting constraint on the time at which such an encounter occurred is set by the existence of the Oort cloud. It was shown in [110] that the encounter had to occur much earlier than  $\sim 10$  My after the formation of Uranus and Neptune, otherwise most of the existing Oort cloud would have been ejected to interstellar space. Moreover, many of the planetesimals at that time in the scattered disk would have had their perihelion distance lifted beyond Neptune, decoupling them from the planet. As

a consequence, the extended scattered-disk population, with  $a > 50$  AU and  $40 < q < 50$  AU, would have had a mass comparable or larger than that of the resulting Oort cloud, hardly compatible with the few detections of extended scattered-disk objects achieved up to now. As discussed in sect. 4.2, a close encounter with a star during the first million years of planetary formation is a possible event if the Sun formed in a stellar cluster. However, at such an early time, presumably the Kuiper belt objects were not yet fully formed [146][88] (unless they accreted very rapidly by gravitational instability). In this case the edge of the belt would be at a heliocentric distance corresponding to a post-encounter eccentricity excitation of  $\sim 0.05$ , a threshold value below which collisional damping is efficient and accretion can recover, and beyond which the objects rapidly grind down to dust [91].

An edge-forming stellar encounter could not be the responsible for the origin of the peculiar orbit of Sedna, unlike what has been proposed in [92]. In fact, such a close encounter would also produce a relative overabundance of bodies with perihelion distance similar to that of Sedna but with semi-major axis in the 50–200 AU range [123]. These bodies have never been discovered, despite of their more favorable observational biases.

#### **Forming a bounded planetesimal disk from an extended gas-dust disk.**

In [168], it was suggested that the outer edge of the Kuiper belt is the result of two facts: *i*) accretion takes longer with increasing heliocentric distance and *ii*) small planetesimals drift inwards due to gas drag. This leads to a steepening of the radial surface density gradient of solids. The edge effect is augmented because, at whatever distance large bodies can form, they capture the  $\sim$ m-sized bodies spiraling inwards from farther out. The net result of the process, as shown by numerical modeling in [168], is the production of an effective edge, where both the surface density of solid matter and the mean size of planetesimals decrease sharply with distance.

A variant of this scenario has been proposed in [179]. In their model, planetesimals could form by gravitational instability in the regions where the local ratio solid/gas was 2-10 times that corresponding to cosmic abundances. According to the authors, this large ratio could be achieved because of a radial variations of orbital drift speeds of millimeter-sized particles induced by gas drag. However, this mechanism would have worked only within some threshold distance from the Sun, so that the resulting planetesimal disk would have had a natural edge.

A third possibility is that planetesimals formed only within a limited heliocentric distance, because of the effect of turbulence. If turbulence in protoplanetary disks is driven by magneto-rotational instability (MRI), one can expect that it was particularly strong in the vicinity of the Sun and at large distances (where solar and stellar radiation could more easily ionize the gas), while it was weaker in the central, optically thick region of the nebula, known as the ‘dead zone’ [151]. The accretion of planetesimals should have been inhibited by strong turbulence, because the latter enhanced the relative velocities of the

grains. Consequently, the planetesimals could have formed only in the dead zone, with well defined outer (and inner) edge(s).

**Truncating the original gas disk.** The detailed observational investigation of star formation regions has revealed the existence of many *proplyds*, i.e. anomalously small proto-planetary disks. It is believed that these disks were originally much larger, but in their distant regions the gas was photo-evaporated by the very energetic radiation emitted by the massive stars of the cluster [1]. Thus, it has been proposed that the outer edge of the Kuiper belt reflects the size of the original solar system proplyd [78].

**Remark on the location of the Kuiper belt edge.** In all the scenarios discussed above, the location of the edge can be adjusted by tuning the relevant parameters of the corresponding model. In all cases, however, Neptune plays no direct role in the edge formation. In this context, it is particularly important to remark from Fig. 3 that the edge of the Kuiper belt appears to coincide precisely with the location of the 1:2 mean-motion resonance with Neptune. This strongly suggests that, whatever mechanism formed the edge, the planet was able to adjust the final location of the edge through gravitational interactions. I will return to this in sect. 5.5.

## 5.4 The mass deficit of the cold population

The scenario proposed in [57] (see sect. 5.2) confines the problem of the mass depletion of the Kuiper belt to just the cold population. In fact, in [57] only  $\sim 0.2\%$  of the bodies initially in the disk swept by Neptune remained in the Kuiper belt on stable high- $i$  orbits at the end of Neptune’s migration. This naturally explains the current low mass of the hot population. However, the population originally in the 40-50 AU range –which would constitute the cold population in the scenario of [57]– should have been only moderately excited and not dynamically depleted, so that it should have preserved most of its primordial mass.

Two general mechanisms have been proposed for the mass depletion: the dynamical ejection of most of the bodies from the Kuiper belt to the Neptune-crossing region and the collisional comminution of most of the mass of the Kuiper belt into dust.

The dynamical depletion mechanism was proposed in [121] and later revisited in [135]. In this scenario, a planetary embryo, with mass comparable to that of Mars or of the Earth, was scattered by Neptune onto a high-eccentricity orbit that crossed the Kuiper belt for  $\sim 10^8$  y. The repeated passage of the embryo through the Kuiper belt excited the eccentricities of the Kuiper belt bodies, the vast majority of which became Neptune crossers and were subsequently dynamically eliminated by the planets’ scattering action. The integrations in [135], however, treated the Kuiper belt bodies as test particles, and therefore their encounters with Neptune did not alter the position of the planet. Thus, similar

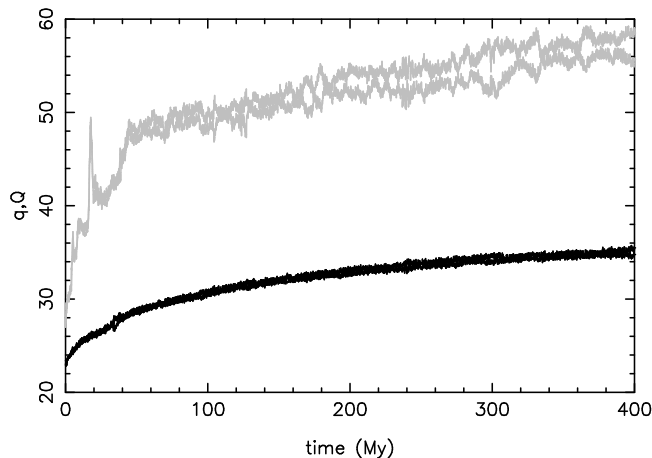


Figure 29: A self-consistent simulation of the scenario proposed in [135] for the excitation and dynamical depletion of the Kuiper belt (from [59]). Neptune is originally placed at  $\sim 23$  AU and an Earth-mass embryo at  $\sim 27$  AU. Both planets are embedded in a  $30 M_{\oplus}$  disk, extending from 10 to 50 AU with a  $r^{-1}$  surface density profile ( $7.5 M_{\oplus}$  between 40 and 50 AU). The black curve shows the evolution of Neptune’s semi-major axis (its eccentricity remains negligible), while the grey curves refer to perihelion and aphelion distances of the embryo. Notice that the embryo is never scattered by Neptune, unlike in [135]. It migrates through the disk faster than Neptune, up to the disk’s outer edge. Neptune interacts with the entire mass of the disk, thanks to the dynamical excitation of the disk due to the presence of the embryo. Therefore, it migrates much further that it would if the embryo were not present, and reaches a final position well beyond 30 AU (40 AU after 1 Gy).

simulations have been re-run in [59], in the framework of a more self-consistent model accounting for planetary migration in response to planetesimal scattering. As expected, the dynamical depletion of the Kuiper belt greatly enhanced Neptune’s migration. The reason for this is that, thanks to the dynamical excitation of the distant disk provided by the embryo, Neptune interacted not only with the portion of the disk in its local neighborhood, but with the entire mass of the disk at the same time. As shown in Fig. 29 even a low mass disk of  $30 M_{\oplus}$  between 10 and 50 AU ( $7.5 M_{\oplus}$  only in the Kuiper belt) could drive Neptune well beyond 30 AU. Halting Neptune’s migration at  $\sim 30$  AU requires a disk mass of  $\sim 15 M_{\oplus}$  or less (depending on Neptune’s initial location). Such a mass and density profile would imply only  $3.75 M_{\oplus}$  of material originally in the Kuiper belt between 40 and 50 AU, which is less than the mass required ( $10\text{--}30 M_{\oplus}$ ) by models of the accretion of Kuiper belt bodies [147][90].

A priori, for what concerns Neptune’s migration, there is no evident difference between the case where the Kuiper belt is excited to Neptune-crossing orbits by a planetary embryo or by some other mechanism, such as the primor-



dial secular resonance sweeping proposed in [129]. Therefore, we conclude that Neptune never ‘saw’ the missing mass of the Kuiper belt. The remaining possibility for a dynamical depletion of the Kuiper belt is that the Kuiper belt objects were kicked directly to hyperbolic or Jupiter-crossing orbits and consequently were eliminated without interacting with Neptune. Only the passage of a star through the Kuiper belt seems to be capable of such an extreme excitation [95].

The collisional grinding scenario was proposed in [148] [27] [26] and then pursued in [89] [91] [93]. In essence, a massive Kuiper belt with large eccentricities and inclinations would undergo a very intense collisional activity. Consequently, most of the mass originally in bodies smaller than 50–100 km in size could be comminuted into dust, and then evacuated by radiation pressure and Poynting-Robertson drag, causing a substantial mass depletion.

To work, the collisional erosion scenario requires that two essential conditions are fulfilled. First, it requires a peculiar primordial size distribution, such that all of the missing mass was contained in small, easy to break, objects, while the number of large object was essentially identical to that in the current population. Some models support the existence of such a size distribution at the end of the accretion phase [88] [90]. However, the collisional formation of the Pluto–Charon binary [17], the capture of Triton onto a satellite orbit around Neptune [144] and the discovery of 2003 UB<sub>313</sub> in the extended scattered disk [15], suggest that the number of big bodies was much larger in the past, consisting of about 1,000 Pluto-sized objects [144]. In principle, it is possible that all of these large bodies were in the planetesimal disk inside 30 AU, swept by Neptune’s migration, while the primordial Kuiper belt contained only the number of large bodies inferred from the current discovery statistics, but this would require that the size distribution in the planetesimal disk had a very sensitive dependence on heliocentric distance.

The second essential condition for substantial collisional grinding is that the massive primordial Kuiper belt had a large eccentricity and inclination excitation, comparable to the current one ( $e \sim 0.25$  and/or  $i \sim 7^\circ$ ). However, as reported at the beginning of this section, in light of [57], the mass depletion problem concerns only the cold Kuiper belt, and the dynamical excitation of the cold population is significantly smaller than that required by the collisional grinding models.

I remark, moreover, that even assuming that the two conditions above are fulfilled, the collisional grinding models still have problems in reducing the total mass of the belt down to the current values of a few percent of an Earth mass. As the mass decreases, the collisional grinding process progressively slows down, and eventually stops when the total mass is still about an Earth mass. The most advanced of the collisional models [93] can reduce the total mass to few  $0.01M_\oplus$  only if a very low specific disruption energy  $Q_*$  is assumed; if more reasonable values of  $Q_*$  (similar to those obtained in hydro-code experiments [8]) are adopted, the final mass achieved by collisional grinding is at least one tenth of the initial mass, namely about  $1 M_\oplus$  or more.

It is very difficult to reach a firm conclusion on the possibility of collisional grinding of the Kuiper belt from the collisional models alone, because of the

sensitivity of the latter on the assumed parameters. Perhaps the best strategy is to assume that the collisional grinding was effective, explore its general consequences and compare them with the available constraints. This work is mostly in progress, but I briefly outline below its preliminary results.

First, most of the binaries in the cold population would not have survived the collisional grinding phase [137]. In fact, the observed Kuiper belt binaries have large separations, so that it can be easily computed that the impact on the satellite of a 100 times less massive projectile with a speed of 1km/s would give the satellite an impulse velocity sufficient to escape to an unbound orbit. If the collisional activity was strong enough to cause an effective reduction of the overall mass of the Kuiper belt, these kind of collisions had to be extremely common, so that we would not expect a significant fraction of widely separated binary objects in the current remaining population.

Second, if the conditions favorable for collisional grinding in the Kuiper belt are assumed for the entire planetesimal disk (5-50 AU), the Oort cloud would not have formed: the planetesimals would have been destroyed before being ejected as in [149] (Charnoz private communication).

Third, as the Kuiper belt mass decreased during the grinding process, the precession frequencies of Neptune and the planetesimals had to change. Consequently, secular resonances had to move, potentially sweeping the belt. Assuming that, when Neptune reached 30 AU, the disk was already depleted inside 35 AU but was still massive in the 35–50 AU region, [59] showed that the  $\nu_8$  secular resonance would have started sweeping through the disk as soon as the mass decreased below  $10 M_{\oplus}$ . The  $\nu_8$  resonance sweeping would have excited the eccentricity of the bodies to Neptune-crossing values and –given the large mass that the Kuiper belt would have still had when this phenomenon started– Neptune would have continued its radial migration well beyond its current location.

## 5.5 Pushing out the Kuiper belt

Given the difficulties of the collisional grinding scenario for the cold Kuiper belt, a dynamical way to solve the mass depletion problem has been proposed in [108]. In this scenario, the primordial edge of the massive proto-planetary disk was somewhere around 30–35 AU and the *entire* Kuiper belt population –not only the hot component as in [57]– formed within this limit and was transported to its current location during Neptune’s migration. The transport process for the cold population had to be different from the one found in [57] for the hot population (but work in parallel with it), because the inclinations of the hot population were excited, while those of the cold population were not.

In the framework of the classical migration scenario [113] [59], the mechanism proposed in [108] was the following: the cold population bodies were initially trapped in the 1:2 resonance with Neptune; then, as they were transported outwards by the resonance, they were progressively released due to the non-smoothness of the planet migration. In the standard adiabatic migration scenario [113] there would be a resulting correlation between the eccentricity

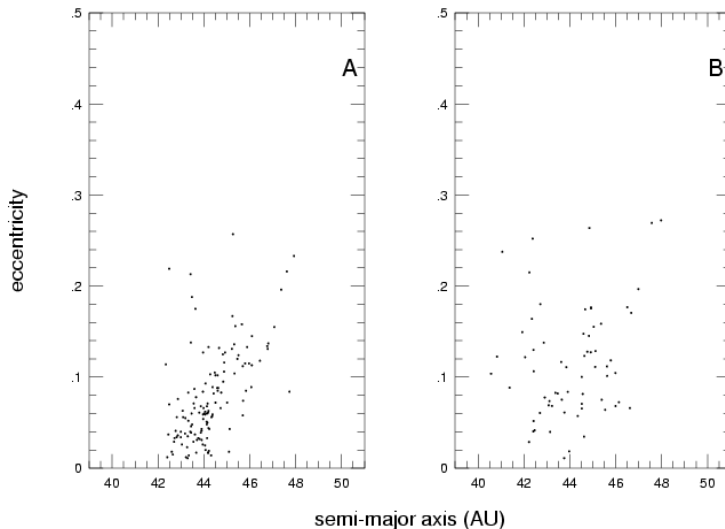


Figure 30: Left: the observed semi-major axis vs. eccentricity distribution of the cold population. Only bodies with multi-opposition orbits and  $i < 4^\circ$  are taken into account. Right: the resulting orbital distribution in the scenario proposed in [108].

and the semi-major axis of the released bodies. However this correlation was broken by a secular resonance embedded in the 1:2 mean-motion resonance. This secular resonance was generated because the precession rate of Neptune's orbit was modified by the torque exerted by the massive proto-planetary disk that drove the migration.

Simulations of this process can match the observed  $(a, e)$  distribution of the cold population fairly well (see Fig. 30), while the initially small inclinations are only very moderately perturbed. In this scenario, the small mass of the current cold population is simply due to the fact that only a small fraction of the massive disk population was initially trapped in the 1:2 resonance and released on stable non-resonant orbits. The preservation of the binary objects would not be a problem because these objects were moved out of the massive disk in which they formed by a gentle dynamical process. The final position of Neptune would simply reflect the primitive truncation of the proto-planetary disk, as in [59]. Most important, this model explains why the current edge of the Kuiper belt is at the 1:2 mean-motion resonance with Neptune, despite that none of the mechanisms proposed for the truncation of the planetesimal disk involves Neptune in a direct way (see sect. 5.3). The location of the edge was modified by the migration of Neptune via its resonance.

On the flip side, the model in [108] re-opens the problem of the origin of different physical properties of the cold and hot populations, because both would have originated within 35 AU, although in somewhat different parts of the disk.

I stress, however, that the strength of [108] is in the idea that pushing out the cold Kuiper belt could solve both the problems related to mass deficit and edge location. The specific mechanism for pushing out the cold belt depends on the specific model of giant planet evolution that is adopted. The classical planet migration scenario used in [108] might not reflect the real evolution of the system (see sect. 6). In this case, alternative push-out mechanisms should be investigated. Whatever the preferred mechanism, it will have to give a predominant role to the 1:2 mean-motion resonance with Neptune in order to explain the current location of the Kuiper belt edge.

## 6 Origin of the Late Heavy Bombardment of the Terrestrial planets

The models proposed in the previous sections for the formation of the Oort cloud and the sculpting of the Kuiper belt seem to offer a quite complete view of the formation and evolution of the Solar System. But they are not entirely satisfactory, because they ignore an important fact in the history of the Solar System: the late heavy bombardment (LHB) of the terrestrial planets.

Below, I review the observational constraints on the LHB, then I describe the models proposed in the past to explain a spike in the bombardment rate and, finally, I will focus on an emerging view of what happened  $\sim 650$  My after the formation of the planets. In section 7 I will discuss how our understanding of Oort cloud and Kuiper belt formation needs to be modified in light of the LHB evidence, pointing also to open problems and prospects for future research.

**Evidence for a late cataclysmic bombardment.** The crust of the Moon crystallized around 4.44 Gy ago, and the morphology of its highlands records a dense concentration of impact craters, excavated prior to the emplacement –around 3.8 Gy ago– of the first volcanic flows in the mare plains [176]. Thus, a period of intense bombardment –the LHB– occurred in the first 600-700 My of the Moon’s history. However, the magnitude and the chronology of the collisions between 4.5 and 4 Gy remains a topic of controversy.

Two explanations have been proposed. According to [71] [176], the frequency of impacts declined slowly and progressively since the end of the accretion period, up to 3.9 Gy ago. In this view, the LBH is not an exceptional event. Rather it is a 600 My tail of the collisional process that built the terrestrial planets.

Another view advocates a rapid decline in the frequency of impacts after the formation of the Moon, down to a value comparable to the current one. This was followed by a cataclysmic period between  $\sim 4.0$  and  $\sim 3.8$  Gy ago, marked by an extraordinarily high rate of collisions [157] [140] [24] [141] [142].

Today, the majority of authors favors the cataclysmic scenario of the LHB. The latter is supported by a series of arguments:

*i)* 600 million years of continual impacts should have left an obvious trace on the Moon. So far, no such trace has not been found. The isotopic dating of both the samples returned by the various Apollo and Luna missions revealed no impact melt-rock older than 3.92 Gy [140] [141]. The lunar meteorites confirm this age limit. The meteorites provide a particularly strong argument because they likely originated from random locations on the Moon [24], unlike the lunar samples collected directly on the Moon. A complete resetting of all ages all over the Moon is possible [64] but highly unlikely, considering the difficulties of completely resetting isotopic ages at the scale of a full planet [28]. The U-PB and Rb-Sr isochrones of lunar highland samples indicate a single metamorphic event at 3.9 Gy ago and between 3.85 and 4 Gy ago respectively [157]. There is no evidence for a resetting of these isotopic systems by intense collisions between 4.4 and 3.9 Gy.

*ii)* The old upper crustal lithologies of the Moon do not show the expected enrichment in siderophile elements (in particular the Platinum Group Elements) implied by an extended period of intense collisions [141].

*iii)* If the elevated mass accretion documented in the period around 3.9 Gy is considered to be the tail end of an extended period of collisions, the whole Moon should have accreted at about 4.1 Gy ago instead of 4.5 Gy [142] [96].

*iv)* The 15 largest impact structures on the Moon, the so-called basins, with diameters between 300 and 1200 Km, have been dated to have formed between 4.0 and 3.9 Gy ago. If the bombardment had declined monotonically since 4.5 Gy ago, it would be strange that the largest impacts all occurred at the end of the bombardment period.

*v)* On Earth, the oxygen isotopic signature of the oldest known zircons (age: 4.4 Gy) indicates formation temperatures compatible with the existence of liquid water [165]. This argument seems contradictory with an extended period of intense collisions, which would have brought the Earth's temperature to exceed the water evaporation threshold.

Therefore, it can be concluded that there is strong evidence for a cataclysmic Late Heavy Bombardment event around 3.9 Gy ago. This cataclysm did not concern just the Moon, but has now been clearly established throughout the inner solar system [98]. The exact duration of the cataclysm is difficult to estimate, though. Based on the cratering record of the Moon, it varies between 20 and 200 My, depending on the mass flux estimate used in the calculation.

**Early models of LHB origin.** The occurrence of a cataclysmic LHB challenges our naive view of a Solar System gradually evolving from chaos to order. Several ideas have been proposed to explain what could have abruptly changed the evolution of the system, causing a spike in the bombardment rate.

The possibility of a stochastic break-up of an asteroid close to a resonance in the main belt has been investigated in [180]. The flux of projectiles inferred from the crater density would require the break-up of an object larger than

Ceres. This event is very implausible and would have left a huge asteroid family in the main belt, of which we see no trace.

If a stochastic break-up is ruled out, then the remaining possibility is that a reservoir of small bodies, which remained stable up to the time of the LHB, suddenly became unstable, with most of its objects achieving planet crossing orbits.

A comet shower from the Oort cloud, possibly triggered by a stellar encounter, is a first possibility. However, a new LPC has a probability to collide with the Earth of about  $10^{-9}$ . Because the mass hitting the Earth during the LHB is estimated to be  $\sim 10^{-5} M_{\oplus}$  ([72]), this would require an Oort cloud initially containing  $10^4$  Earth masses, which –as discussed in sect. 4– is impossible.

In [18] it was proposed that a fifth terrestrial planet, with a mass comparable to that of Mars, became unstable after  $\sim 600$  My of evolution, and crossed the asteroid belt before being dynamically removed. Invaded by this new perturber, the asteroid belt became unstable and most of its objects acquired planet crossing eccentricities. The simulations presented in [18] show that a late instability of a 5 terrestrial planet system is indeed possible, but it requires that the rogue planet was initially at about 1.9 AU, with an inclination of  $\sim 15^\circ$ . Whether this initial configuration was consistent with terrestrial planets formation models was not discussed. Similarly, the resulting orbital distribution in the asteroid belt, after the removal of the rogue planet, was not investigated. Moreover, in most simulations the rogue planet was removed by a collision with Mars, whereas the red planet does not show any sign of such a gigantic strike.

In [111] it was proposed that the LHB was associated with a ‘late appearance’ of Uranus and Neptune in the planetesimal disk. That paper showed that the planetesimals scattered away from the neighborhoods of the ice giants would have been sufficient to cause a bombardment on the Moon with a magnitude comparable to that of the LHB. Moreover, the dynamical removal of these planetesimals would have caused a radial migration of Jupiter and Saturn, which in turn would have forced the  $\nu_6$  secular resonance to sweep across the main asteroid belt [55]. Their eccentricities being excited by the resonance passage, most asteroids would have acquired planet crossing orbits. Consequently, they would have contributed to –or even dominated– the terrestrial planets cratering process. The problem in this work was that the ‘late appearance’ of Uranus and Neptune was postulated, rather than explained. The authors argued that these planets might have formed very slowly, although this seems implausible given that they accreted hydrogen atmospheres of 1–2 Earth masses from the proto-solar nebula [63], which should have dissipated within  $\sim 10$  My ([69]). Later, in [106] it was proposed that Uranus and Neptune formed in between Jupiter and Saturn. The system remained stable for 600 My, until an instability was produced. Consequently, Uranus and Neptune were scattered outwards by Jupiter and Saturn; the interaction with the disk eventually damped the planets’ eccentricities and parked them on stable orbits. In this process, the planetesimal disk was destroyed as in [111]. The simulations in [106] showed that a late instability of a Jupiter-Uranus-Neptune-Saturn system is indeed possible. However, the instability time depends critically on the initial conditions,

and it is unclear if those adopted in the successful simulations could be consistent with giant planet formation models. More importantly, the scattering of Uranus and Neptune by Jupiter and Saturn would have destabilized the regular satellites systems of all the planets. Finally, the massive planetesimal disk required to stabilize the orbits of Uranus and Neptune would have forced the latter to migrate well beyond its current position. Thus, as admitted by the authors themselves, this scenario had to be considered as a ‘fairy tale’.

**The great comet-asteroid alliance: an emerging view on the LHB origin.** Starting from two key considerations:

- i)* planet migration through the planetesimal disk induces a bombardment of the terrestrial planets of sufficient magnitude to explain the LHB (from [111]),
- ii)* at the end of the migration phase, the Solar System is essentially identical to the current one (namely there are no more reservoirs of planetesimals to destabilize),

it was realized in [124] that solving the problem of the LHB origin required to find a plausible mechanism to trigger planet migration at a late time.

Pursuing this goal, in [61] the authors remarked that, in all previous simulations, planet migration started immediately because planetesimals were placed close enough to the planets to be violently unstable. While this type of initial condition was reasonable for the goals of those works, it is unlikely. Planetesimal driven migration is probably not important for planet dynamics as long as the gaseous massive nebula exists (the nebula accounts for about 100 times more mass than the planetesimals). The initial conditions in simulations of the planetesimal driven migration should therefore represent the system that existed at the time the nebula dissipated. Thus, the planetesimal disk should contain only those particles that had dynamical lifetimes longer than the lifetime of the solar nebula (a few million years), because the planetesimals initially on orbits with shorter dynamical lifetimes should have been eliminated earlier, during the nebula era. If this constraint on the initial conditions is fulfilled, then the resulting migration is necessarily slow, because it depends on the rate at which disk particles evolve onto planet-crossing orbits, which is long by definition. If the planetary system, in absence of planetesimals, is stable, this slow migration can continue for a long time, slightly accelerating or damping depending on the disk’s surface density [59]. Conversely, if the planet system is –or becomes– unstable, then the planets tend to increase their orbital separation. The outermost planet penetrates into the disk and this starts a fast migration, similar to that obtained in previous simulations, where the planets are embedded in the disk from the very beginning. Thus the problem of triggering the LHB is reduced to the problem of understanding how the giant planets, during their slow migration, could pass from a stable configuration to an unstable one.

A solution of this problem has been proposed in [164]. This work postulated that, at the time of the dissipation of the gas disk, the four giant planets were

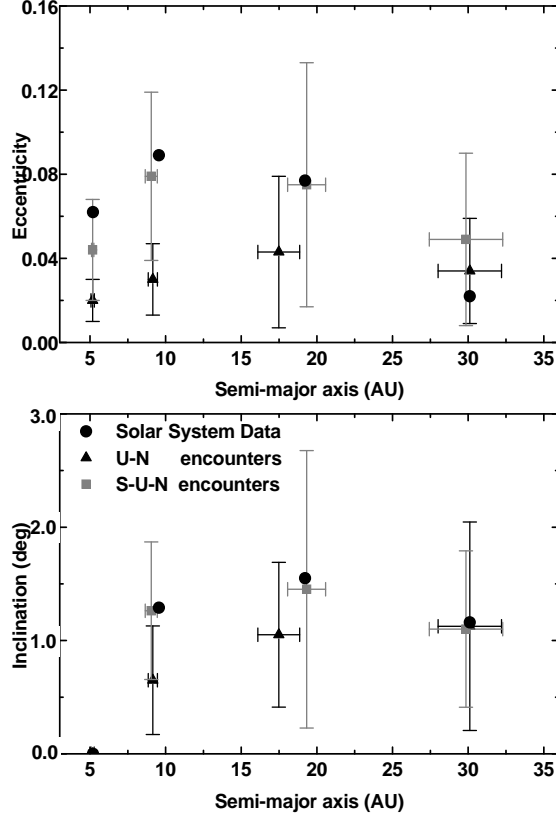


Figure 31: Comparison of the synthetic final planetary systems obtained in [164] with the real outer Solar System. Top: Proper eccentricity vs. semi-major axis. Bottom: Proper inclination vs. semi-major axis. Here, proper eccentricities and inclinations are defined as the maximum values acquired over a 2 My time-span and were computed from numerical integrations. The inclinations are measured relative to Jupiter’s orbital plane. The values for the real planets are presented with filled black dots. The gray squares mark the mean of the proper values for the runs with no planetary encounters involving Saturn, while the black triangles mark the same quantities for the runs where at least one ice giant encountered the ringed planet (about 15 runs in each case). The error bars represent one standard deviation of the measurements. From [164].

in a compact configuration, with quasi-circular, quasi-coplanar orbits with radii ranging from 5.5 to 13–17 AU. Saturn and Jupiter were close enough to have a ratio of orbital periods less than 2. This choice of the initial conditions for the two giant planets is supported by simulations of their evolution during the gas-disk phase [116] [126]. The assumption of initial small eccentricities and inclination is consistent with planet formation models. The small eccentricities ensure the



stability of such a compact planet configuration. In the scenario of [164], during their migration in divergent directions, Jupiter and Saturn eventually crossed their mutual 1:2 mean-motion resonance. This resonance crossing excited their eccentricities to values comparable to those currently observed (for eccentricity excitation due to resonance crossing see also [21]). The acquired eccentricities of Jupiter and Saturn destabilized the planetary system as a whole. The planetary orbits became chaotic and started to approach each other. Thus, a short phase of encounters followed the resonance-crossing event. Consequently, both ice giants were scattered outward, deeply into the disk. As discussed above, this abruptly increased the migration rates of the planets. During this fast migration phase, the eccentricities and inclinations of the planets decreased by the dynamical friction exerted by the planetesimals and the planetary system was finally stabilized.

With a planetesimal disk of about  $35M_{\oplus}$ , the simulations in [164] remarkably reproduced the current architecture of the giant planets orbits, in terms of semi-major axes, eccentricities and inclinations. In particular, this happened in the simulations where at least one of the ice giants encountered Saturn (see Fig. 31). Conversely, in the simulations where encounters with Saturn never occurred, Uranus typically ended its evolution on an orbit too close to the Sun and the final eccentricities and inclinations of all planets were too small.

With this result in hand [61] could put all the elements together in a coherent scenario for the LHB origin. Assuming an initial planetary system as in [164], the planetesimal disk fulfilled the lifetime constraint discussed above only if its inner edge was located about 1 AU beyond the position of the last planet. With this kind of disk, the 1:2 resonance crossing event that destabilized the planetary system occurred at a time ranging from 192 My to 875 My (see Fig. 32). Modifying the planetary orbits also led to changes in the resonance crossing time, pushing it up to 1.1 Gy after the beginning of the simulation. This range of instability times well brackets the estimated date of the LHB from lunar data.

The top panel of Fig. 33 shows the giant planets' evolution in a representative simulation of [61]. Initially, the giant planets migrated slowly due to the leakage of particles from the disk (Figure 3a). This phase lasted 875 My, at which point Jupiter and Saturn crossed their 1:2 resonance. At the resonance crossing event, as in [164], the orbits of the ice giants became unstable and they were scattered into the disk by Saturn. They disrupted the disk and scattered objects all over the Solar System, including the inner regions. Eventually they stabilized on orbits very similar to the current ones, at  $\sim 20$  and  $\sim 30$  AU respectively. The solid curve in the bottom panel shows the amount of material that struck the Moon as a function of time. As predicted in [111], the amount of material hitting the Moon after resonance crossing is consistent with the mass ( $6 \times 10^{21}$  g) estimated from the number and size distribution of lunar basins that formed around the time of the LHB epoch [72].

As discussed in [111] though, the planetesimals from the distant disk –which can be identified as ‘comets’– were not the only ones to hit the terrestrial planets. The radial migration of Jupiter and Saturn forced the secular resonances

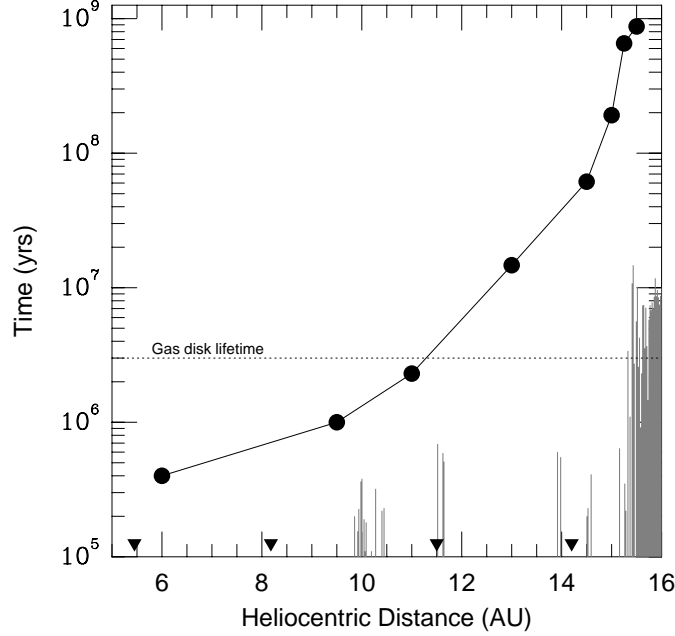


Figure 32: Disk location and LHB timing. The histogram reports the average dynamical lifetime of massless test particles placed in a planetary system with Jupiter, Saturn and the ice giants on nearly-circular, coplanar orbits at 5.45, 8.18, 11.5, 14.2 AU, respectively (marked as black triangles on the plot). The dynamical lifetime was computed by placing 10 particles with  $e = i = 0$  and random mean anomaly at each semi-major axis. Each vertical bar in the plot represents the average lifetime for those 10 particles, after having removed stable Trojan cases. The ‘lifetime’ is defined as the time required for a particle to encounter a planet within a Hill radius. A comparison between the histogram and the putative lifetime of the gaseous nebula [69] argues that, when the latter dissipated, the inner edge of the planetesimal disk had to be about 1–1.5 AU beyond the outermost ice giant. The time at which Jupiter and Saturn crossed their 1:2 mean-motion resonance, as a function of the location of the planetesimal disk’s inner edge, is shown with filled dots. From [61].

$\nu_6$  and  $\nu_{16}$  to sweep across the asteroid belt [55], exciting eccentricities and inclinations of asteroids. The fraction of the main belt population that acquired planet-crossing eccentricities depends quite crucially on the orbital distribution that the belt had before the LHB, which is not well known. The asteroid belt could not be a massive, dynamical cold disk at the time of the LHB. If it did,

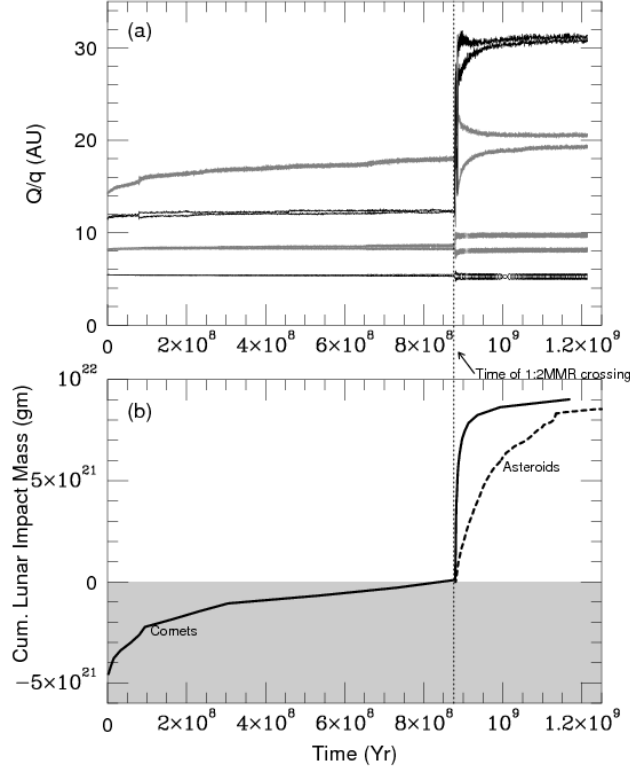


Figure 33: Planetary migration and the associated mass flux towards the inner Solar System from a representative simulation of [61]. Top: the evolution of the 4 giant planets. Each planet is represented by a pair of curves – the top and bottom curves are the aphelion and perihelion distances, respectively. Jupiter and Saturn cross their 1:2 mean-motion resonance at 880 My. Bottom: the cumulative mass of comets (solid curve) and asteroids (dashed curve) accreted by the Moon. The comet curve is offset so that the value is zero at the time of 1:2 resonance crossing. The estimate of the total asteroidal contribution is very uncertain, but should be roughly of the same order of magnitude as the cometary contribution, and occur over a longer time-span. From [61].

essentially all asteroids would have been ejected onto planet-crossing orbits, the bombardment of the Moon would have been orders of magnitude more intense than that recorded by the LHB [111] and the few asteroids surviving in the belt after the secular resonance sweeping would have an orbital distribution inconsis-

tent with that currently observed [55]. Presumably, the asteroid belt underwent a first phase of dynamical depletion and excitation at the time of terrestrial planet formation [173] [136] and then a second dynamical depletion at the time of the LHB. If, at the end of the first phase, the orbital distribution in the belt was comparable to the current one, then the secular resonance sweeping at the time of the LHB would have left  $\sim 10\%$  of the objects in the asteroid belt [61]. Assuming this figure, the pre-LHB main belt contained roughly  $5 \times 10^{-3} M_{\oplus}$  (10 times the current mass) and the total mass of the asteroids hitting the Moon was comparable to that of the comets (see Fig. 33). However, slight changes in the pre-LHB asteroid distribution and in the migration rate of Jupiter and Saturn (also highly variable from simulation to simulation, depending on the chaotic evolution of Neptune), can change this result for the asteroidal contribution to the Lunar cratering rate by a factor of several. In conclusion, the model in [61] cannot state whether asteroids or comets dominated the impact rate on the terrestrial planets. What it can say, however, is that the asteroidal contribution came later and more slowly than the cometary contribution (see Fig. 33), possibly erasing much of the signature of the comet bombardment.

The issue of which population dominated the impact rate can be solved by looking for constraints on the Moon. In [98], analysis of Lunar impact melts indicated that at least one of the projectiles that hit the Moon, and probably more, had a chemistry inconsistent with carbonaceous chondrites or comets. In [155] it was found that the impact melt at the landing site of Apollo 17 was caused by a projectile of LL-chondritic composition. These results imply that the bombardment was dominated by asteroids typical of the inner belt.

In [152] the comparison of size distributions of the craters formed at the time of the LHB on Mercury, Mars and the Moon allowed the calculation of the ratios among the impact velocities on these planets, leading to the conclusion that most projectiles had a semi-major axis between 1 and 2 AU. Comets never acquire such a small semi-major axis during their evolution, so that this argument again favors a predominant contribution from the inner main belt. More recently, [153] found that the crater size distribution on the lunar highlands is consistent with the size distribution currently observed in the main belt.

Taken altogether, these results point with little doubt to asteroids being the dominating (or, possibly, latest-arriving) projectile population for the terrestrial planets at the time of the LHB. However, they do not imply that the asteroids *triggered* the LHB. On the contrary, the result in [153] implies that the LHB was triggered by a distant disk of comets as in [61], for the reasons explained below.

The remarkable match between the size distributions of craters and main belt asteroids, pointed out in [153], implies that –at the LHB time– asteroids have been ejected from the main belt onto planet-crossing orbits in proportions independent of their size<sup>11</sup>. Only the sweeping of secular resonances can give a size-independent ejection throughout the main belt. At the time of the LHB,

<sup>11</sup>unlike the current Near Earth Asteroids (NEAs) which, escaping from the belt due to non-gravitational forces, have a size distribution steeper than that of the main belt population

the gas disk was already totally dissipated. Thus, secular resonance sweeping could only be caused by the radial displacement of Jupiter and Saturn. Now, even assuming that the entire LHB on the terrestrial planets was caused by asteroids, from the mass hitting the Moon at that time [72] and the Moon collision probability typical of NEAs, one can easily compute that the total asteroid mass on planet crossing orbits was about  $0.01 M_{\oplus}$ . This mass was too small to cause a significant migration of the giant planets. In conclusion, a more massive disk –which could only be trans-Neptunian– had to trigger and drive planet migration. Comets mandated the bombardment and asteroids executed it.

**Note on Trojans and satellites of the giant planets.** To validate or reject a model, it is important to look at the largest possible number of constraints. Two populations immediately come to mind when considering the LHB scenario proposed in [61]: the Trojans and the satellites. Is their existence consistent with that scenario?

Jupiter has a conspicuous Trojan population. These objects, usually referred to as ‘asteroids’, follow essentially the same orbit as Jupiter, but lead or trail that planet by an angular distance of  $\sim 60$  degrees, librating around the Lagrange triangular equilibrium points. The first Trojan of Neptune was recently discovered [20]; detection statistics imply that the Neptune Trojan population could be comparable in number to that of Jupiter, and possibly even 10 times larger [22].

The simulations in [164] [61] led to the capture of several particles on long-lived Neptune Trojan orbits (2 per run, on average, with a lifetime larger than 80 My). Their eccentricities reached values smaller than 0.1. These particles were eventually removed from the Trojan region, but this probably is an artifact of the graininess of Neptune’s migration in the simulation, due to the quite large individual mass of the planetesimals ([68]).

Jupiter Trojans are a more subtle issue that is described in detail in [127]. There is a serious argument in the literature against the idea that Jupiter and Saturn crossed their 1:2 mean-motion resonance: if the crossing had happened, any pre-existing Jovian Trojans would have become violently unstable, and Jupiter’s co-orbital region would have emptied [55] [118]. However, the dynamical evolution of a gravitating system of objects is time reversible. Thus, if the original objects can escape the Trojan region when the latter becomes unstable, other bodies can enter the same region and be temporarily trapped. Consequently, a transient Trojan population can be created if there is an external source of objects. In the framework of the scenario in [61], the source consists of the very bodies that are forcing the planets to migrate, which must be a very large population given how much the planets must move. When Jupiter and Saturn get far enough from the 1:2 resonance, so that the co-orbital region becomes stable, the population that happens to be there at that time remains trapped. It becomes the population of permanent Jovian Trojans still observable today.

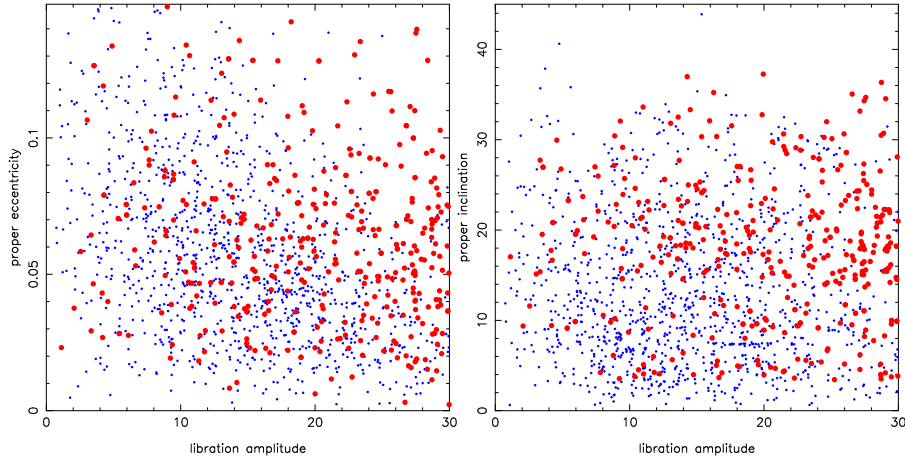


Figure 34: Comparison of the orbital distribution of Trojans between the simulations in [127] and observations. The simulation results are shown as red circles and the observations as blue dots in the planes of proper eccentricity vs. libration amplitude (left) and proper inclination vs. libration amplitude (right). The distribution of the simulated Trojans is somewhat skewed towards large libration amplitudes, relative to the observed population. However, this is not a serious problem because a fraction of the planetesimals with the largest amplitudes would leave the Trojan region during the subsequent 4 Gy of evolution[102], leading to a better match. The similarity between the two inclination distributions provides strong support for the LHB model in [61].

This possibility has been tested with numerical simulations in [127]. Among the particles that were Jupiter or Saturn crossers during the critical period of Trojan instability, between  $2.4 \times 10^{-6}$  and  $1.8 \times 10^{-5}$  remained permanently trapped as Jovian Trojans. More importantly, at the end of the simulations, the distribution of the trapped Trojans in the space of the three fundamental quantities for Trojan dynamics –the *proper* eccentricity, inclination and libration amplitude [119]– was remarkably similar to the current distribution of the observed Trojans, as illustrated in Fig. 34. In particular, this is the only model proposed thus far which explains the inclination distribution of Jovian Trojans. The latter was considered to be the hardest problem in the framework of the classical scenario, according to which the Trojans formed locally and were captured at the time of Jupiter’s growth [115].

The capture probabilities reported above allowed [127] to conclude that the total mass of the captured Trojan population was between  $\sim 4 \times 10^{-6}$  and  $\sim 3 \times 10^{-5} M_{\oplus}$ . Previous estimates from detection statistics [84] concluded that the current mass of the Trojan population is  $\sim 10^{-4} M_{\oplus}$ . However, taking into account modern, more refined knowledge of the Trojans absolute magnitude distribution (discussed in [127]), mean albedo [49] and density [114], the estimate of the current mass of the Trojan population is reduced to  $7 \times 10^{-6} M_{\oplus}$ , consistent

with the simulations in [127]. The bulk density of  $0.8^{+0.2}_{-0.1}\text{g/cm}^3$ , measured for the binary Trojan 617 Patroclus [114] is a confirmation by itself of the model of chaotic capture of Trojans from the original trans-Neptunian disk. In fact, this density is significantly smaller than any density measured so far in the asteroid belt, including for the most primitive objects, while it is essentially identical to the bulk densities inferred for the trans-Neptunian objects Varuna [85] and 1997 CQ<sub>29</sub> [132].

In conclusion, the properties of Jovian Trojans are not simply consistent with the LHB model of [61]: they constitute a strong indication –if not a smoking gun– in support of the 1:2 mean-motion resonance crossing of Jupiter and Saturn, which is at the core of the model in [61].

I now briefly come to the satellites of the giant planets. As discussed above, the non-survivability of the regular satellite systems is one of the killing arguments against the exotic scenario proposed in [106]. Because Saturn, Uranus and Neptune also have encounters with each other in the model of [164][61], it is important to look at the satellites' fates in this new framework. The issue has been addressed in [164]. The authors recorded all encounters deeper than one Hill-radius occurring in eight simulations. Then, they integrated the evolution of the regular satellite systems of Saturn, Uranus and Neptune during a re-enactment of these encounters. They found that, in half of the simulations, all of the satellite systems survived the entire suite of encounters with final eccentricities and inclinations smaller than 0.05. The difference with respect to the case of [106] is that, in the latter model, both ice giants had to have close and strong encounters with Jupiter or Saturn, whereas in the evolutions of [164][61] encounters with Jupiter never occur, and encounters with Saturn are typically distant ones, with moderate effects. Thus, the survivability of the regular satellites is not a problem for the LHB model. However, the more distant, irregular satellites would not survive the planetary encounters. Thus, if the LHB model is correct they must have been captured at the time of the LHB (see sect. 7).

## 7 Building a coherent view of solar system history: perspectives for future work.

From the emerging view of the events that led to the origin of the LHB, it appears that the evolution of the Solar System was characterized by three main phases:

- i) *the planetary accretion phase.* The giant planets formed in a few million years, in a compact orbital configuration embedded in a gas disk. The terrestrial planets presumably formed on a timescale of several  $10^7$  y [2] [177] [143]. Planetesimals formed out to a threshold distance of  $\sim 30\text{--}35$  AU. The asteroid belt underwent a first dynamical depletion and excitation during this phase [136], while planetesimals in the giant planets region were removed, leaving a massive planetesimal disk existing only beyond

the orbit of the outermost giant planet [61].

- ii) *a long quiescent phase* lasting 600 My, during which the distant planetesimal disk was gradually eroded at its inner edge by the planetary perturbations, leading to a slow migration of the giant planet orbits [61].
- iii) *the current phase*, lasting since 3.8 Gy ago, during which the Solar System has maintained essentially the same structure [62].

The LHB marks the cataclysmic transition between phase ii) and phase iii).

From this template of the Solar System history I will dare to try to put in a new context the various scenarios discussed in the previous sections for the origin of the comet reservoirs, and to suggest new directions for future research.

The Oort cloud should have formed in two stages. The first stage occurred as soon as (or even during the time that) the giant planets formed. This occurred very early, when the system was still rich in gas, and presumably the Solar System was still embedded in a stellar cluster. Appropriate simulations should thus account for a dense galactic environment, close and frequent stellar encounters as in [46], but using particles on initial quasi-circular and coplanar orbits in the planetary region and accounting for gas drag. The decoupling of Sedna and 2000 CR<sub>105</sub> from the scattering action of the planets should have occurred in this phase. The second stage occurred at the LHB time, when the original outer planetesimal disk was destroyed and a massive scattered disk was formed. The classical simulations discussed in sect. 4 are pertinent for this last phase. The inferred ratio between the number of comets currently in the Oort cloud and in the scattered disk (see sect. 4.1) argues that the first stage was more effective than the second one.

The Kuiper belt took shape at the LHB time. As the outer planetesimal disk was destroyed by the eccentric and migrating ice giants, a fraction of a percent of the planetesimals managed to be pushed outwards and be implanted in a region of orbital space that became stable when the planets finally settled on their current orbits. Thus the principle of the push-out scenario for the Kuiper belt should remain valid, although the simulations discussed in sects. 5.2 and 5.5 are not really pertinent. In fact, they assumed a smooth, long-range migration of Neptune, which is not what the LHB simulations in [61] show. Simulations in progress seem to indicate that the mechanism proposed in [57] for the origin of the hot population still applies (Gomes, private communication). For the cold population the mechanism proposed in [108] has to be substituted with a new one. It turns out that, during the short phase when Neptune is eccentric, the Kuiper belt is totally unstable up to the 1:2 mean-motion resonance with Neptune. It can therefore be visited by planetesimals coming from inside the outer edge of the disk. This builds a sort of steady state population in the Kuiper belt region, which remains permanently trapped when Neptune's eccentricity damps by dynamical friction, and the Kuiper belt becomes stable again (Levison, private communication). This process would therefore be analogous to that leading to the capture of Jovian Trojans. If the damping of Neptune's eccentricity occurred sufficiently fast, as found in the LHB model of [61]



describes, the planetesimals that remained trapped in the Kuiper belt by this mechanism would not have had enough time to develop large inclinations, and therefore the population trapped by this process would produce the cold Kuiper belt. In this scenario, the current size distribution of the Kuiper belt should be a fossil of that acquired during the  $\sim 600$  My time-span that the objects spent in the massive planetesimal disk, before being pushed out [133].

The irregular satellites of (at least) Saturn, Uranus and Neptune, if they existed before the LHB, would have been lost during the phase of encounters among the planets. Thus, those currently observed had to be captured later, from the flux of planetesimals coming from the distant disk. At this late stage, the capture process could not be related to gas drag, nor to a fast growth of the planetary masses (the so-called pull-down scenario); it is likely related to three-body interactions (i.e. interactions between planetesimals inside the Hill's sphere of a planet), although the exact mechanism has not been demonstrated yet. This view is consistent with that proposed in [86], from the comparative analysis of the size distributions of the irregular satellite populations of the 4 giant planets. Moreover, in this scenario the irregular satellites should have the same composition as Kuiper belt objects, given that both populations were extracted from the same primordial planetesimal disk. The recent data collected on the satellite Phoebe by the Cassini mission argue in this direction [23][87].

The new LHB scenario also has important implications for aspects of Solar System formation and primordial evolution not discussed in this chapter. The formation of the terrestrial planets should be revisited, accounting for giant planets on more compact, circular orbits, as required in [61]. Similarly, the evolution of the asteroid belt should also be re-assessed. As mentioned before, the belt should have suffered two phases of dynamical depletion and excitation. The first one during the formation of the terrestrial planets, and the second one during the LHB. Therefore, during the 600 My period between the end of terrestrial planet accretion and the LHB, the asteroid belt should have remained about 10–20 times more massive than the current belt, in a dynamically excited state. The collisional evolution during this period should have been very important, and the current size distribution in the main belt should be a fossil of the one that was developed during this phase. A study similar to [13] should be done, but taking into account this two-stage evolution of the belt.

Finally, the LHB scenario constrains the orbital architecture of the giant planets at the end of the gas disk phase. Future simulations of the formation of these planets and of their interactions with the nebula will have to meet these constraints. In particular, the compact configuration of the planetary orbits and the presence of a massive disk of planetesimals outside the orbit of the outermost planet constrain the maximum range of radial migration that the giant planets could suffer during the gas phase. For instance, if Jupiter had formed, say, at 30 AU and migrated down to 5 AU during the gas-disk lifetime, the outer planetesimal disk required to trigger the LHB would have been destroyed. Most probably, the cores of all giant planets formed within 10–15 AU from the Sun [159] and, for some reason not yet totally clear, never migrated substantially.

### Acknowledgments:

I wish to thank N. Thomas and W. Benz for their invitation to present a series of lectures at the 35th Saas-Fee advanced course, from which this chapter has been derived. I also thank R. Jedicke and D. Jewitt for their invitation to re-present the same lectures at the Institute for Astronomy of the University of Hawaii. I am grateful to all the colleagues with whom I had stimulating discussions on comet dynamics and the formation of the cometary reservoirs, in particular L. Dones and H. Levison. I also acknowledge that I re-cycled pieces of text originally written by M. Brown and Ph. Claeys in papers that we made together on the Kuiper belt and on the Late Heavy Bombardment. I'm in debt to all those who read carefully the draft of this manuscript and gave valuable suggestions for improvements: D. O'Brien, W. Benz. Finally, I wish to devote this chapter to the memory of Michel Festou. This great French expert of comets was particularly aware of the importance of dynamics for understanding the role of these icy objects in the framework of Solar System formation. My discussions with him greatly motivated me –originally an asteroid person– to know more about the primordial evolution of the outer Solar System.

## References

- [1] Adams, F. C., Hollenbach, D., Laughlin, G., Gorti, U. 2004. Photoevaporation of Circumstellar Disks Due to External Far-Ultraviolet Radiation in Stellar Aggregates. *Astrophysical Journal* 611, 360-379.
- [2] Allegre, C.J., G. Manhes and C. Gopel 1995. The age of the Earth. *Geochimica et Cosmochimica Acta*. 59, 1445-1456.
- [3] Allen, R.L., Bernstein, G.M., Malhotra, R. 2001. The edge of the solar system. *Astroph. J.*, **549**, L241-L244.
- [4] Allen, R.L., Bernstein, G.M., Malhotra, R. 2002. Observational Limits on a Distant Cold Kuiper Belt. *Astron. J.*, **124**, 2949-2954.
- [5] Astakhov, S. A., Lee, E. A., Farrelly, D. 2005. Formation of Kuiper-belt binaries through multiple chaotic scattering encounters with low-mass intruders. *Monthly Notices of the Royal Astronomical Society* 360, 401-415.
- [6] Bailey, M. E., Clube, S. V. M., Hahn, G., Napier, W. M., Valsecchi, G. B. 1994. Hazards Due to Giant Comets: Climate and Short-term Catastrophism. in *Hazards Due to Comets and Asteroids*, (T. Gehrels and M.S. Matthews eds), 479–533, Univ Arizona Press, Tucson.
- [7] Bailey, M. E., Stagg, C. R. 1988. Cratering constraints on the inner Oort cloud - Steady-state models. *Monthly Notices of the Royal Astronomical Society* 235, 1-32.
- [8] Benz, W., Asphaug, E. 1999. Catastrophic Disruptions Revisited. *Icarus* 142, 5-20.

- [9] Bernstein, G. M., Trilling, D. E., Allen, R. L., Brown, M. E., Holman, M., Malhotra, R. 2004. The Size Distribution of Trans-Neptunian Bodies. *Astronomical Journal* 128, 1364-1390.
- [10] Binney, J., Tremaine, S. 1987. *Galactic dynamics*. Princeton, NJ, Princeton University Press, 1987, 747 p. .
- [11] Binzel, R. P., Rivkin, A. S., Stuart, J. S., Harris, A. W., Bus, S. J., Burbine, T. H. 2004. Observed spectral properties of near-Earth objects: results for population distribution, source regions, and space weathering processes. *Icarus* 170, 259-294.
- [12] Bottke, W. F., Morbidelli, A., Jedicke, R., Petit, J.-M., Levison, H. F., Michel, P., Metcalfe, T. S. 2002. Debiased Orbital and Absolute Magnitude Distribution of the Near-Earth Objects. *Icarus* 156, 399-433.
- [13] Bottke, W. F., Durda, D. D., Nesvorný, D., Jedicke, R., Morbidelli, A., Vokrouhlický, D., Levison, H. 2005. The fossilized size distribution of the main asteroid belt. *Icarus* 175, 111-140.
- [14] Brown M. 2001. The Inclination Distribution of the Kuiper Belt. *Astron. J.*, **121**, 2804-2814.
- [15] Brown, M. E., Trujillo, C. A., Rabinowitz, D., Tourtellotte, S., Marsden, B. G. 2005. 2003 UB313. Minor Planet Electronic Circulars 41.
- [16] Brunini A., Melita M. 2002. The existence of a planet beyond 50 AU and the orbital distribution of the classical Edgeworth Kuiper belt objects. *Icarus*, **160**, 32-43.
- [17] Canup, R. M. 2005. A Giant Impact Origin of Pluto-Charon. *Science* 307, 546-550.
- [18] Chambers, J. E., Lissauer, J. J. 2002. A New Dynamical Model for the Lunar Late Heavy Bombardment. Lunar and Planetary Institute Conference Abstracts 33, 1093.
- [19] Chiang, E.I., Brown, M.E. 1999. Keck pencil-beam survey for faint Kuiper belt objects. *Astron. J.*, **118**, 1411-1422.
- [20] Chiang E.I., Jordan A.B., Millis R.L., Buie M.W., Wasserman L.H., Elliot J.L., Kern S.D., Trilling D.E., Meech K.J. and Wagner R.M. 2003. Resonance Occupation in the Kuiper Belt: Case Examples of the 5:2 and Trojan Resonances. *Astron. J.*, **126**, 430-443
- [21] Chiang, E. I. 2003. Excitation of Orbital Eccentricities by Repeated Resonance Crossings: Requirements. *Astrophysical Journal* 584, 465-471.
- [22] Chiang, E. I., Lithwick, Y. 2005. Neptune Trojans as a Test Bed for Planet Formation. *Astrophysical Journal* 628, 520-532.

- [23] Clark, R. N., and 25 colleagues 2005. Compositional maps of Saturn's moon Phoebe from imaging spectroscopy. *Nature* 435, 66-69.
- [24] Cohen, B.A., Swindle, T.D., and Kring, D.A., 2000, Support for the Lunar Cataclysm Hypothesis from Lunar Meteorite Impact Melt Ages: *Science*, v. 290, p. 1754-1756.
- [25] Danby J.M.A. (1962) *Fundamentals of Celestial Mechanics*. Willmann-Bell Inc. Richmond, Virginia.
- [26] Davis D. R., Farinella P. 1998, Collisional Erosion of a Massive Edgeworth-Kuiper Belt: Constraints on the Initial Population. In *Lunar Planet. Science Conf.* **29**, 1437-1438.
- [27] Davis D. R., Farinella P. 1997. Collisional Evolution of Edgeworth-Kuiper Belt Objects. *Icarus*, **125**, 50-60.
- [28] Deutsch, A., and Schrärer, U., 1994, Dating terrestrial impact craters: Meteoritics, v. 29, p. 301-322.
- [29] Dones, L., Weissman, P. R., Levison, H. F., Duncan, M. J. 2004. Oort cloud formation and dynamics. *Comets II* 153-174.
- [30] Dones L., Levison H.F., Duncan M.J., Weissman P.R., 2005. Simulations of the formation of the Oort Cloud I. the reference model. *Icarus*, in press.
- [31] Doressoundiram A., Barucci M.A., Romon J., Veillet C. 2001. Multicolor Photometry of Trans-neptunian Objects. *Icarus*, **154**, 277-286.
- [32] Doressoundiram, A., Peixinho, N., Doucet, C., Mousis, O., Barucci, M. A., Petit, J. M., Veillet, C. 2005. The Meudon Multicolor Survey (2MS) of Centaurs and trans-neptunian objects: extended dataset and status on the correlations reported. *Icarus* 174, 90-104.
- [33] Duncan, M., Quinn, T., Tremaine, S. 1987. The formation and extent of the solar system comet cloud. *Astronomical Journal* 94, 1330-1338.
- [34] Duncan, M., Quinn, T., Tremaine, S. 1988. The origin of short-period comets. *Astrophysical Journal* 328, L69-L73.
- [35] Duncan, M. J., Levison, H. F., Budd, S. M. 1995, The long-term stability of orbits in the Kuiper belt, *Astron. J.*, **110**, 3073-3083.
- [36] Duncan, M. J., Levison, H. F. 1997, Scattered comet disk and the origin of Jupiter family comets, *Science*, **276**, 1670-1672.
- [37] Duncan M., Levison H.F. and Dones L. 2004. Dynamical evolution of ecliptic comets. in *Comet II*, Festou et al. eds., University Arizona Press, Tucson, Az., 193-204.

- [38] Elliot, J. L., and 10 colleagues 2005. The Deep Ecliptic Survey: A Search for Kuiper Belt Objects and Centaurs. II. Dynamical Classification, the Kuiper Belt Plane, and the Core Population. *Astronomical Journal* 129, 1117-1162
- [39] Fernandez, J. A. 1978. Mass removed by the outer planets in the early solar system. *Icarus* 34, 173-181.
- [40] Fernandez, J. A. 1980. Evolution of comet orbits under the perturbing influence of the giant planets and nearby stars. *Icarus* 42, 406-421.
- [41] Fernandez, J. A. 1980. On the existence of a comet belt beyond Neptune. *Monthly Notices of the Royal Astronomical Society* 192, 481-491.
- [42] Fernandez, J. A., Ip, W.-H. 1984. Some dynamical aspects of the accretion of Uranus and Neptune - The exchange of orbital angular momentum with planetesimals. *Icarus* 58, 109-120.
- [43] Fernandez, J.A., Gallardo, T. 1994. The transfer of comets from parabolic orbits to short-period orbits: Numerical studies. *Astronomy and Astrophysics* 281, 911-922.
- [44] Fernandez, J. A. 1997. The Formation of the Oort Cloud and the Primitive Galactic Environment. *Icarus* 129, 106-119.
- [45] Fernández, J. A., Tancredi, G., Rickman, H., Licandro, J. 1999. The population, magnitudes, and sizes of Jupiter family comets. *Astronomy and Astrophysics* 352, 327-340.
- [46] Fernández, J. A., Brunini, A. 2000. The buildup of a tightly bound comet cloud around an early Sun immersed in a dense Galactic environment: Numerical experiments. *Icarus* 145, 580-590.
- [47] Fernández, J. A., Gallardo, T., Brunini, A. 2002. Are There Many Inactive Jupiter-Family Comets among the Near-Earth Asteroid Population?. *Icarus* 159, 358-368.
- [48] Fernández, J. A., Gallardo, T., Brunini, A. 2004. The scattered disk population as a source of Oort cloud comets: evaluation of its current and past role in populating the Oort cloud. *Icarus* 172, 372-381.
- [49] Fernández, Y. R., Sheppard, S. S., Jewitt, D. C. 2003. The Albedo Distribution of Jovian Trojan Asteroids. *Astronomical Journal* 126, 1563-1574.
- [50] Fernández, Y. R., Jewitt, D. C., Sheppard, S. S. 2005. Albedos of Asteroids in Comet-Like Orbits. *Astronomical Journal* 130, 308-318.
- [51] Funato, Y., Makino, J., Hut, P., Kokubo, E., Kinoshita, D. 2004. The formation of Kuiper-belt binaries through exchange reactions. *Nature* 427, 518-520.

- [52] Gladman, B., Kavelaars, J.J., Nicholson, P.D., Lored, T.J., Burns, J.A. 1998. Pencil-beam surveys for faint trans-Neptunian objects. *Astron. J.*, **116**, 2042-2054.
- [53] Gladman B., Holman M., Grav T., Kaavelars J.J., Nicholson P., Aksnes K., Petit J.M. 2002. Evidence for an extended scattered disk. *Icarus*, **157**, 269-279.
- [54] Goldreich P., Lithwick Y., Sari R. 2002. Formation of Kuiper-belt binaries by dynamical friction and three-body encounters. *Nature*, **420**, 643-646.
- [55] Gomes, R. S. 1997. Dynamical Effects of Planetary Migration on the Primordial Asteroid Belt. *Astronomical Journal* 114, 396-401.
- [56] Gomes R. S. 2000. Planetary Migration and Plutino Orbital Inclinations *Astron. J.*, **120**, 2695-2707.
- [57] Gomes, R. S. 2003. The origin of the Kuiper Belt high-inclination population. *Icarus* 161, 404-418.
- [58] Gomes, R. 2003. The Common Origin of the High Inclination TNO's. *Earth Moon and Planets* 92, 29-42.
- [59] Gomes, R. S., Morbidelli, A., Levison, H. F. 2004. Planetary migration in a planetesimal disk: why did Neptune stop at 30 AU?. *Icarus* 170, 492-507.
- [60] Gomes, R. S., Gallardo, T., Fernández, J. A., Brunini, A. 2005. On The Origin of The High-Perihelion Scattered Disk: The Role of The Kozai Mechanism And Mean Motion Resonances. *Celestial Mechanics and Dynamical Astronomy* 91, 109-129.
- [61] Gomes, R., Levison, H. F., Tsiganis, K., Morbidelli, A. 2005. Origin of the cataclysmic Late Heavy Bombardment period of the terrestrial planets. *Nature* 435, 466-469.
- [62] Grieve R. A. and Shoemaker E. M. (1994) The record of past impacts on Earth. In *Hazards Due to Comets and Asteroids* (T. Gehrels, M. S. Matthews, eds.), pp. 417-462, University of Arizona press, Tucson.
- [63] Guillot, T. 1999. Interior of Giant Planets Inside and Outside the Solar System. *Science* 286, 72-77.
- [64] Grinspoon D., 1989. Large impact events and atmospheric evolution on the terrestrial planets. *Ph.D. thesis*, University of Arizona, Tucson, Arizona.
- [65] Hainaut, O. 2002 <http://www.sc.eso.org/~ohainaut/MBOSS/>
- [66] Hayashi C. 1981. Structure of the solar nebula, growth and decay of magnetic fields and effects of magnetic and turbulent viscosities on the nebula. *Prog. Theor. Phys. Suppl.*, **70**, 35-53.

- [67] Hahn, J. M., Malhotra, R. 1999. Orbital Evolution of Planets Embedded in a Planetesimal Disk. *Astronomical Journal* 117, 3041-3053.
- [68] Hahn, J. M., Malhotra, R. 2005. Neptune's Migration into a Stirred-Up Kuiper Belt: A Detailed Comparison of Simulations to Observations. *Astron. J.* in press.
- [69] Haisch K.E., Lada E.A. and Lada C.J. Disk frequencies and lifetimes in young clusters. *Astroph. J.*, 553, L153–156 (2001)
- [70] Harris, N. W., Bailey, M. E. 1998. Dynamical evolution of cometary asteroids. *Monthly Notices of the Royal Astronomical Society* 297, 1227-1236.
- [71] Hartmann, W.K., 1975, Lunar cataclysm: A misconception?: *Icarus*, v. 24, p. 181-187.
- [72] Hartmann, W. K., Ryder, G., Dones, L., Grinspoon, D. 2000. The Time-Dependent Intense Bombardment of the Primordial Earth/Moon System. *Origin of the earth and moon*, edited by R.M. Canup and K. Righter and 69 collaborating authors. Tucson: University of Arizona Press., p.493-512
- [73] Heisler, J., Tremaine, S. 1986. The influence of the galactic tidal field on the Oort comet cloud. *Icarus* 65, 13-26.
- [74] Heisler, J., Tremaine, S., Alcock, C. 1987. The frequency and intensity of comet showers from the Oort cloud. *Icarus* 70, 269-288.
- [75] Heisler, J. 1990. Monte Carlo simulations of the Oort comet cloud. *Icarus* 88, 104-121.
- [76] Henrard J. 1982. Capture into resonance - An extension of the use of adiabatic invariants. *Cel. Mech.*, **27**, 3–22.
- [77] Hills, J. G. 1981. Comet showers and the steady-state infall of comets from the Oort cloud. *Astronomical Journal* 86, 1730-1740.
- [78] Hollenbach, D., Adams, F. C. 2004. Dispersal of Disks Around Young Stars: Constraints on Kuiper Belt Formation. *ASP Conf. Ser.* 324: Debris Disks and the Formation of Planets 324, 168.
- [79] Holman, M. J., Wisdom, J. 1993. Dynamical stability in the outer solar system and the delivery of short period comets. *Astronomical Journal* 105, 1987-1999.
- [80] Hut, P., Alvarez, W., Elder, W. P., Kauffman, E. G., Hansen, T., Keller, G., Shoemaker, E. M., Weissman, P. R. 1987. Comet showers as a cause of mass extinction. *Nature* 329, 118-126.

- [81] Ida S., Larwood J., Burkert A. 2000. Evidence for Early Stellar Encounters in the Orbital Distribution of Edgeworth-Kuiper Belt Objects. *Astroph. J.*, **528**, 351–356.
- [82] Jewitt, D. C., Luu, J. X. 1993, Discovery of the candidate Kuiper belt object 1992 QB1, *Nature*, **362**, 730–732.
- [83] Jewitt, D., Luu, J., Trujillo, C. 1998. Large Kuiper belt objects: The Mauna Kea 8K CCD survey. *Astron. J.*, **115**, 2125–2135.
- [84] Jewitt, D. C., Trujillo, C. A., Luu, J. X. 2000. Population and Size Distribution of Small Jovian Trojan Asteroids. *Astronomical Journal* 120, 1140–1147.
- [85] Jewitt, D. C., Sheppard, S. S. 2002. Physical Properties of Trans-Neptunian Object (20000) Varuna. *Astronomical Journal* 123, 2110–2120
- [86] Jewitt, D., Sheppard, S. 2005. Irregular Satellites in the Context of Planet Formation. *Space Science Reviews* 116, 441–455.
- [87] Johnson, T. V., Lunine, J. I. 2005. Saturn’s moon Phoebe as a captured body from the outer Solar System. *Nature* 435, 69–71.
- [88] Kenyon, S.J., Luu, J.X. 1998. Accretion in the early Kuiper belt: I. Coagulation and velocity evolution. *Astron. J.*, **115**, 2136–2160.
- [89] Kenyon, S.J., Luu, J.X. 1999a. Accretion in the early Kuiper belt: II. Fragmentation. *Astron. J.*, **118**, 1101–1119.
- [90] Kenyon, S.J., Luu, J.X. 1999b. Accretion in the early outer solar system. *Astrophys. J.*, **526**, 465–470
- [91] Kenyon S.J. and Bromley B.C. 2002. Collisional Cascades in Planetesimal Disks. I. Stellar Flybys. *Astron. J.*, **2002**, 1757–1775.
- [92] Kenyon, S. J., Bromley, B. C. 2004. Stellar encounters as the origin of distant Solar System objects in highly eccentric orbits. *Nature* 432, 598–602.
- [93] Kenyon, S. J., Bromley, B. C. 2004. The Size Distribution of Kuiper Belt Objects. *Astronomical Journal* 128, 1916–1926.
- [94] Knežević Z., Milani A., Farinella P., Froeschlé Ch. and Froeschlé C. (1991) Secular resonances from 2 to 50 AU. *Icarus*, **93**, 316.
- [95] Kobayashi H., Ida S. 2001. The Effects of a Stellar Encounter on a Planetesimal Disk. *Icarus*, **153**, 416–429.
- [96] Koeberl, C., 2004, The late heavy bombardment in the inner solar system: Earth, Moon and Planets, v. 92, p. 79–87.



- [97] Kozai, Y. 1962. Secular Perturbations of Asteroids with High Inclination and Eccentricity.. *Astronomical Journal* 67, 579.
- [98] Kring, D. A., Cohen, B. A. 2002. Cataclysmic bombardment throughout the inner solar system 3.9-4.0 Ga. *Journal of Geophysical Research (Planets)* 107, 4-1.
- [99] Kuchner M.J., Brown M.E., Holman M. 2002. Long-Term Dynamics and the Orbital Inclinations of the Classical Kuiper Belt Objects. *Astron. J.*, **124**, 1221-1230.
- [100] Kuiper, G.P. 1951. On the origin of the Solar System. In *Astrophysics*, ed. Hynek, J.A., McGraw-Hill, New York, 357 pp.
- [101] Levison, H. F. 1996. Comet Taxonomy. ASP Conf. Ser. 107: Completing the Inventory of the Solar System 107, 173-191.
- [102] Levison, H., Shoemaker, E. M., Shoemaker, C. S. 1997. The dispersal of the Trojan asteroid swarm. *Nature* 385, 42-44.
- [103] Levison, H.F., & Duncan, M. J. 1997, From the Kuiper Belt to Jupiter-Family Comets: The Spatial Distribution of Ecliptic Comets, *Icarus*, **127**, 13-32.
- [104] Levison H.F., Stern S.A. 2001. On the Size Dependence of the Inclination Distribution of the Main Kuiper Belt. *Astron. J.*, **121**, 1730-1735.
- [105] Levison, H. F., Dones, L., Duncan, M. J. 2001. The Origin of Halley-Type Comets: Probing the Inner Oort Cloud. *Astronomical Journal* 121, 2253-2267.
- [106] Levison, H. F., Dones, L., Chapman, C. R., Stern, S. A., Duncan, M. J., Zahnle, K. 2001. Could the Lunar "Late Heavy Bombardment" Have Been Triggered by the Formation of Uranus and Neptune?. *Icarus* 151, 286-306.
- [107] Levison, H. F., Morbidelli, A., Dones, L., Jedicke, R., Wiegert, P. A., Bottke, W. F. 2002. The Mass Disruption of Oort Cloud Comets. *Science* 296, 2212-2215.
- [108] Levison, H. F., Morbidelli, A. 2003. The formation of the Kuiper belt by the outward transport of bodies during Neptune's migration. *Nature* 426, 419-421.
- [109] Levison, H. F., Duncan, M. J., Dones, L., Gladman, B. 2004. The Scattered Disk as a Source of Halley-Type Comets. AAS/Division for Planetary Sciences Meeting Abstracts 36, .
- [110] Levison, H. F., Morbidelli, A., Dones, L. 2004. Sculpting the Kuiper Belt by a Stellar Encounter: Constraints from the Oort Cloud and Scattered Disk. *Astronomical Journal* 128, 2553-2563.

- [111] Levison, H. F., Thommes, E., Duncan, M. J., Dones, L. 2004. A Fairy Tale about the Formation of Uranus and Neptune and the Lunar Late Heavy Bombardment. ASP Conf. Ser. 324: Debris Disks and the Formation of Planets 324, 152.
- [112] Malhotra, R. 1993. The Origin of Pluto's Peculiar Orbit. *Nature* 365, 819.
- [113] Malhotra, R. 1995. The Origin of Pluto's Orbit: Implications for the Solar System Beyond Neptune. *Astronomical Journal* 110, 420.
- [114] Marchis, F., and 16 colleagues 2005. The Orbit of 617 Patroclus Binary Trojan System from Keck LGS AO observations. AAS/Division for Planetary Sciences Meeting Abstracts 37, and *Nature*, submitted.
- [115] Marzari F., Scholl H., Murray C. and Lagerkvist C. Origin and evolution of Trojan asteroids. in *Asteroids III*, Bottke W.F., Cellino A., Paolicchi P. and Binzel R.P. eds., University of Arizona Press., 725-738 (2002)
- [116] Masset, F., Snellgrove, M. 2001. Reversing type II migration: resonance trapping of a lighter giant protoplanet. *Monthly Notices of the Royal Astronomical Society* 320, L55-L59.
- [117] Melita M., Larwood J., Collander-Brown S, Fitzsimmons A., Williams I.P., Brunini A. 2002. The edge of the Edgeworth-Kuiper belt: stellar encounter, trans-Plutonian planet or outer limit of the primordial solar nebula? In *Asteroid, Comet, Meteors*, ESA Spec. Publ. series, in press.
- [118] Michtchenko T.A., Beaugé C. and Roig F. Planetary Migration and the Effects of Mean Motion Resonances on Jupiter's Trojan Asteroids. *Astronomical Journal* 122, 3485-3491 (2001)
- [119] Milani, A. 1993. The Trojan asteroid belt: Proper elements, stability, chaos and families. *Celestial Mechanics and Dynamical Astronomy* 57, 59-94.
- [120] Morbidelli A., Thomas F. and Moons M. (1995a) The resonant structure of the Kuiper belt and the dynamics of the first five trans-Neptunian objects. *Icarus*, **118**, 322.
- [121] Morbidelli A., Valsecchi G. B. 1997. Neptune scattered planetesimals could have sculpted the primordial Edgeworth-Kuiper belt, *Icarus*, **128**, 464-468.
- [122] Morbidelli A., 2002. *Modern Celestial Mechanics: aspects of Solar System dynamics*, in "Advances in Astronomy and Astrophysics", Taylor & Francis, London.
- [123] Morbidelli, A., Levison, H. F. 2004. Scenarios for the Origin of the Orbits of the Trans-Neptunian Objects 2000 CR<sub>105</sub> and 2003 VB<sub>12</sub> (Sedna). *Astronomical Journal* 128, 2564-2576.

- [124] Morbidelli, A. 2004. How Neptune Pushed the Boundaries of Our Solar System. *Science* 306, 1302-1304.
- [125] Morbidelli A. and Brown M. 2004. The Kuiper Belt and the primordial evolution of the solar system. in *Comet II*, Festou et al. eds., University Arizona Press, Tucson, Az., 175–192.
- [126] Morbidelli, A., Crida, A., Masset, F. 2005. Preventing Type II Migration of Jupiter and Saturn. AAS/Division for Planetary Sciences Meeting Abstracts 37, .
- [127] Morbidelli, A., Levison, H. F., Tsiganis, K., Gomes, R. 2005. Chaotic capture of Jupiter’s Trojan asteroids in the early Solar System. *Nature* 435, 462-465.
- [128] Murray-Clay R.A. and Chiang H.I. 2005. Stochastic migration in planetesimal disks. preprint.
- [129] Nagasawa M., Ida S. 2000. Sweeping Secular Resonances in the Kuiper Belt Caused by Depletion of the Solar Nebula. *Astron. J.*, **120**, 3311–3322.
- [130] Nesvorný D. and Roig F. (2000) Mean motion resonances in the trans-neptunian region: Part I: The 2:3 resonance with Neptune. *Icarus*, in press.
- [131] Nesvorný D. and Roig F. (2001) Mean motion resonances in the trans-neptunian region: Part II: the 1:2, 3:4 and weaker resonances. *Icarus*, in press.
- [132] Noll, K. S., Stephens, D. C., Grundy, W. M., Osip, D. J., Griffin, I. 2004. The Orbit and Albedo of Trans-Neptunian Binary (58534) 1997 CQ<sub>29</sub>. *Astronomical Journal* 128, 2547-2552.
- [133] O’Brien, D. P., Morbidelli, A., Bottke, W. F. 2005. Collisional Evolution of the Primordial Trans-Neptunian Disk: Implications for Planetary Migration and the Current Size Distribution of TNOs. AAS/Division for Planetary Sciences Meeting Abstracts 37, .
- [134] Oort, J. H. 1950. The structure of the cloud of comets surrounding the Solar System and a hypothesis concerning its origin. *Bulletin of the Astronomical Institute of the Netherlands* 11, 91-110.
- [135] Petit J. M., Morbidelli A., Valsecchi, G. B. 1999. Large scattered planetesimals and the excitation of the small body belts. *Icarus*, **141**, 367-387.
- [136] Petit, J.-M., Morbidelli, A., Chambers, J. 2001. The Primordial Excitation and Clearing of the Asteroid Belt. *Icarus* 153, 338-347.
- [137] Petit, J.-M., Mousis, O. 2004. KBO binaries: how numerous were they?. *Icarus* 168, 409-419.

- [138] Pittich, E. M., D'Abramo, G., Valsecchi, G. B. 2004. From Jupiter-family to Encke-like orbits. The rôle of non-gravitational forces and resonances. *Astronomy and Astrophysics* 422, 369-375.
- [139] Rickman, H., Froeschlé, C., Froeschlé, C., Valsecchi, G. B. 2004. Stellar perturbations on the scattered disk. *Astronomy and Astrophysics* 428, 673-681.
- [140] Ryder, G., 1990, Lunar samples, lunar accretion and the Early bombardment of the Moon: *Eos Transactions AGU*, v. 71, p. 313-323.
- [141] Ryder, G., Koeberl, C., and Mojzsis, S.J., 2000, Heavy bombardment on the Earth at 3.85: The search for petrographical and geochemical evidence, in Canup, R.M., and Richter, K., eds., *Origin of the Earth and Moon*: Tucson, Arizona, University of Arizona Press, p. 475-492.
- [142] Ryder, G., 2002, Mass flux in the ancient Earth-Moon system and the benign implications for the origin of life on Earth: *Journal Geophysical Research-Planets*, v. 107, p. 6-14.
- [143] Sasaki, T., Abe, Y. 2004. Partial Resetting on Hf-W System by Giant Impacts. *Lunar and Planetary Institute Conference Abstracts* 35, 1505.
- [144] Stern, S. A. 1991, On the number of planets in the outer solar system - Evidence of a substantial population of 1000-km bodies, *Icarus*, 90, 271-281
- [145] Stern S. A. 1995. Collisional time scales in the Kuiper disk and their implications. *Astron. J.*, **110**, 856-868.
- [146] Stern, S. A. 1996, On the Collisional Environment, Accretion Time Scales, and Architecture of the Massive, Primordial Kuiper Belt., *Astron. J.*, **112**, 1203-1210.
- [147] Stern, S. A., Colwell, J. E. 1997a, Accretion in the Edgeworth-Kuiper Belt: Forming 100-1000 KM Radius Bodies at 30 AU and Beyond. *Astron. J.*, **114**, 841-849.
- [148] Stern, S. A., Colwell, J. E. 1997b, Collisional Erosion in the Primordial Edgeworth-Kuiper Belt and the Generation of the 30-50 AU Kuiper Gap, *Astroph. J.*, **490**, 879-885.
- [149] Stern, S. A., Weissman, P. R. 2001. Rapid collisional evolution of comets during the formation of the Oort cloud. *Nature* 409, 589-591.
- [150] Stern, S.A. 2002. Evidence for a collisional mechanism affecting Kuiper belt object colors. *Astron. J.*, **124**, 2300-2304.
- [151] Stone, J. M., Gammie, C. F., Balbus, S. A. and Hawley, J. F. in *Protostars and Planets IV* (eds Mannings, V., Boss, A. P. and Russell, S. S.) 589 (Univ. Arizona Press, Tucson, 1998)

- [152] Strom, R. G., Neukum, G. 1988. The cratering record on Mercury and the origin of impacting objects. Mercury, University of Arizona Press 336-373.
- [153] Strom, R. G., Malhotra, R., Ito, T., Yoshida, F., Kring, D. A. 2005. The Origin of Planetary Impactors in the Inner Solar System. *Science* 309, 1847-1850.
- [154] Stuart, J. S. 2001. A Near-Earth Asteroid Population Estimate from the LINEAR Survey. *Science* 294, 1691-1693.
- [155] Tagle, R. 2005. LL-Ordinary Chondrite Impact on the Moon: Results from the 3.9 Ga Impact Melt at the Landing Site of Apollo 17. 36th Annual Lunar and Planetary Science Conference 36, 2008.
- [156] Tegler, S. C. and Romanishin, W. 2000. Extremely red Kuiper-belt objects in near-circular orbits beyond 40 AU. *Nature*, **407**, 979-981.
- [157] Tera, F., Papanastassiou, D.A., and Wasserburg, G.J., 1974, Isotopic evidence for a terminal lunar cataclysm: *Earth and Planetary Science Letters*, v. 22, p. 1-21.
- [158] Thebault P. and Doeressoundiram A. 2003. A numerical test of the collisional resurfacing scenario. Could collisional activity explain the spatial distribution of color-index within the Kuiper belt? *Icarus*, **162**, 27-37.
- [159] Thommes, E. W., Duncan, M. J., Levison, H. F. 2003. Oligarchic growth of giant planets. *Icarus* 161, 431-455.
- [160] Trujillo, C. A., Jewitt D. C., Luu J. X. 2001. Properties of the Trans-Neptunian Belt: Statistics from the Canada-France-Hawaii Telescope Survey. *Astron. J.*, **122**, 457-473.
- [161] Trujillo C.A., Brown M.E. 2001. The Radial Distribution of the Kuiper Belt. *Astroph. J.*, **554**, 95-98.
- [162] Trujillo C.A., Brown M.E. 2002. A Correlation between Inclination and Color in the Classical Kuiper Belt. *Astroph. J.*, **566**, 125-128.
- [163] Trujillo C.A., 2003. The Caltech Wide Area Sky Survey: Beyond (50000) Quaoar. In *Proceedings of the First Decadal Review of the Edgeworth-Kuiper Belt Meeting in Antofagasta, Chile, Earth Moon and Planets*, **92**, 99-112.
- [164] Tsiganis, K., Gomes, R., Morbidelli, A., Levison, H. F. 2005. Origin of the orbital architecture of the giant planets of the Solar System. *Nature* 435, 459-461.
- [165] Valley J. W., Peck W. H., King E. M., and Wilde S. A. (2002). A cool early Earth. *Geology* 30, 351-354.

- [166] Valsecchi, G. B., Morbidelli, A., Gonczi, R., Farinella, P., Froeschle, C., Froeschle, C. 1995. The dynamics of objects in orbits resembling that of P/Encke. *Icarus* 118, 169.
- [167] Weidenschilling S. 2002. On the Origin of Binary Transneptunian Objects. *Icarus*, **160**, 212–215.
- [168] Weidenschilling S. 2003. Formation of Planetesimals/Cometesimals in the Solar nebula. in *Comet II*, Festou et al. eds., University Arizona Press, Tucson, Az.. 97–104.
- [169] Weissman, P. R. 1978. Physical and Dynamical Evolution of Long-Period Comets. Ph.D. thesis, Univ. of California, Los Angeles.
- [170] Weissman, P. R. 1990. The Oort cloud. *Nature* 344, 825-830.
- [171] Weissman, P. R. 1996. The Oort Cloud. ASP Conf. Ser. 107: Completing the Inventory of the Solar System 107, 265-288.
- [172] Weissman, P. R., Lowry, S. C. 2003. The Size Distribution of Jupiter-Family Cometary Nuclei. Lunar and Planetary Institute Conference Abstracts 34, 2003.
- [173] Wetherill, G. W. 1992. An alternative model for the formation of the asteroids. *Icarus* 100, 307-325.
- [174] Whitman K., Morbidelli A. and Jedicke R. 2005. The size-frequency distribution of dormant Jupiter family comets. *Icarus*, submitted.
- [175] Wiegert, P., Tremaine, S. 1999. The Evolution of Long-Period Comets. *Icarus* 137, 84-121.
- [176] Wilhems, D. E. (1987). Geologic history of the Moon. US Geological Survey, Professional Paper 1348. 302 p. Reston, Virginia.
- [177] Yin, Q., Jacobsen, S. B., Yamashita, K., Blichert-Toft, J., Télouk, P., Albarède, F. 2002. A short timescale for terrestrial planet formation from Hf-W chronometry of meteorites. *Nature* 418, 949-952.
- [178] Yeomans, D. K., Chodas, P. W., Sitarski, G., Szutowicz, S., Królikowska, M. 2004. Cometary orbit determination and nongravitational forces. in *Comets II* (M. Festou et al. eds.), 137-151., University of Arizona press, Tucson.
- [179] Youdin, A. N., Shu, F. H. 2002. Planetesimal Formation by Gravitational Instability. *Astrophysical Journal* 580, 494-505.
- [180] Zappala, V., Cellino, A., Gladman, B. J., Manley, S., Migliorini, F. 1998. NOTE: Asteroid Showers on Earth after Family Breakup Events. *Icarus* 134, 176-179.